Magneto-Optical Response of 2-Dimensional Lattices

João Carlos Carneiro Guerra
Mestrado em Física
Departamento de Física e Astronomia
2018

Orientador
João Viana Lopes, Prof. Auxiliar Convidado
Faculdade de Ciências

Todas as correções determinadas pelo júri, e só essas, foram efetuadas.

O Presidente do Júri,

Porto, / /

Acknowledgments

Before heading into this work, I must first express my thanks to everyone that supported me during my endeavor into writing this work. First of all, I want to thank my supervisor Prof. João Viana Lopes, who was not only extremely available to discuss all the questions and problems I had, but who also constantly pushed me into doing the best work I could despite all the setbacks, and Prof. João Lopes dos Santos, whose insight in these subjects managed to be extremely useful in solving some problems. Secondly, I want to thank my friends that have accompanied me during my academic course: António, Bruno, João Pedro, Maria, and Simão. A special thanks is due to Simão for proofreading my thesis and for teaching me how to work with KITE. Lastly, I want to thank my family for their unconditional support throughout this journey.

Abstract

As indicated by its title, this work consists of a study of graphene under a constant magnetic field.

In Chapter 1, we start by studying the properties the square and lattice without a magnetic field in order to become familiarized with their basic properties.

In Chapter 2, we apply a constant magnetic field to the systems studied in Chapter 1 and determine its wavefunctions. The expressions we arrive at are approximations, and as such, we compare them with numerical results provenient from diagonalization of the tight-binding Hamiltonian.

Chapter 3 introduces the formalism necessary to calculate the conductivity of a general lattice, culminating in Kubo's formula, which will become the equation from which the conductivity will be calculated. Following this, on Chapter 4, we apply the results obtained in Chapter 2 in order to determine the linear conductivity of graphene. After doing so, we compare the obtained expressions against numerical results obtained by the software KITE, which uses the Kernel Polynomial Method to obtain its results faster than other programs. As such, a small introduction to KPM using the density of states as an example is also presented.

Contents

Introduction

Since the first time it was isolated in 2004 [1], graphene has been shown to possess a variety of optical and magneto-optical properties that make it a unique material, leading to an intensive study that has been conducted in recent years. In particular, one of the fields that has been subject to a lot of investigation is graphene's linear and non-linear behavior when an external magnetic field is applied. Some of the studied phenomena studied include the high non-linear optical conductivity [2, 3, 4, 5], four-wave mixing [2, 3, 6], Faraday rotation [7, 8, 9, 10], third harmonic generation [6, 4], Kerr effects [6, 4], fractional quantum Hall effect and magnetoplasmons [7, 11]. These phenomena are all absent or different from the case when there is no magnetic field applied, which makes the study of graphene's linear and non-linear properties study a very promising one.

Chapter 1

Magnetic Field in a Crystal

In this chapter we start by introducing the tight-binding model to describe the electrons' behavior in a crystal. We then follow by introducing a magnetic field in the tight-binding description. This will be applied to the square lattice, where we determine its energy spectrum and wavefunctions, and compare it with numerical results.

1.1 Magnetic Field in a Tight-Binding Model

In order to study the effects of the magnetic field in a crystal, we must first introduce a model that describes the electrons in a crystal. After introducing the tight-binding model, we will introduce the magnetic field through the Peierls substitution.

1.1.1 Tight-Binding Model in a Periodic Lattice

A periodic lattice is generated by the translation of a unit cell. Thus, we can write the position of a unit cell as

$$\boldsymbol{R} = \sum_{i=1}^{D} m_i \boldsymbol{a}_i \tag{1.1.1}$$

where D is the lattice dimension, $\{\boldsymbol{a}_i\}$ are the basis vectors that generate the lattice, and m_i are integer coefficients.

Inside unit cells, we can have more than one atom, whose positions inside the cell are given by $\boldsymbol{\delta}_\alpha$ (α is a label that represents the atoms inside the unit cell). With this, we can write the position of any atom in the lattice as

$$\boldsymbol{r}^\alpha = \boldsymbol{R} + \boldsymbol{\delta}_\alpha. \tag{1.1.2}$$

For the 2D case, we write the position of a unit cell as

$$\boldsymbol{R} = m\boldsymbol{a}_1 + n\boldsymbol{a}_2$$

where m and n correspond to m_1 and m_2 of eq.(1.1.1).

Having explained our notation for the positions of atoms in a 2D lattice, we are now ready to introduce the tight-binding model. A tight-binding model [18], is an approximation made for studying the dynamics of electrons moving on an atomic lattice. Such model Hamiltonians may arise from a finite differences approximation of the Schrodinger Hamiltonian, from the hybridization between electron orbitals of nearby atoms, or even postulated as phenomenological models. At any rate, their

general form in the Wanier basis (and disregarding electron-electron interactions) is

$$\sum_i \varepsilon(\boldsymbol{r}_i)|\varphi(\boldsymbol{r}_i)\rangle\langle\varphi(\boldsymbol{r}_i)| - \sum_{i\neq j} t(\boldsymbol{r}_i,\boldsymbol{r}_j)|\varphi(\boldsymbol{r}_i)\rangle\langle\varphi(\boldsymbol{r}_j)|,$$

where $\varepsilon(\boldsymbol{r}_i)$ are the on-site energies, and $t(\boldsymbol{r}_i,\boldsymbol{r}_j)$ is the hopping integral, which is associated to the probability amplitude for the electron to hop between the atoms in position $\boldsymbol{r}_i$ and $\boldsymbol{r}_j$. In second quantization, this looks like

$$H = \sum_i \varepsilon\left(\boldsymbol{r}_i\right) c^\dagger\left(\boldsymbol{r}_i\right) c\left(\boldsymbol{r}_i\right) - t\sum_{\langle i,j\rangle} c^\dagger\left(\boldsymbol{r}_i\right) c\left(\boldsymbol{r}_j\right),$$

where the usual approximation of nearest neighbor hoppings was considered.

1.1.2 Magnetic Field and Peierls Phase

A magnetic field is introduced in the tight-binding Hamiltonian by adding a phase to the hopping

$$t\left(\boldsymbol{r}_i,\boldsymbol{r}_j\right) \to t\left(\boldsymbol{r}_i,\boldsymbol{r}_j\right) e^{i\varphi(\boldsymbol{r}_i,\boldsymbol{r}_j)}$$

where this phase, known as Peierls phase [12], is defined as

$$\varphi(\boldsymbol{r}_i,\boldsymbol{r}_j) = \frac{e}{\hbar}\int_{\boldsymbol{r}_i}^{\boldsymbol{r}_j} \boldsymbol{A}(\boldsymbol{r},t)\cdot d\boldsymbol{r} \tag{1.1.3}$$

where e is the electron charge and $\boldsymbol{A}$ is the vector potential, which is related to the magnetic field through its curl

$$\boldsymbol{\nabla}\times\boldsymbol{A} = \boldsymbol{B}. \tag{1.1.4}$$

Knowing that

$$\nabla\times(\nabla f) = 0$$

for any function f, we can add a gradient to $\boldsymbol{A}$ without altering the magnetic field. This is called a Gauge freedom, in the choice of $\boldsymbol{A}$, and is useful in choosing a vector potential that simplifies the calculations.

1.2 Square Lattice

Although the focus of this work is the study of graphene, we will start by studying the square lattice. Due to its simpler structure, the calculations turn out less complex than for graphene, but at the same time, many of the results and tendencies observed also hold for graphene.

Furthermore, we will focus our discussion on the square lattice with periodic boundary conditions. The reason to do so is because very large systems with open boundaries are well described by smaller lattices with periodic boundaries. This point shall also be discussed in the following section when we compare numerical results for both open and periodic boundaries.

1.2.1 No Magnetic Field

The tight-binding Hamiltonian for the square lattice is

$$H = -t \sum_{m,n=0}^{L-1} c^\dagger(m,n)c(m+1,n) + c^\dagger(m,n)c(m-1,n) + c^\dagger(m,n)c(m,n+1) + c^\dagger(m,n)c(m,n-1) \tag{1.2.1}$$

when considering hoppings only between nearest-neighbors. In this case, the hopping integral t is the same for all four neighbors. The periodic boundary conditions are inserted in the Hamiltonian by making the identifications

$$c^\dagger(m,n) = c^\dagger(m+L_x,n) \tag{1.2.2}$$

$$c^\dagger(m,n) = c^\dagger(m,n+L_y) \tag{1.2.3}$$

where L_x and L_y are the periods of the lattice along x and y. The Hamiltonian is invariant by translations of any lattice vector $\boldsymbol{R} = ma\hat{e}_x + na\hat{e}_y$, where a is the lattice parameter. This means that the Hamiltonian commutes with the translation operator for such vectors. From this, we can say that the eigenfunctions of the translation operator will also be the eigenfunctions of the Hamiltonian [13]. These eigenfunctions can be written in single-particle basis as

$$|\psi(k_x,k_y)\rangle = \sum_{n,m=0}^{L-1} \psi_{k_x,k_y}(m,n)|m,n\rangle \tag{1.2.4}$$

where k_x and k_y can, for now, take any value and

$$\psi_{k_x,k_y}(m,n) = \frac{1}{L}e^{-i\boldsymbol{k}\cdot\boldsymbol{r}} = \frac{1}{L}e^{-ia(k_x m + k_y n)} \tag{1.2.5}$$

The periodic boundary conditions impose that $\psi_{k_x,k_y}(m,n)$ must have the same value after translations of $L_x\boldsymbol{a}_1$ and $L_y\boldsymbol{a}_2$. Checking for the periodicity along x, we arrive at a constraint for k_x:

$$\begin{aligned} \psi_{k_x,k_y}(m,n) &= \psi_{k_x,k_y}(m+L_x,n) \\ e^{-iak_xL_x} &= 1 \\ k_x &= \frac{2\pi}{L_x a}n_x \end{aligned} \tag{1.2.6}$$

where n_x is any integer between 0 and $L_x - 1$. The same result applies to k_y when checking for the periodic conditions in the y direction.

Having obtained the eigenfunctions of the Hamiltonian, we can get an expression for the eigenvalues by applying the Hamiltonian to the eigenfunctions

$$E|\psi(k_x,k_y)\rangle = H|\psi(k_x,k_y)\rangle \tag{1.2.7}$$

which results in

$$\begin{aligned} E(k_x,k_y)|\psi(k_x,k_y)\rangle &= -t\left[e^{iak_x} + e^{-iak_x} + e^{iak_y} + e^{-iak_y}\right]|\psi(k_x,k_y)\rangle \\ E(k_x,k_y) &= -2t\left[\cos(k_x a) + \cos(k_y a)\right] \end{aligned} \tag{1.2.8}$$

This dispersion relation is plotted in Fig.1.1.

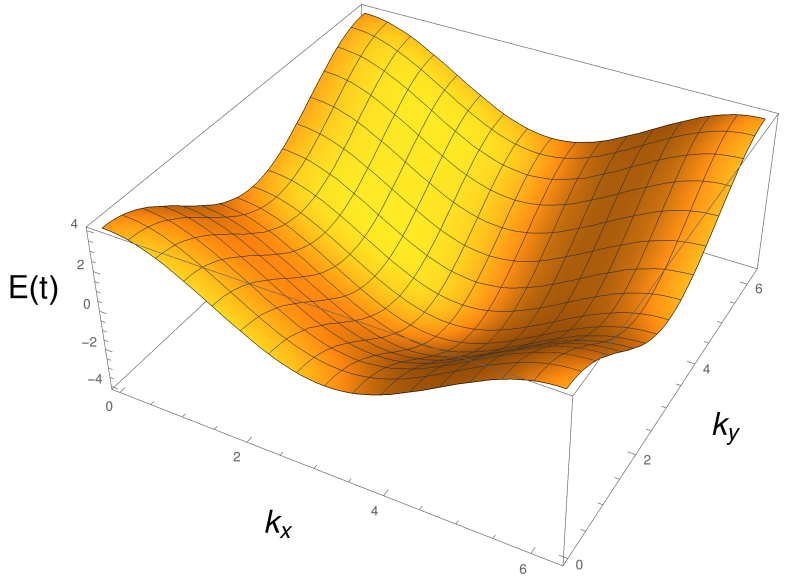

Figure 1.1: Dispersion relation for the square lattice with periodic boundary conditions. The energy is written in units of the hopping integral t.

We can now use this result to write the diagonal Hamiltonian

$$H = \sum_{k_x,k_y} E(k_x,k_y)|\psi(k_x,k_y)\rangle\langle\psi(k_x,k_y)| \tag{1.2.9}$$

where k_x and k_y go from 0 to $2\pi/a$ as seen before. In second quantization, this Hamiltonian is written as

$$H = \sum_{k_x,k_y} E(k_x,k_y)c^\dagger(k_x,k_y)c(k_x,k_y)$$

where $c^\dagger(k_x,k_y)$ and $c(k_x,k_y)$ are given by

$$c^\dagger(k_x,k_y) = \frac{1}{L}\sum_{n,m} e^{ia(k_x m+k_y n)}c^\dagger(m,n) \tag{1.2.10}$$

$$c(k_x,k_y) = \frac{1}{L}\sum_{n,m} e^{-ia(k_x m+k_y n)}c(m,n). \tag{1.2.11}$$

Conversely, we can also write the creation and annihilation operators in real space as a sum of the ones for k-space:

$$c^\dagger(m,n) = \frac{1}{L}\sum_{k_x,k_y} e^{-i\boldsymbol{k}\cdot\boldsymbol{r}}c^\dagger(k_x,k_y) \tag{1.2.12}$$

$$c(m,n) = \frac{1}{L}\sum_{k_x,k_y} e^{i\boldsymbol{k}\cdot\boldsymbol{r}}c(k_x,k_y) \tag{1.2.13}$$

We can now easily diagonalize a tight-binding Hamiltonian with translation symmetry by replacing the creation and annihilation operators in position basis by their expressions in eqs.1.2.12 and 1.2.13. This will be helpful when working in graphene, as its Hamiltonian is also invariant by translations of lattice vectors.

1.2.2 Constant Magnetic Field

A magnetic field is introduced in a tight-binding Hamiltonian through the following substitution

$$t(\boldsymbol{r}_i, \boldsymbol{r}_j) \to e^{i\varphi(\boldsymbol{r}_i, \boldsymbol{r}_j)} t(\boldsymbol{r}_i, \boldsymbol{r}_j)$$

where $\varphi(\boldsymbol{r}_i, \boldsymbol{r}_j)$ is called the Peierls phase. This phase is given by

$$\varphi(\boldsymbol{r}_i, \boldsymbol{r}_j) = \frac{e}{\hbar} \int_{\boldsymbol{r}_i}^{\boldsymbol{r}_j} \boldsymbol{A}(\boldsymbol{r}) \cdot d\boldsymbol{r}$$

where e is the electron charge and $\boldsymbol{A}(\boldsymbol{r})$ the vector potential that describes the magnetic field.

For the case of the square lattice, the Peierls phases between nearest neighbors are

$$\varphi(\boldsymbol{r}_i, \boldsymbol{r}_i \pm a\hat{e}_x) = \frac{e}{\hbar} \int_{\boldsymbol{r}_i}^{\boldsymbol{r}_i \pm a\hat{e}_x} A_x \cdot dx \tag{1.2.14}$$

$$\varphi(\boldsymbol{r}_i, \boldsymbol{r}_i \pm a\hat{e}_y) = \frac{e}{\hbar} \int_{\boldsymbol{r}_i}^{\boldsymbol{r}_i \pm a\hat{e}_y} A_y \cdot dy \tag{1.2.15}$$

By choosing a gauge such that one of the components of $\boldsymbol{A}$ is zero, two of the four phases will become zero. As such, we make $A_y = 0$. From this choice, we have that the vector potential that gives us a constant magnetic field on the z direction is

$$\boldsymbol{A} = -By\hat{e}_x \tag{1.2.16}$$

which can be verified by evaluating its curl

$$\boldsymbol{\nabla} \times \boldsymbol{A} = B\hat{e}_z. \tag{1.2.17}$$

Having chosen $\boldsymbol{A}$, we can now replace it in eq.(1.2.14) and calculate the two non-zero Peierls phases:

$$\varphi(\boldsymbol{r}_i, \boldsymbol{r}_i \pm a\hat{e}_x) = \frac{e}{\hbar} B \int_{ma}^{(m\pm1)a} y dx = \pm \frac{e}{\hbar} Bay \tag{1.2.18}$$

Because we are working on a discrete lattice, we can write the coordinate y as na. This allows us to write the phase in terms of the flux on a unitary cell $\phi = Ba^2$, the quantum of flux $\phi_0 = \frac{h}{e}$, and the coordinate n.

$$\varphi(\boldsymbol{r}_i, \boldsymbol{r}_i \pm a\hat{e}_x) = \pm 2\pi \frac{\phi}{\phi_0} n \tag{1.2.19}$$

Looking at the Hamiltonian with the Peierls phase, it is clear that it has a different periodicity than that of the lattice.

$$\begin{aligned} H = -t \sum_{m,n} & e^{2\pi i \frac{\phi}{\phi_0} n} c^\dagger(m,n) c(m+1,n) + e^{-2\pi i \frac{\phi}{\phi_0} n} c^\dagger(m,n) c(m-1,n) \\ & + c^\dagger(m,n) c(m,n+1) + c^\dagger(m,n) c(m,n-1) \end{aligned}$$

As the phase depends on n, the Hamiltonian will no longer have translation symmetry in general. If

we want to impose periodic boundary conditions, we have to constrain the flux to specific values.

1.2.3 Boundary Conditions

When imposing periodic boundary conditions, the flux will be constrained to certain values, as the Peierls phase must be the same after a translation of the lattice period. Looking at the expression for the phases, we can outright see that they do not depend on x, meaning that the boundary conditions along this direction do not impose any constraints on the phase. Imposing boundary conditions along y, we get that

$$\varphi(\boldsymbol{r}_i, \boldsymbol{r}_j) = \varphi(\boldsymbol{r}_i, \boldsymbol{r}_j + L_y a) + 2\pi M \tag{1.2.20}$$

where M is any integer. After inputting the expression for the phases, this equation becomes

$$2\pi \frac{\phi}{\phi_0} L_y = 2\pi M \iff \frac{\phi}{\phi_0} = \frac{M}{L_y} \tag{1.2.21}$$

This means that the only allowed values of the flux for the square lattice with periodic boundary conditions are multiples of ϕ_0/L_y.

Going back to the Hamiltonian, and introducing the phases, we have

$$H = -t\sum_{m,n} e^{2\pi i \frac{\phi}{\phi_0} n} c^\dagger(m,n)c(m+1,n) + e^{-2\pi i \frac{\phi}{\phi_0} n} c^\dagger(m,n)c(m-1,n) \\ + c^\dagger(m,n)c(m,n+1) + c^\dagger(m,n)c(m,n-1)$$

At this point, we would want to do the same as in the case without magnetic field: write the creation and annihilation operators in momentum space and find the dispersion relation. However, due to the dependence of the phases in n, there is no translation symmetry along the y direction, meaning that the solutions studied earlier do not apply. However, as there is no dependence on x in the phase, the translation symmetry along this direction is not broken. This allows for the expansion of the creation and annihilation operators in terms of plane waves along x. After simplifying, we obtain

$$H = -t\sum_{k_x,n} 2\cos\left(k_x a + 2\pi \frac{\phi}{\phi_0} n\right) c^\dagger(k_x,n)c(k_x,n) + c^\dagger(k_x,n)c(k_x,n+1) + c^\dagger(k_x,n)c(k_x,n-1) \tag{1.2.22}$$

As this Hamiltonian is diagonal in k_x, we can write it by blocks

$$H = \sum_{k_x} c^\dagger(k_x) H(k_x) c(k_x) \tag{1.2.23}$$

where $c^\dagger(k_x) = \begin{pmatrix} c^\dagger(k_x,0) & \dots & c^\dagger(k_x, L-1) \end{pmatrix}$, $c(k_x)$ is its Hermitian conjugate, and $H(k_x)$ is given by

$$-t\begin{bmatrix} 2\cos(k_xa+2\pi\frac{\phi}{\phi_o}) & 1 & 0 & \dots & 1 \\ 1 & 2\cos(k_xa+4\pi\frac{\phi}{\phi_o}) & 1 & \dots & 0 \\ 0 & 1 & \ddots & \vdots & \vdots \\ \vdots & \vdots & \dots & 2\cos(k_xa+2\pi(L-1)\frac{\phi}{\phi_o}) & 1 \\ 1 & 0 & \dots & 1 & 2\cos(k_xa+2\pi L\frac{\phi}{\phi_o}) \end{bmatrix} \tag{1.2.24}$$

Notice the 1 in the positions $(1, L)$ and $(L, 1)$ of the matrix. These entries represent the hoppings between the sites 0 and $L-1$, assuring the periodic boundaries along y. For the case of open boundaries in the y direction, the result is very similar to this one. The differences are that the flux does not have any restriction on the values it can take, and the entries $(1, L)$ and $(L, 1)$ of $H(k_x)$ are 0.

1.2.4 Continuum Approximation

As the Hamiltonian is diagonal in k_x, the eigenvectors of the Hamiltonian are going to be some linear combination of the position states $|n\rangle$

$$|\phi_\lambda\rangle = \sum_n \alpha_\lambda(k_x, n)|k_x, n\rangle \tag{1.2.25}$$

where λ is a label for the associated eigenvalue. In order to determine these α coefficients, we use eq.(1.2.7), obtaining

$$E_\lambda\alpha_\lambda(k_x, n) = -t\left[2\cos\left(2\pi\frac{\phi}{\phi_0}n + k_xa\right)\alpha_\lambda(k_x, n) + \alpha_\lambda(k_x, n-1) + \alpha_\lambda(k_x, n+1)\right] \tag{1.2.26}$$

This result is not one equation, but actually a set of L equations, one for each value of n. As it proves to be impossible to find a solution to this system, we approximate α to a continuum function (which is a valid approximation for a very large L). This makes it possible to expand $\alpha(k_x, n+1)$ and $\alpha(k_x, n-1)$ in a power series of n around $\alpha(k_x, n)$

$$\alpha_\lambda(k_x, n \pm 1) = \alpha_\lambda(k_x, n) \pm \frac{d\alpha_\lambda}{dn}(k_x, n) + \frac{1}{2}\frac{d^2\alpha_\lambda}{dn^2}(k_x, n) \tag{1.2.27}$$

In this case, we expand to second order because the first order terms will cancel. Replacing in eq.(1.2.26), we obtain a differential equation for $\alpha_\lambda(k_x, n)$:

$$E_\lambda\alpha_\lambda(k_x, n) = -t\left[\left(2\cos\left(2\pi\frac{\phi}{\phi_0}n + k_xa\right) + 2\right)\alpha_\lambda(k_x, n) + \frac{d^2\alpha_\lambda}{dn^2}\right] \tag{1.2.28}$$

Due to the co-sine term, we cannot find an exact solution to this differential equation. However, notice that this equation is the wavefunction equation for a particle in a potential given by

$$V(k_x, n) = -2t\left[\cos\left(2\pi\frac{\phi}{\phi_0}n + k_xa\right) + 1\right] \tag{1.2.29}$$

and mass $-\frac{\hbar^2}{2ta^2}$. As we cannot find the exact solution, we can approximate the potential around its minimum and determine approximated wavefunctions for the lowest energies of the system. Defining

n' as the value of n where the potential is minimum, we have

$$2\pi\frac{\phi}{\phi_0}n' + k_x a = 2\pi q \tag{1.2.30}$$

where q is any integer. Using the expressions we already found for k_x (eq.(1.2.6)) and ϕ/ϕ_0 (eq.(1.2.21)), n' becomes

$$n' = \frac{1}{M}\left(Lq - n_x\right) \tag{1.2.31}$$

From this expression, we can learn some information about this system. As n varies between 0 and $L-1$, q has to be an integer between 0 and $M-1$. This is so because when $q = M$, the value of n' will have an added factor of L compared to when $q = 0$, and because of the periodic boundary conditions, those two points would be the same. This means that the number of minima of the potential, which is the number of values q can take, will be equal to M. Furthermore, the variation of k_x induces a translation of the minima.

With an expression for the minima, we can expand the co-sine around it, yielding

$$\cos\left(2\pi\frac{\phi}{\phi_0}n + k_x a\right) \approx 1 - \frac{1}{2}\left(\frac{a}{l_B}\right)^4 (n-n')^2 \tag{1.2.32}$$

where l_B is called the magnetic length and its expression is given by

$$l_B = \sqrt{\frac{\phi_0 a^2}{2\pi\phi}} = \sqrt{\frac{La^2}{2\pi M}} \tag{1.2.33}$$

Going back to the differential equation, replacing the expansion of the co-sine, we have

$$-t\frac{d^2\alpha_\lambda}{dn^2} + t\left(\frac{a}{l_B}\right)^4 (n-n')^2\alpha_\lambda(k_x,n) = (E_\lambda + 4t)\alpha_\lambda(k_x,n) \tag{1.2.34}$$

which has a striking resemblance with the equation for the quantum harmonic oscillator. Applying a change of variable to n

$$n \to x = n - n'$$

we obtain exactly that:

$$-t\frac{d^2\alpha_\lambda}{dx^2} + t\left(\frac{a}{l_B}\right)^4 x^2\alpha_\lambda(k_x,x) = (E_\lambda + 4t)\alpha_\lambda(k_x,x) \tag{1.2.35}$$

We now have transformed the problem of finding the coefficients of the wave functions into an harmonic oscillator problem. The solutions for this equation can be found in any introductory quantum mechanics textbook, such as [12]. In order to obtain the solutions for this problem, we write the solution for the quantum harmonic oscillator, but with the coefficients of the above equation

$$m \to \frac{\hbar^2 a^2}{2t}$$

$$\omega \to \frac{2t}{\hbar}\left(\frac{a}{l_B}\right)^2$$

obtaining

$$\alpha_0(k_x, n) = \left(\frac{1}{\pi}\left(\frac{a}{l_B}\right)^2\right)^{\frac{1}{4}} e^{-\frac{1}{2}\frac{a^2}{l_B^2}(n-n')^2} \tag{1.2.36}$$

for the lowest energy level. The coefficients for higher energy levels can be obtained from this one as

$$\alpha_\lambda(k_x, n) = \frac{1}{\sqrt{\lambda!}}\frac{1}{\sqrt{2^\lambda}}\left[\frac{a}{l_B}n - \frac{l_B}{a}\frac{d}{dn}\right]^\lambda \alpha_0(k_x, n) \tag{1.2.37}$$

We can now analyze how $\alpha_0(k_x, n)$ behaves as the system's parameters vary. Looking at the form of its expression, $\alpha_0(k_x, n)$ is a Gaussian centered on n' and $\sigma = (l_B/a)^2$. From eq.(1.2.33) we see that l_B^2 is inversely proportional to the flux ϕ, which means that increasing it will decrease the width of the Gaussian, causing it to be more dense around n'.

From eq.(1.2.35) we can also take the values of the energy associated with the coefficients. Knowing that the energy of a quantum harmonic oscillator is quantized as

$$E_\lambda = \hbar\omega\left(\lambda + \frac{1}{2}\right) \tag{1.2.38}$$

where λ is a non-negative integer. Identifying the second term of eq.(1.2.35) with it, we get

$$E_\lambda = \frac{4\pi\phi}{\phi_0}\left(\lambda + \frac{1}{2}\right)t - 4t \tag{1.2.39}$$

As with the α coefficients, there is also a dependence on ϕ in the energy. In this case, for higher values of the flux, the spacing between energy levels will become larger.

With this, we have reached an approximation for the lowest energy values of the square lattice with a magnetic field and its respective wavefunctions.

1.2.5 Magnetic Cell

In order to better understand what happens to the electrons on a periodic lattice when we increase the magnetic field, we can introduce the concept of magnetic cell. Writing the flux as

$$\frac{\phi}{\phi_0} = \frac{M}{L} \tag{1.2.40}$$

where L is the period of the lattice, made the same in both directions, and M divides L and is greater than one, we call a cell with size $L' = L/M$ the magnetic cell. Using this definition of magnetic cell, we can rewrite the coordinate n as

$$n \to n + mL' \tag{1.2.41}$$

where m labels the magnetic cells that constitute a period of the lattice and n is now between 0 and $L' - 1$. This introduces a new dimension in the problem, which, as we will see, will end up simplifying it. Using this definition on the Hamiltonian, we get

$$\begin{aligned} H = -t\sum_{k_x}\sum_{m=0}^{M-1}\sum_{n=0}^{L'-1} & V(k_x, m, n)c^\dagger(k_x, m, n)c(k_x, m, n) \\ & + c^\dagger(k_x, m, n)c(k_x, m, n+1) + c^\dagger(k_x, m, n)c(k_x, m, n-1) \\ & + c^\dagger(k_x, m, 0)c(k_x, m-1, L'-1) + c^\dagger(k_x, m, L'-1)c(k_x, m+1, 0) \end{aligned} \tag{1.2.42}$$

where

$$V(k_x, m, n) = 2\cos\left(2\pi\frac{\phi}{\phi_0}\left(n + mL'\right) + k_x a\right) \tag{1.2.43}$$

The last two terms of the Hamiltonian represent the hoppings between the last atom of a magnetic cell and the first of the next one. We can simplify this Hamiltonian by noticing that $V(k, m, n)$ does not actually depend on m

$$\begin{aligned} V(k_x, m, n) &= 2\cos\left(2\pi\frac{M}{L}\left(m\frac{L}{M} + n\right) + k_x a\right) \\ &= 2\cos\left(2\pi m + 2\pi\frac{\phi}{\phi_0}n + k_x a\right) \\ &= 2\cos\left(2\pi\frac{\phi}{\phi_0}n + k_x a\right) \end{aligned} \tag{1.2.44}$$

This makes the Hamiltonian invariant by translations along m. Expanding the operators as we did in eqs.1.2.12 and 1.2.13 but now for m, we obtain

$$\begin{aligned} H = &-t\sum_{k_x k_m}\sum_{n=0}^{L'-1} V(k_x, n)c^\dagger(k_x, k_m, n)c(k_x, k_m, n) \\ &+ c^\dagger(k_x, k_m, n)c(k_x, k_m, n+1) + c^\dagger(k_x, k_m, n)c(k_x, k_m, n-1) \\ &+ e^{-ik_m aL'}c^\dagger(k_x, k_m, 0)c(k_x, k_m, L'-1) + e^{ik_m aL'}c^\dagger(k_x, k_m, L'-1)c(k_x, k_m, 0) \end{aligned} \tag{1.2.45}$$

We can write this Hamiltonian similarly to eq.(1.2.23)

$$H = \sum_{k_x, k_m} c^\dagger(k_x, k_m)H(k_x, k_m)c(k_x, k_m) \tag{1.2.46}$$

where

$$c(k_x, k_m) = \begin{pmatrix} c(k_x, k_m, 0) & \dots & c(k_x, k_m, L'-1) \end{pmatrix} \tag{1.2.47}$$

$c^\dagger(k_x, k_m)$ is its hermitian conjugate and $H(k_x, k_m)$ is defined as

$$-t\begin{bmatrix} 2\cos(k_x a) & 1 & 0 & \dots & e^{-ik_m aL'} \\ 1 & 2\cos(k_x a + 2\pi\frac{\phi}{\phi_0}) & 1 & \dots & 0 \\ 0 & 1 & \ddots & \vdots & \vdots \\ \vdots & \vdots & \dots & 2\cos(k_x a + 2\pi(L'-2)\frac{\phi}{\phi_0}) & 1 \\ e^{ik_m aL'} & 0 & \dots & 1 & 2\cos(k_x a + 2\pi(L'-1)\frac{\phi}{\phi_0}) \end{bmatrix} \tag{1.2.48}$$

which has a very similar form to the one in eq.(1.2.24). By writing the Hamiltonian in this form, the process of obtaining the eigenvalues is much easier, as we now have to determine the eigenvalues of M $L' \times L'$ matrices, instead of a $ML' \times ML'$ matrix, which would take M times longer.

As for the wavefunctions, we can write them as

$$\psi_{\lambda, k_x, k_m}(x, n, m) = e^{ik_x x}e^{ik_m aL'm}\psi_{\lambda, k_x, k_m}(n) \tag{1.2.49}$$

where $\psi_{\lambda, k_x, k_m}(n)$ are the eigenvectors obtained from the diagonalization of the Hamiltonian in 1.2.48. This means that $\psi_{\lambda, k_x, k_m}(n)$ will be the same for both magnetic cells, which is equivalent to saying that the wavefunctions for the $L \times L$ lattice will be the wavefunctions for the $L' \times L'$ magnetic cell,

repeated through all magnetic cells.

1.3 Numerical Results

Having arrived at approximated expressions for the energy and wavefunctions for the square lattice, we want to know how good our results are. One way to do this is to compute the eigenvalues and eigenvectors of the Hamiltonian and plot them against the results we obtained. In this section we will make these comparisons for the energy and wavefunctions, and analyze how they change by varying the system's parameters. The numerical results were obtained using Wolfram Mathematica.

1.3.1 Energy

In Fig. 1.2 a), we have plotted eq.(1.2.39) against the eigenvalues of the Hamiltonian in eq.(1.2.24) for the lowest 31 levels and $\phi/\phi_0 = 1/2048$. For the range of energies represented, the two sets of points are very close to one another, which indicates that our approximation holds. We can also see, however, that for higher energy levels, the two sets of points start growing farther from one another, which indicates that as we increase the energy, our approximation becomes less efficient. This is to be expected, as we expanded the potential around its minima, so we naturally have that the lower the energy, the better the approximation.

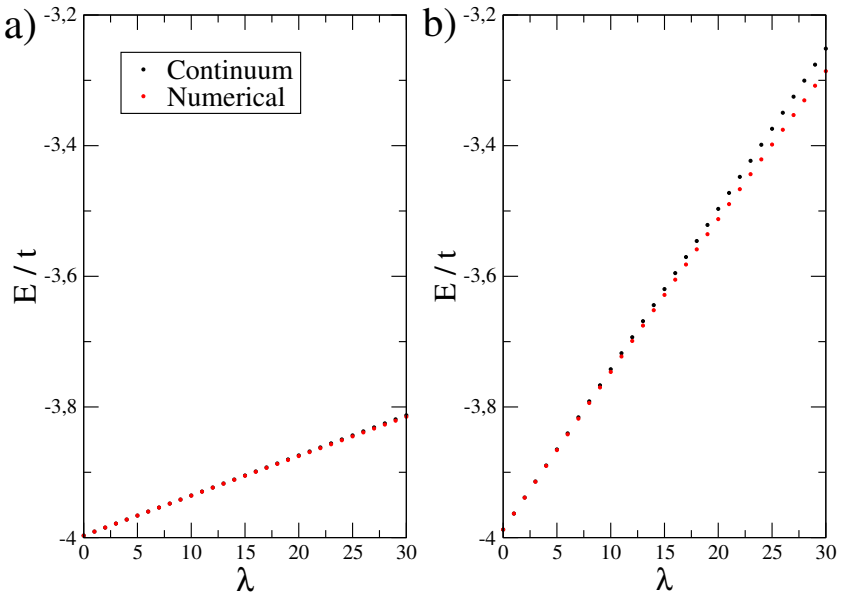

Figure 1.2: Lowest 31 values for the energy in units of the hopping integral, represented as function of the energy level λ. The system's parameters are $L = 2048$ and $\phi/\phi_0 = 1/L$ for a) and $\phi/\phi_0 = 4/L$ for b). Red dots represent the eigenvalues calculated through numerical diagonalization of the Hamiltonian while black ones are the energy values obtained through eq.(1.2.39).

In Fig.1.2 b) we plotted the same system, but with $\phi/\phi_0 = 1/512$. We can see here that, as observed in the previous section, by increasing the magnetic field, the energy difference between energy levels increases. Also, fixing the level λ, we notice that the approximation in Fig.1.2 b) becomes worse than the one in a), which means that the quality of the approximation is determined by the energy and not by the level. So, if we want to obtain many energy levels where our approximation is valid, we just need to lower the magnetic field (which in turn means increasing the period of the system, seeing as the lowest allowed value for ϕ is proportional to $1/L$)

Another important aspect that cannot be seen in Fig.1.2 is the degeneracy of the eigenvalues. As seen in the previous section, the potential is periodic, meaning that the eigenvalues of the Hamiltonian will have a degeneracy equal to the number of times the potential repeats itself from 0 to $n-1$. Using the fact that the potential is a co-sine, the number of times it repeats itself will be equal to the number of minima, which, as calculated earlier, is $m = L\phi/\phi_0$. Applying this to Fig.1.2 b), ($L = 2048$ and $\phi/\phi_0 = 1/512$), we see that its eigenvalues are 4-times degenerate, which agrees with the numerical results obtained.

Having seen the limits of our approximation, we can now plot how the full spectrum of the eigenvalues of the Hamiltonian varies with the magnetic field. The result is presented in Fig. 1.3 and the resulting image is known as "Hofstadter Butterfly". This plot shows us how complex a lattice under a magnetic field is, which is why we restrict our study to low energies.

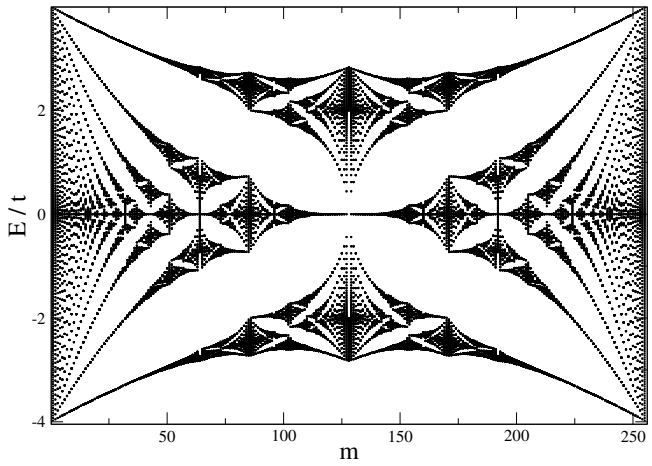

Figure 1.3: Eigenvalues of a 256×256 square lattice with periodic boundary conditions as function of $m = L\phi/\phi_0$

1.3.2 Wavefunctions

In Fig.1.4, we plot some of the low energy wavefunctions, both from the analytical expression and from the numerical diagonalization of the Hamiltonian of eq.(1.2.24). As it can be seen, there is an almost complete overlap between both curves. However, as the energy associated to the wavefunction increases, differences start to appear between the curves.

Similarly to what we did to the energy, we can see how the wavefunctions change by varying the magnetic field. The result, shown in Fig. 1.5, is just as foretold when we introduced the concept of magnetic cell: the wavefunction repeats itself for all the magnetic cells. This is what we see in Fig., where for $\phi/\phi_0 = 4/L$ we get that for the lowest energy, we have four points around which there is a harmonic oscillator behavior. Using the expression for n', these points are 0, $L/4$, $L/2$ and $3L/4$, which is in agreement with the figure.

Additionally, we also plot eq.(1.2.36) in Fig.1.5. As we are representing the wavefunctions for the lowest energy, we obtain a very good fit, which is why there only appears to be one curve.

1.3.3 Open Boundary Conditions

Up until now, we focused on studying the square lattice with periodic boundary conditions, which is an approximation for an open system with a very large L. Although we do not have an expression to describe the energy bands or the wavefunctions of a system with open boundaries, we can use the

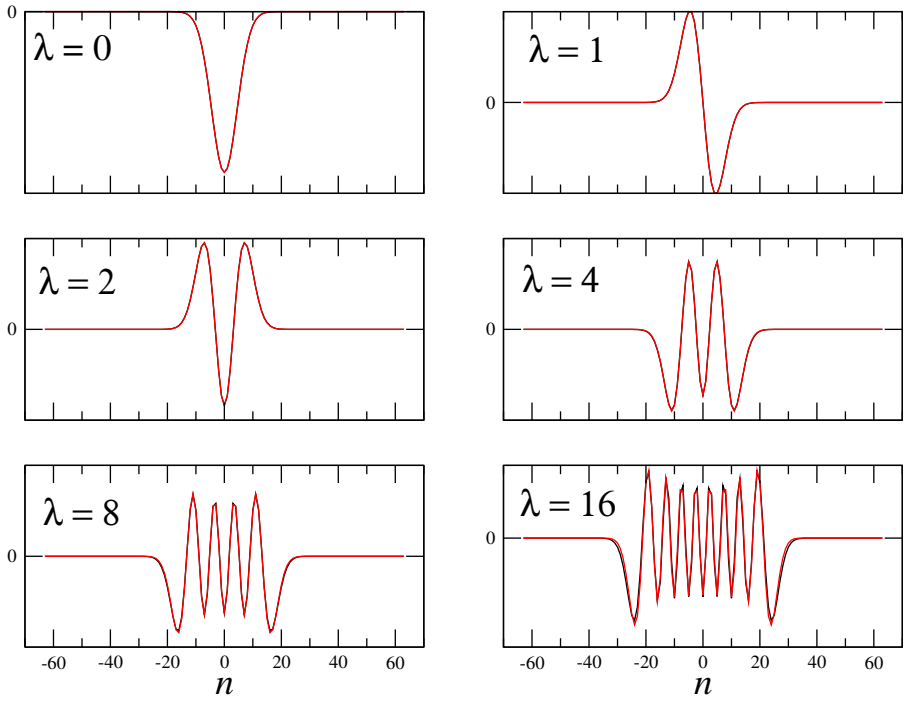

Figure 1.4: Square lattice wavefunctions represented as function of n (the lattice sites along the y direction) obtained through diagonalization of a 128×128 Hamiltonian with $\phi/\phi_0 = 1/L$ and $k = 0$ (black) and the analytical solutions obtained through eqs. 1.2.36 and 1.2.37 for the same parameters (red).

Hamiltonian of eq.(1.2.24) to describe such a system and obtain numerical results. We can see how these results evolve as we increase the size of the system, and see if they converge to the results obtained with periodic boundaries.

We will start by plotting the energy as a function of k_x. In the case of periodic boundaries, the energy does not depend on k_x, which means that the Landau levels will be constant. However the same does not happen when the system has open boundaries, as we can see in Fig.1.6. In this figure, for values of k_x close to 0 and 2π, the energy starts to increase for the open boundaries case. Going back to eq.(1.2.30), we see that these values of k_x correspond to wavefunctions centered around the edges of the lattice. This makes sense, as the states that differ between periodic and open boundaries description should be the ones near the edges. The increase in energy can be justified with the high

Another quantity that we can analyze in order to study the effect of the open boundaries is the density of states. In Fig.1.7, we represent the lowest Landau level of the density of states of a square lattice with open and periodic boundaries. As we increase L, the states that appear far from the peak start to decrease in amplitude. This means that by increasing L, the density of states of an open system tends to the one for periodic boundaries.

1.4 Determining the Phases for a General Lattice

In the case of the square lattice, the constraints of periodic boundary conditions on the phases were determined without problems. This is due to the fact that in the square lattice, the lattice vectors are orthogonal, and there is only one atom per unit cell. However, for other lattices, this may not be the case: finding expressions for the phases that can satisfy periodic boundary conditions can become a troublesome task. With this in mind, we will develop in this section a method through which we can obtain the Peierls phases for any lattice with periodic boundary conditions.

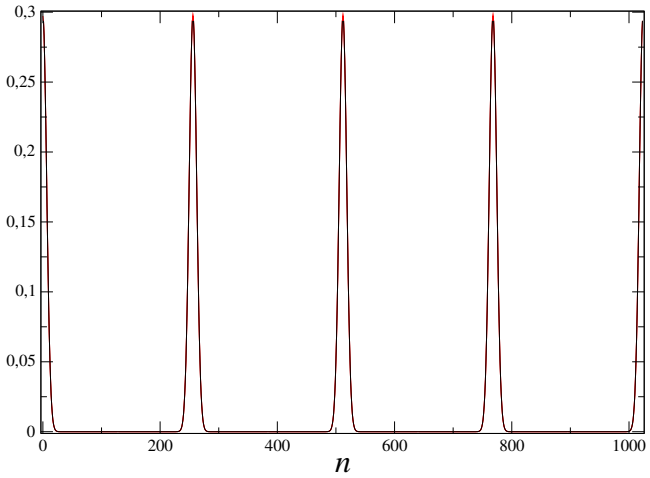

Figure 1.5: Wavefunction for the lowest energy level of a square lattice with period $L = 1024$, $k_x = 0$ and $\phi/\phi_0 = 4/L$ calculated by diagonalization of the Hamiltonian 1.2.24 (black) and by eq.(1.2.36) (red).

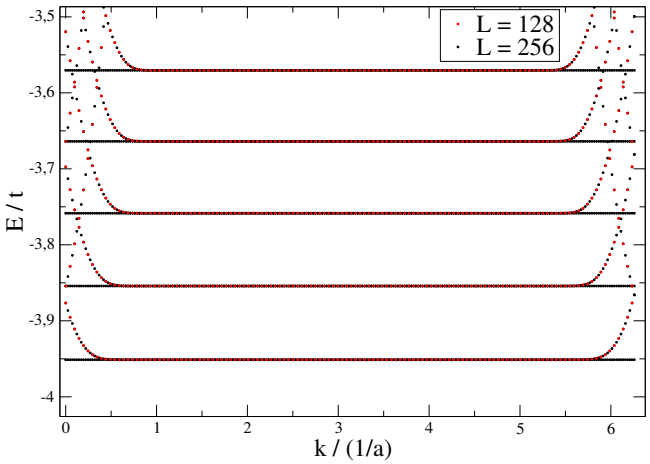

Figure 1.6: Lowest Landau levels for a square lattice with open boundaries and $\phi/\phi_0 = 1/128$.

1.4.1 The Vector Potential A

Using the lattice vectors, we can define the reciprocal lattice vectors $\boldsymbol{b}_i$ through the orthogonality relation

$$\boldsymbol{a}_i \cdot \boldsymbol{b}_j = 2\pi\delta_{ij} \tag{1.4.1}$$

Like the lattice vectors, the reciprocal lattice vectors constitute a complete basis of the space we are working in (in the 2D case, of the plane). As such, we can write the vector potential $\boldsymbol{A}(\boldsymbol{r})$ as

$$\boldsymbol{A}(\boldsymbol{r}) = \sum_i A_i(\boldsymbol{r})\boldsymbol{b}_i \tag{1.4.2}$$

As we are studying the case where the magnetic field is constant, this means that the components of $\boldsymbol{A}$ will depend linearly on $\boldsymbol{r}$, that is, $A_i(\boldsymbol{r})$ will be a linear combination of the various components of $\boldsymbol{r}$. In particular, we can write $\boldsymbol{r}$ in the reciprocal lattice basis, yielding

$$\boldsymbol{A}(\boldsymbol{r}) = \sum_{ij} \left(A_{ij}\boldsymbol{r} \cdot \boldsymbol{b}_j\right) \boldsymbol{b}_i \tag{1.4.3}$$

where A_{ij} are coefficients that will determine the magnetic field. We can also write the transpose of

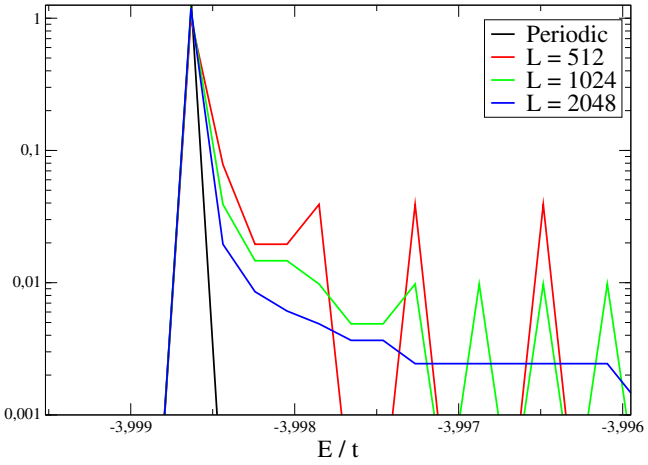

Figure 1.7: Zoom-in of the density of states of a square lattice on the lowest Landau level with $\phi/\phi_0 = 1/4096$. The black curve represents periodic boundary conditions, while the other three are for open boundaries with different sizes. Only one Landau level is shown because, otherwise, the image would become visually confusing.

$\boldsymbol{A}$ as

$$\boldsymbol{A}^T(\boldsymbol{r}) = \sum_{ij} \left(A_{ij}\boldsymbol{r}\cdot\boldsymbol{b}_i\right)\boldsymbol{b}_j.$$

which has the following property

$$\boldsymbol{A}(\boldsymbol{r}_1)\cdot\boldsymbol{r}_2 = \boldsymbol{A}^T(\boldsymbol{r}_2)\cdot\boldsymbol{r}_1.$$

This property will be very important when determining the constraints on the phases due to periodic boundaries.

1.4.2 Relation to the Magnetic Field

Let us write $\boldsymbol{A}$ as function of the magnetic field. Starting from

$$\boldsymbol{B} = \boldsymbol{\nabla}\times\boldsymbol{A}$$

and using eq.(1.4.3), for the 2D case, we arrive at

$$\boldsymbol{B} = \frac{(2\pi)^2}{V}\left(A_{21} - A_{12}\right)\hat{e}_z.$$

where V is the area if a unit cell. Writing $\boldsymbol{B} = B\hat{e}_z$, this expression becomes

$$B = \frac{(2\pi)^2}{V}\left(A_{21} - A_{12}\right) \tag{1.4.4}$$

Fixing the magnetic field, we just need to choose A_{12} and A_{21} such that this equality holds. This means that A_{11} and A_{22} can take any value.

1.4.3 Periodic Boundary Conditions

Let us start by considering the case where there is only one atom per unit cell. As $\boldsymbol{A}$ is linear in $\boldsymbol{r}$, the Peierls phase between two points $\boldsymbol{r}_i$ and $\boldsymbol{r}_j$ becomes

$$\frac{\hbar}{e}\varphi(\boldsymbol{r}_i,\boldsymbol{r}_j)=\int_{\boldsymbol{r}_i}^{\boldsymbol{r}_j} d\boldsymbol{r}\cdot\boldsymbol{A}(\boldsymbol{r})=(\boldsymbol{r}_j-\boldsymbol{r}_i)\cdot\boldsymbol{A}\left(\frac{\boldsymbol{r}_i+\boldsymbol{r}_j}{2}\right). \tag{1.4.5}$$

Now, we have to impose the periodic boundary conditions on the phase. Writing the period of the lattice along the direction $\boldsymbol{a}_n$ as L_n, the boundary conditions along that dictate that

$$e^{i\varphi(\boldsymbol{r}_i+L_n\boldsymbol{a}_n,\boldsymbol{r}_j+L_n\boldsymbol{a}_n)}=e^{i\varphi(\boldsymbol{r}_i,\boldsymbol{r}_j)}$$

which is equivalent to

$$\frac{e}{\hbar}(\boldsymbol{r}_j-\boldsymbol{r}_i)\cdot\boldsymbol{A}\left(L_n\boldsymbol{a}_n\right)=2\pi\lambda \tag{1.4.6}$$

where λ is some integer. Unwinding the definitions of the position vectors and the vector potential, this equation becomes

$$\begin{aligned}\frac{e}{\hbar}\sum_{m,p,q}\left(x_j^m-x_i^m\right)\boldsymbol{a}_m\cdot\boldsymbol{b}_pA_{pq}\left(L_n\boldsymbol{a}_n\cdot\boldsymbol{b}_q\right)&=2\pi\lambda\\ \frac{e}{\hbar}(2\pi)^2\sum_m\left(x_j^m-x_i^m\right)A_{mn}L_n&=2\pi\lambda\\ \frac{e}{\hbar}\sum_m\left(x_j^m-x_i^m\right)2\pi A_{mn}L_n&=\lambda\end{aligned} \tag{1.4.7}$$

As $\left(x_j^m-x_i^m\right)$ and L_n are already integers, it should suffice that $\frac{e}{\hbar}2\pi A_{mn}$ be an integer. However, as we want to obtain the lowest possible values for A_{mn}, we instead impose that $\frac{e}{\hbar}2\pi A_{mn}L_n$ be an integer, which is equivalent to writing

$$A_{mn}=\frac{\phi_0 M_{mn}}{(2\pi)^2L_n} \tag{1.4.8}$$

where M_{mn} is a matrix of integers. Using eq.(1.4.4), we can write the values the to which the magnetic field is constrained:

$$B=\frac{\phi_0}{V}\left(\frac{M_{21}}{L_1}-\frac{M_{12}}{L_2}\right).$$

Choosing $M_{21}=0$ is a particular choice of gauge (Landau gauge), which leads to

$$\frac{\phi}{\phi_0}=\frac{M_{12}}{L_1} \tag{1.4.9}$$

where $\phi=BV$ is the flux through a unit cell. As M_{12} is any integer, this result agrees with the one we obtained earlier for the square lattice.

Let us now study how this solution fits our problem when we have more than one atom per unit cell. Rewriting eq.(1.4.6) for this case, we have

$$\begin{aligned}\frac{e}{\hbar}(\boldsymbol{r}_j^\beta-\boldsymbol{r}_i^\alpha)\cdot\boldsymbol{A}\left(L_n\boldsymbol{a}_n\right)&=2\pi\lambda\\ \frac{e}{\hbar}(\boldsymbol{r}_j-\boldsymbol{r}_i)\cdot\boldsymbol{A}\left(L_n\boldsymbol{a}_n\right)+(\boldsymbol{\delta}^\beta-\boldsymbol{\delta}^\alpha)\cdot\boldsymbol{A}\left(L_n\boldsymbol{a}_n\right)&=2\pi\lambda\end{aligned} \tag{1.4.10}$$

The term without the orbitals vanishes when we write A_{ij} as in eq.(1.4.8). Applying it to the previous equation, we have

$$\frac{e}{\hbar}\sum_{m,p,q}(\delta_m^\beta-\delta_m^\alpha)\boldsymbol{a}_m\cdot\boldsymbol{b}_p\frac{\phi_0 M_{pq}}{(2\pi)^2 L_q}(L_n\boldsymbol{a}_n\cdot\boldsymbol{b}_q)=2\pi\lambda$$
$$\sum_m(\delta_m^\beta-\delta_m^\alpha)M_{mn}=\lambda \tag{1.4.11}$$

Unlike in the case of the lattice vectors, $(\delta_m^\beta-\delta_m^\alpha)$ will not in general be an integer. This means that the choice of M_{mn} will have to be so that $(\delta_m^\beta-\delta_m^\alpha)M_{mn}$ is an integer. However, this is only possible if $(\delta_m^\beta-\delta_m^\alpha)$ is a rational number, which may not be the case.

In order to solve this, we make use of the Gauge freedom when writing $\boldsymbol{A}$. Adding the gradient of a function $F(\boldsymbol{r})$ to $\boldsymbol{A}$, the Peierls phase becomes

$$\frac{e}{\hbar}\varphi(\boldsymbol{r}_i^\alpha,\boldsymbol{r}_j^\beta)=(\boldsymbol{r}_j^\beta-\boldsymbol{r}_i^\alpha)\cdot\boldsymbol{A}\left(\frac{\boldsymbol{r}_i^\alpha+\boldsymbol{r}_j^\beta}{2}\right)+F(\boldsymbol{r}_j^\beta)-F(\boldsymbol{r}_i^\alpha).$$

Choosing $F(\boldsymbol{r})$ as

$$F(r_i^\alpha)=-\boldsymbol{A}(\boldsymbol{r}_i^\alpha)\cdot\boldsymbol{\delta}^\alpha \tag{1.4.12}$$

satisfies the periodic boundary conditions for any lattice. Rewriting the vector potential with this $F(\boldsymbol{r})$, the Peierls phases become

$$\frac{e}{\hbar}\varphi(\boldsymbol{r}_i^\alpha,\boldsymbol{r}_j^\beta)=(\boldsymbol{r}_j^\beta-\boldsymbol{r}_i^\alpha)\cdot\boldsymbol{A}\left(\frac{\boldsymbol{r}_i^\alpha+\boldsymbol{r}_j^\beta}{2}\right)+\boldsymbol{A}(\boldsymbol{r}_j^\beta)\cdot\boldsymbol{\delta}^\beta-\boldsymbol{A}(\boldsymbol{r}_i^\alpha)\cdot\boldsymbol{\delta}^\alpha. \tag{1.4.13}$$

This expression, with a choice of $\boldsymbol{A}$ that satisfies eq.(1.4.4), allows us to calculate the Peierls phases for any lattice, with the guarantee that the periodic boundary conditions are obeyed.

Chapter 2

Graphene

Having seen how a magnetic field is introduced in a 2D lattice, we are now ready to study the case of graphene under a constant magnetic field. First, we will make a brief introduction of the properties of graphene when no magnetic field is applied. This will be followed by the introduction of the magnetic field in the tight-binding Hamiltonian, which will lead to a system of equations for which we will obtain an approximate solution. Additionally, we will also introduce the magnetic field in a way that is much more used in the literature: minimal coupling on the approximated Hamiltonian around the Dirac points. we will compare the two methods and discuss the results they yield. The last section will consist of numerical results that will plotted against the obtained expressions, just as we did for the square lattice.

2.1 Graphene without Magnetic Field

Graphene's structure can be described by two triangular Bravais lattices displaced by a vector $\boldsymbol{\delta}$. This means that each unit cell has two atoms, which makes the problem more complex than in the case of the square lattice.

The lattice vectors of graphene and the displacement vector $\boldsymbol{\delta}$ can be chosen as:

$$\boldsymbol{a}_1 = a\,(1, 0) \tag{2.1.1}$$

$$\boldsymbol{a}_2 = \frac{a}{2}\left(1, -\sqrt{3}\right) \tag{2.1.2}$$

$$\boldsymbol{\delta} = \frac{a}{2}\left(1, -\frac{1}{\sqrt{3}}\right) \tag{2.1.3}$$

where a is the length of the lattice vectors. This lattice structure is represented in Fig. 2.1 a). The two different Bravais lattices are labeled as sublattice A and B. As for the reciprocal lattice vectors, they are obtained by the orthogonality relation with the lattice vectors, $\boldsymbol{a}_i \cdot \boldsymbol{b}_j = 2\pi\delta_{ij}$, and read

$$\boldsymbol{b}_1 = \frac{2\pi}{a}\left(1, \frac{1}{\sqrt{3}}\right) \tag{2.1.4}$$

$$\boldsymbol{b}_2 = \frac{2\pi}{a}\left(0, -\frac{2}{\sqrt{3}}\right). \tag{2.1.5}$$

The first Brillouin zone generated by these vectors is represented in Fig.2.1 b). The $\boldsymbol{k}$ vectors inside the first Brillouin zone can be written as

$$\boldsymbol{k} = k_1\boldsymbol{b}_1 + k_2\boldsymbol{b}_2 = \frac{m_1}{L}\boldsymbol{b}_1 + \frac{m_2}{L}\boldsymbol{b}_2 \tag{2.1.6}$$

where m_1 and m_2 are integers between 0 and $L-1$.

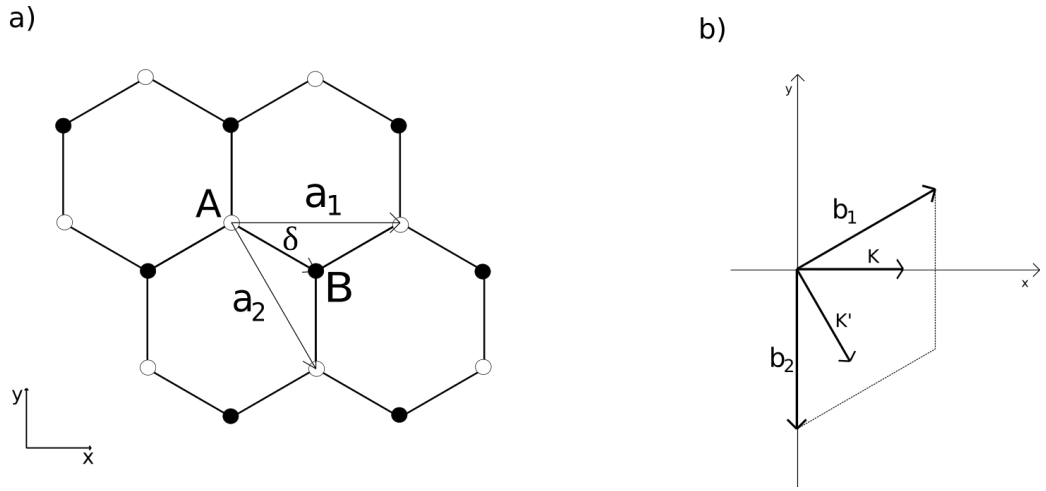

Figure 2.1: a) Graphene structure with the lattice vectors $\boldsymbol{a}_1$ and $\boldsymbol{a}_2$ and the displacement vector $\boldsymbol{\delta}$. The sublattices A (white circles) and B (black circles) are also represented. b) First Brillouin Zone of graphene, with the reciprocal lattice vectors and Dirac points $\boldsymbol{K}$ and $\boldsymbol{K'}$.

Each atom has three nearest neighbors, all of which belong to the opposite sublattice. With this choice of lattice and displacement vectors, the tight-binding Hamiltonian for this system will be [14]:

$$H = -t\sum_{m,n} a^\dagger(m,n)b(m,n) + a^\dagger(m,n)b(m-1,n) + a^\dagger(m,n)b(m,n-1) + h.c \tag{2.1.7}$$

where $a^\dagger$ and a are the creation and annihilation operators for atoms in the sublattice A, $b^\dagger$ and b for the sublattice B, and the sum is over all unit cells. Notice that each term contains the hoppings between the A atom and its neighbors (the first three terms) and the hoppings between the B atom of the same cell and its neighbors (the hermitian conjugate). Thus, by summing over all unit cells we are taking into account every atom of the lattice.

Similarly to the square lattice, graphene's Hamiltonian is invariant by translations of the lattice vectors. This allows us to write the creation operators in momentum-space (eqs.1.2.12 and 1.2.13) as

$$a^\dagger(m,n) = \frac{1}{L}\sum_{k_1,k_2} e^{-i2\pi k_1 m} e^{-i2\pi k_2 n} a^\dagger(k_1,k_2) \tag{2.1.8}$$

$$b^\dagger(m,n) = \frac{1}{L}\sum_{k_1,k_2} e^{-i\frac{2\pi}{3}(k_1+k_2)} e^{-i2\pi k_1 m} e^{-i2\pi k_2 n} b^\dagger(k_1,k_2) \tag{2.1.9}$$

where the sum on k_1 and k_2 is over the first Brillouin zone. Replacing these expressions for the operators in the Hamiltonian, we obtain

$$H = -t\sum_{k_1,k_2} e^{i\frac{2\pi}{3}(k_1+k_2)} \left(1 + e^{-i2\pi m_1} + e^{-i2\pi m_2}\right) a^\dagger(k_1,k_2)\, b(k_1,k_2) + h.c \tag{2.1.10}$$

This Hamiltonian can also be written in matrix form

$$H = \sum_{\boldsymbol{k}} \begin{pmatrix} a^\dagger(\boldsymbol{k}) & b^\dagger(\boldsymbol{k}) \end{pmatrix} H_{\boldsymbol{k}} \begin{pmatrix} a(\boldsymbol{k}) \\ b(\boldsymbol{k}) \end{pmatrix} \tag{2.1.11}$$

where

$$H_{\boldsymbol{k}} = -t \begin{pmatrix} 0 & s_{\boldsymbol{k}} \\ s_{\boldsymbol{k}}^* & 0 \end{pmatrix} \tag{2.1.12}$$

$$s_{\boldsymbol{k}} = e^{i\boldsymbol{k}\cdot\boldsymbol{\delta}} \left(1 + e^{-i2\pi k_1} + e^{-i2\pi k_2}\right). \tag{2.1.13}$$

Writing the Hamiltonian in this form, we can see that the energy values for each $\boldsymbol{k}$ will be the eigenvalues of $H_{\boldsymbol{k}}$, which are

$$E(\boldsymbol{k}) = \pm|s_{\boldsymbol{k}}| = \pm t \left[3 + 2\left(\cos\left(2\pi k_1\right) + \cos\left(2\pi k_2\right) + \cos\left(2\pi\left(k_1 - k_2\right)\right)\right)\right]^{\frac{1}{2}}. \tag{2.1.14}$$

This is the dispersion relation for graphene, which is represented in Fig.2.2. In the first Brillouin zone, this expression has two zeros

$$\boldsymbol{K} = \frac{2}{3}\boldsymbol{b}_1 + \frac{1}{3}\boldsymbol{b}_2 = \frac{2\pi}{a}\left(\frac{2}{3}, 0\right) \tag{2.1.15}$$

$$\boldsymbol{K}' = \frac{1}{3}\boldsymbol{b}_1 + \frac{2}{3}\boldsymbol{b}_2 = \frac{2\pi}{a}\left(\frac{1}{3}, -\frac{1}{\sqrt{3}}\right) \tag{2.1.16}$$

which are called Dirac points. In order to study what happens at low energies, we make a linear expansion of the dispersion relation around these Dirac points. This results in

$$E(\boldsymbol{q}) \simeq \pm v_F \hbar q \tag{2.1.17}$$

where $\boldsymbol{q}$ is the momentum relative to the Dirac points and q is its module. This is a very interesting result, as this dispersion relation has a relativistic form, where instead of the speed of light we have the Fermi velocity.

$$v_F = \frac{\sqrt{3}}{2}\frac{ta}{\hbar} \approx 10^6 m/s. \tag{2.1.18}$$

Just as we wrote the dispersion relation near the Dirac points, we can do the same for the Hamiltonian. Starting with an approximation around $\boldsymbol{q} = \boldsymbol{k} - \boldsymbol{K}$, $s_{\boldsymbol{q}}$ becomes

$$s_{\boldsymbol{q}} = e^{i(\boldsymbol{K}+\boldsymbol{q})\cdot\boldsymbol{\delta}} \left[1 + e^{-i2\pi K_1}(1 - 2\pi i q_1) + e^{-i2\pi K_2}(1 - 2\pi i q_2)\right]. \tag{2.1.19}$$

Working this expression, we obtain a simplified result

$$s_{\boldsymbol{q}} = 2\pi\left[-\frac{\sqrt{3}}{2}q_1 + i\left(\frac{q_1}{2} - q_2\right)\right] \tag{2.1.20}$$

$$= \frac{\sqrt{3}}{2}a(q_x + iq_y). \tag{2.1.21}$$

In the last step we decomposed q_1 and q_2 on its components along the coordinated axes, which brings about a simpler expression. With this, the Hamiltonian around $\boldsymbol{K}$ becomes

$$H_{\boldsymbol{q}} = -v_F \begin{pmatrix} 0 & q_x - iq_y \\ q_x + iq_y & 0 \end{pmatrix} \tag{2.1.22}$$

This expression can be written in a more compact way by introducing the Pauli matrices. Doing so,

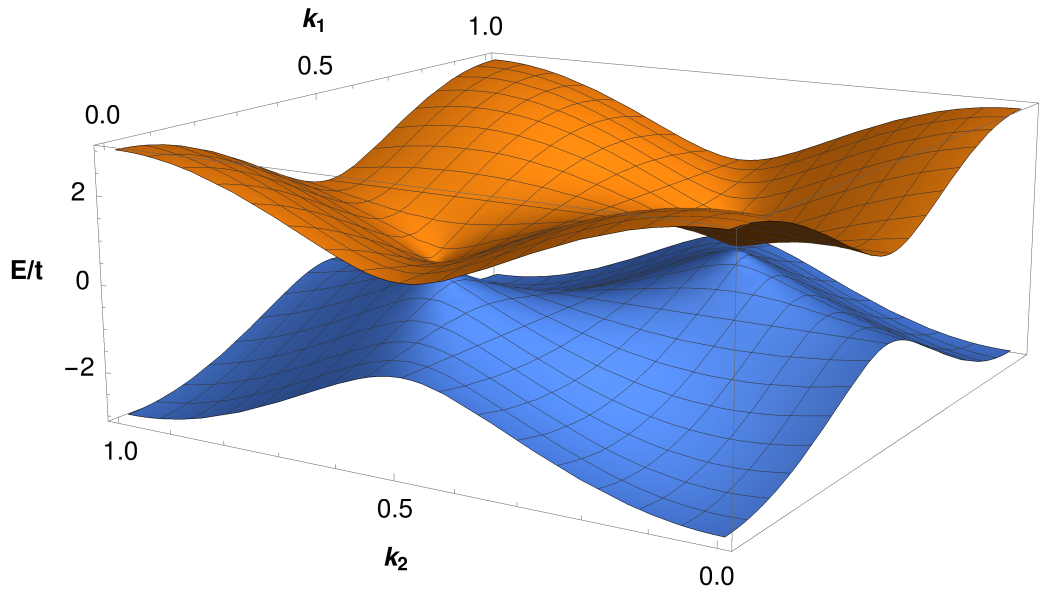

Figure 2.2: Graphene's dispersion relation as a function of k_1 and k_2. The orange part is the positive solution and the blue one the negative one. Both solutions are zero in two points - the Dirac points.

results in

$$H_{\boldsymbol{q}} = -v_F \boldsymbol{\sigma} \cdot \boldsymbol{q} \tag{2.1.23}$$

The case for the other Dirac point is entirely analogous, yielding

$$H_{\boldsymbol{q}'} = -v_F \boldsymbol{\sigma}^\dagger \cdot \boldsymbol{q}' \tag{2.1.24}$$

where $\boldsymbol{q}' = \boldsymbol{k} - \boldsymbol{K}'$.

These Hamiltonians resemble the Dirac Hamiltonian for a massless particle in 2 dimensions (hence the name Dirac points for $\boldsymbol{K}$ and $\boldsymbol{K}'$). This approximated Hamiltonian, due to being linear in the momentum, will make some calculations further ahead more simple; however, as this is a linear approximation, some phenomena may not be described by this Hamiltonian, so we have to bare in mind that this is just an approximation.

2.2 Peierls Substitution in Graphene

We will now introduce a magnetic field through Peierls substitution. For each term, we have three phases we need to calculate: $\varphi((m,n),(m,n)+\boldsymbol{\delta})$, $\varphi((m,n),(m-1,n)+\boldsymbol{\delta})$ and $\varphi((m,n),(m,n-1)+\boldsymbol{\delta})$, which we will call φ_1, φ_2 and φ_3. To determine them, we will use the results obtained in Section 1.4. Writing the potential vector as

$$\boldsymbol{A} = A_{12}\,(\boldsymbol{r} \cdot \boldsymbol{b}_2)\,\boldsymbol{b}_1 + \nabla F(\boldsymbol{r}) \tag{2.2.1}$$

where $A_{12} = \frac{\phi}{(2\pi)^2}$ and $F(\boldsymbol{r})$ is as defined in eq.(1.4.12), the phases become

$$\begin{aligned}\varphi_1 &= 0\\ \varphi_2 &= -2\pi\frac{\phi}{\phi_0}\left(\frac{\pi}{6}+n\right)\\ \varphi_3 &= 0.\end{aligned} \tag{2.2.2}$$

Due to the periodic boundary conditions, the minimum flux allowed is $\frac{\phi_0}{L}$, as seen in eq.(1.4.9).

We could now add these phases to the tight-binding Hamiltonian in order to obtain a description of graphene in a magnetic field; however, we will not utilize this gauge, but the more common Landau gauge, which is given by

$$\boldsymbol{A}(\boldsymbol{r}) = -By\hat{e}_x. \tag{2.2.3}$$

The reason for doing this is because we want to compare the results obtained through Peierls substitution in the tight-binding Hamiltonian with those usually obtained in literature through minimal coupling on eqs.(2.1.23) and (2.1.24). Denoting $\boldsymbol{A}_1(\boldsymbol{r})$ the vector potential of eq.(2.2.1) and $\boldsymbol{A}_2(\boldsymbol{r})$ the one in the Landau gauge, the gauge transformation that takes one into the other is

$$\boldsymbol{A}_2(\boldsymbol{r}) = \boldsymbol{A}_1(\boldsymbol{r}) + \nabla F'(\boldsymbol{r}) \tag{2.2.4}$$

where

$$F'(\boldsymbol{r}) = -F(\boldsymbol{r}) + \frac{\phi}{2\pi\phi_0}\left[\frac{(\boldsymbol{r}\cdot\boldsymbol{b}_2)^2}{4} - \frac{(\boldsymbol{r}\cdot\boldsymbol{b}_2)}{6} - \frac{(\boldsymbol{r}\cdot\boldsymbol{b}_1)}{3}\right]. \tag{2.2.5}$$

In this expression, the first term, $-F(\boldsymbol{r})$ cancels the same term in the initial Gauge. The second term is responsible for transforming the non-gradient part of the vector potential from being along $\boldsymbol{b}_1$, into being along $\hat{e}_x$.

The Peierls phases we obtain in the Landau gauge are

$$\varphi_1 = \pi\frac{\phi}{\phi_0}n \tag{2.2.6}$$

$$\varphi_2 = -\pi\frac{\phi}{\phi_0}n \tag{2.2.7}$$

$$\varphi_3 = 0.$$

Applying periodic conditions to these phases, we obtain a result different from the ones in eq.(2.2.2). Exemplifying for φ_1, we obtain

$$\varphi_1(n+L) - \varphi_1(n) = 2\pi M \Longrightarrow \frac{\phi}{\phi_0} = \frac{2}{L}M \tag{2.2.8}$$

where M is any integer. This the double of the value we obtained in the initial gauge. This means that, when working on the Landau gauge, we will quantize the flux according to this expression. However, we must bare in mind that when applying periodic boundary conditions on graphene with magnetic field, the minimum flux we can obtain is $\phi = \frac{\phi_0}{L}$.

2.2.1 Wavefunctions and Energy

Putting the phases obtained for the Landau gauge in the Hamiltonian, it becomes

$$H = -t\sum_{m,n} e^{i\frac{\pi\phi}{\phi_0}n}a^\dagger(m,n)b(m,n) + e^{-i\frac{\pi\phi}{\phi_0}n}a^\dagger(m,n)b(m-1,n) + a^\dagger(m,n)b(m,n-1) + h.c \quad (2.2.9)$$

As we introduced the magnetic field through a vector potential that only depends on n, the Hamiltonian still has translation symmetry along m, which allows us to write the operators as a function of k_1. Using eqs.(2.1.8) and (2.1.9), but making the expansion only for k_1, we have

$$a^\dagger(m,n) = \frac{1}{\sqrt{L}}\sum_{k_1} e^{-i2\pi k_1 m}a^\dagger(k_1,n) \quad (2.2.10)$$

$$b^\dagger(m,n) = \frac{1}{\sqrt{L}}\sum_{k_1} e^{-i\frac{2\pi}{3}k_1}e^{-i2\pi k_1 m}b^\dagger(k_1,n) \quad (2.2.11)$$

Replacing the operators in the Hamiltonian, we obtain

$$H = -t\sum_{k_1,n} e^{i\frac{2\pi}{3}k_1}\left(e^{i\frac{\pi\phi}{\phi_0}n} + e^{-i\frac{\pi\phi}{\phi_0}n}e^{-i2\pi k_1}\right)a^\dagger(k_1,n)b(k_1,n) + e^{i\frac{2\pi}{3}k_1}a^\dagger(k_1,n)b(k_1,n-1) + h.c \quad (2.2.12)$$

$$= -t\sum_{k_1,n} e^{-i\frac{\pi}{3}k_1}2\cos\left(\frac{\pi\phi}{\phi_0}n + \pi k_1\right)a^\dagger(k_1,n)b(k_1,n) + e^{i\frac{2\pi}{3}k_1}a^\dagger(k_1,n)b(k_1,n-1) + h.c \quad (2.2.13)$$

This Hamiltonian resembles the one we obtained for the square lattice, but it has one key difference: we have two sublattices, which, as will become evident, will complicate the equations we will obtain.

With an expression for the Hamiltonian, we can now study the wavefunctions and energy of this system. By applying the Hamiltonian to a general eigenstate $|\psi_\lambda\rangle$, written as

$$|\psi_\lambda\rangle = \sum_n \alpha_\lambda(k_1,n)a^\dagger(k_1,n) + \beta_\lambda(k_1,n)b^\dagger(k_1,n) \quad (2.2.14)$$

and equaling it to $E_\lambda|\psi_\lambda\rangle$, we obtain two sets of coupled equations:

$$E_\lambda\alpha_\lambda(k_1,n) = -t\left[2e^{-i\frac{\pi}{3}k_1}\cos\left(\pi\frac{\phi}{\phi_0}n - \pi k_1\right)\beta_\lambda(k_1,n) + e^{i\frac{2\pi}{3}k_1}\beta_\lambda(k_1,n-1)\right] \quad (2.2.15)$$

$$E_\lambda\beta_\lambda(k_1,n) = -t\left[2e^{i\frac{\pi}{3}k_1}\cos\left(\pi\frac{\phi}{\phi_0}n - \pi k_1\right)\alpha_\lambda(k_1,n) + e^{-i\frac{2\pi}{3}k_1}\alpha_\lambda(k_1,n+1)\right]. \quad (2.2.16)$$

Altough we cannot find an exact solution to these equations, we can try to study them for certain regimes. First, we will make a variable change in order to eliminate the complex exponentials

$$\tilde{\alpha}_\lambda(k_1,n) = e^{-i\pi k_1\left(n-\frac{1}{6}\right)}\alpha_\lambda(k_1,n) \quad (2.2.17)$$

$$\tilde{\beta}_\lambda(k_1,n) = e^{-i\pi k_1\left(n+\frac{1}{6}\right)}\beta_\lambda(k_1,n). \quad (2.2.18)$$

We can now start by studying the solutions for zero energy,

$$0 = -t\left[2\cos\left(\pi\frac{\phi}{\phi_0}n - \pi k_1\right)\tilde{\beta}_\lambda(k_1,n) + \tilde{\beta}_\lambda(k_1,n-1)\right] \quad (2.2.19)$$

$$0 = -t\left[2\cos\left(\pi\frac{\phi}{\phi_0}n - \pi k_1\right)\tilde{\alpha}_\lambda(k_1,n) + \tilde{\alpha}_\lambda(k_1,n+1)\right]. \quad (2.2.20)$$

which lead us to a recursion relation for the coefficients $\tilde{\alpha}$ and $\tilde{\beta}$. As both equations are very similar, we will only show the calculations for the first one. In this case, we obtain a recursion relation for the $\tilde{\beta}$ coefficients:

$$\tilde{\beta}_\lambda(k_1, n-1) = -2\cos\left(\pi\frac{\phi}{\phi_0}n - \pi k_1\right)\tilde{\beta}_\lambda(k_1, n). \tag{2.2.21}$$

In the limit of a very large L, we need the amplitude of the wavefunction to vary smoothly between neighboring sites. This means that the wavefunctions for zero energy will be localized around points n' such that

$$\left|2\cos\left(\pi\frac{\phi}{\phi_0}n' - \pi k_1\right)\right| = 1. \tag{2.2.22}$$

Fixing the value of k_1, we can solve this equation for n':

$$\pi\frac{\phi}{\phi_0}n' - \pi k_1 = \theta \Longrightarrow n' = \frac{\phi_0}{\pi\phi}\left(\theta + \pi k_1\right) \tag{2.2.23}$$

where θ is any angle such that $\cos(\theta) = \pm\frac{1}{2}$. Note that, as in the square lattice, the number of points n' depends on the flux. Using the definition of n', we can write eq.(2.2.21) in a more suggestive way:

$$\tilde{\beta}_\lambda(k_1, n-1) = -2\cos\left(\theta + \pi\frac{\phi}{\phi_0}(n-n')\right)\tilde{\beta}_\lambda(k_1, n). \tag{2.2.24}$$

Al tough we assured that the amplitude varies slowly, depending on the value of θ, there may be a change of the phase between neighboring sites. In the case of $\cos(\theta) = -\frac{1}{2}$, the coefficients all have the same phase; however, when $\cos(\theta) = \frac{1}{2}$, we have a phase difference of π. In order to eliminate this, we make a variable change

$$\tilde{\tilde{\beta}}_\lambda(k_1, n) = e^{i\pi n}\tilde{\beta}_\lambda(k_1, n) \tag{2.2.25}$$

which leads to

$$\tilde{\tilde{\beta}}_\lambda(k_1, n-1) = 2\cos\left(\theta + \pi\frac{\phi}{\phi_0}(n-n')\right)\tilde{\tilde{\beta}}_\lambda(k_1, n). \tag{2.2.26}$$

In this case, as $\cos(\theta) = \frac{1}{2}$, the coefficients $\tilde{\tilde{\beta}}_\lambda$ will vary slowly. These coefficients will be very similar to the $\tilde{\beta}$ in the case when $\cos(\theta) = -\frac{1}{2}$, as the only difference in the equations is a minus sign.

We saw that there are solutions whose amplitude varies slowly around certain n' points for zero energy. We can use this result as an approximation to study states with energy close to zero. Doing so, we can write eq.(2.2.19) as:

$$E_\lambda\tilde{\alpha}_\lambda(k_1, n) = -t\left[2\cos\left(\theta + \pi\frac{\phi}{\phi_0}(n-n')\right)\tilde{\beta}_\lambda(k_1, n) + \tilde{\beta}_\lambda(k_1, n-1)\right] \tag{2.2.27}$$

where $\cos(\theta) = -\frac{1}{2}$. As we have already seen that these coefficients vary slowly, we can expand them in a Taylor series up to first order:

$$\tilde{\beta}_\lambda(k_1, n-1) \approx \tilde{\beta}_\lambda(k_1, n) - \frac{d\tilde{\beta}_\lambda}{dn} \tag{2.2.28}$$

which, replacing in eq.(2.2.27), becomes

$$E_\lambda\tilde{\alpha}_\lambda(k_1, n) = -t\left[\left(2\cos\left(\theta + \pi\frac{\phi}{\phi_0}(n-n')\right) + 1\right)\tilde{\beta}_\lambda(k_1, n) - \frac{d}{dn}\tilde{\beta}_\lambda\right]. \tag{2.2.29}$$

We could uncouple both equations and try to find a solution for the coefficients. However, due to the complexity of the resulting differential equation, it is not possible. In order to transform these two

equations into solvable ones, we need to expand the co-sine around $n = n'$ (just as we did for the square lattice). Doing this, the differential equation becomes

$$E_\lambda \alpha_\lambda(k_1, n) = -t\left[\left(\pm\sqrt{3}\frac{\pi\phi}{\phi_0}(n-n')\right)\tilde{\beta}_\lambda(k_1, n) - \frac{d}{dn}\tilde{\beta}_\lambda\right]. \tag{2.2.30}$$

where the signal depends on the value of θ. Writing this and the other differential equation in matrix form, we get

$$-ta\frac{\sqrt{3}}{2}\begin{bmatrix} 0 & \mp\frac{1}{l_B^2}(y-y') - \frac{d}{dy} \\ \mp\frac{1}{l_B^2}(y-y') + \frac{d}{dy} & 0 \end{bmatrix}\begin{bmatrix} \tilde{\alpha}_\lambda(k_1, y) \\ \tilde{\beta}_\lambda(k_1, y) \end{bmatrix} = E_\lambda \begin{bmatrix} \tilde{\alpha}_\lambda(k_1, y) \\ \tilde{\beta}_\lambda(k_1, y) \end{bmatrix} \tag{2.2.31}$$

where $l_B^2 = \frac{\hbar}{eB}$ is the magnetic length we defined in the previous chapter, and the n coordinate is now written as $y = -\frac{\sqrt{3}}{2}na$. This equation can be simplified even further by defining $\tilde{y} = \frac{y-y'}{l_B}$, which results in

$$-\frac{ta}{l_B}\frac{\sqrt{3}}{2}\begin{bmatrix} 0 & \mp\tilde{y} - \frac{d}{d\tilde{y}} \\ \mp\tilde{y} + \frac{d}{d\tilde{y}} & 0 \end{bmatrix}\begin{bmatrix} \tilde{\alpha}_\lambda(\tilde{y}) \\ \tilde{\beta}_\lambda(\tilde{y}) \end{bmatrix} = E_\lambda \begin{bmatrix} \tilde{\alpha}_\lambda(\tilde{y}) \\ \tilde{\beta}_\lambda(\tilde{y}) \end{bmatrix}. \tag{2.2.32}$$

This problem can now be solved by defining the staircase operators as functions of $\tilde{y}$ and $\partial_{\tilde{y}}$, as is done in [14],

$$c = \frac{1}{\sqrt{2}}(\tilde{y} + \partial_{\tilde{y}}) \tag{2.2.33}$$

$$c^\dagger = \frac{1}{\sqrt{2}}(\tilde{y} - \partial_{\tilde{y}}) \tag{2.2.34}$$

and the coefficients α and β as quantum harmonic oscillator functions. Writing eq.(2.2.32) for $\theta = \frac{2\pi}{3}$ (for the minus sign), we obtain

$$\frac{\sqrt{2}ta}{l_B}\frac{\sqrt{3}}{2}\begin{bmatrix} 0 & c \\ c^\dagger & 0 \end{bmatrix}\begin{bmatrix} C_1\phi_\lambda(\tilde{y}) \\ C_2\phi_{\lambda'}(\tilde{y}) \end{bmatrix} = E_\lambda \begin{bmatrix} C_1\phi_\lambda(\tilde{y}) \\ C_2\phi_{\lambda'}(\tilde{y}) \end{bmatrix} \tag{2.2.35}$$

where C_1 and C_2 are normalization constants and ϕ_λ is the quantum harmonic oscillator function of the λ level. Working one of the equations that come from this system, we obtain

$$\frac{\sqrt{2}ta}{l_B}\frac{\sqrt{3}}{2}C_2\sqrt{\lambda'}\phi_{\lambda'-1}(\tilde{y}) = E_\lambda C_1\phi_\lambda(\tilde{y}) \tag{2.2.36}$$

which imposes that $\lambda = \lambda' - 1$. The other equation yields the same result. From these equations we can also take the values of the energy and a relation between the normalization constants. Writing the two equations, now with the constraint on λ', we have

$$\frac{\sqrt{2}ta}{l_B}\frac{\sqrt{3}}{2}C_2\sqrt{\lambda+1} = E_\lambda C_1 \tag{2.2.37}$$

$$\frac{\sqrt{2}ta}{l_B}\frac{\sqrt{3}}{2}C_1\sqrt{\lambda+1} = E_\lambda C_2 \tag{2.2.38}$$

which yields a condition for C_2

$$C_1^2 = C_2^2 \Longrightarrow C_1 = \pm C_2. \tag{2.2.39}$$

Replacing in eq.(2.2.37), we obtain an expression for the energy

$$E_\lambda = \pm\frac{\sqrt{2}ta}{l_B}\frac{\sqrt{3}}{2}\sqrt{\lambda+1} \tag{2.2.40}$$

where the sign depends on the values of C_1 and C_2. With this, we can write our coefficients $\tilde{\alpha}$ and $\tilde{\beta}$ as

$$\begin{bmatrix} \tilde{\alpha}_\lambda(\tilde{y}) \\ \tilde{\beta}_\lambda(\tilde{y}) \end{bmatrix} = C_1 \begin{bmatrix} \phi_\lambda(\tilde{y}) \\ \pm\phi_{\lambda+1}(\tilde{y}) \end{bmatrix} \tag{2.2.41}$$

where the plus (minus) sign represents the state associated with the positive (negative) energy in eq.(2.2.40). As for the normalization constant, it will depend on λ. As ϕ_λ is already a normalized function, for the general case, $C_1 = \frac{1}{\sqrt{2}}$. However, when $\lambda = -1$, $\phi_\lambda = 0$, which means that C_1 has to be 1.

Going back to eq.(2.2.32), we still need to analyze the case of $\theta = \frac{4\pi}{3}$ (the plus sign). This yields a similar system to the one we just solved, through which we obtain the following solutions for the coefficients

$$\begin{bmatrix} \tilde{\alpha}_\lambda(\tilde{y}) \\ \tilde{\beta}_\lambda(\tilde{y}) \end{bmatrix} = C_1 \begin{bmatrix} \phi_{\lambda+1}(\tilde{y}) \\ \pm\phi_\lambda(\tilde{y}) \end{bmatrix}. \tag{2.2.42}$$

and the energy solutions are the same.

As for the case when $\cos(\theta) = \frac{1}{2}$, the equations we obtain for $\tilde{\tilde{\beta}}(k_1, n)$ are the same as eqs.(2.2.30), where the minus sign refers to $\theta = \frac{5\pi}{3}$ and the plus sign refers to $\theta = \frac{\pi}{3}$. Thus for $\theta = \frac{\pi}{3}$, we have

$$\begin{bmatrix} \tilde{\alpha}_\lambda(\tilde{y}) \\ \tilde{\beta}_\lambda(\tilde{y}) \end{bmatrix} = e^{i\pi n} C_1 \begin{bmatrix} \phi_\lambda(\tilde{y}) \\ \pm\phi_{\lambda+1}(\tilde{y}) \end{bmatrix} \tag{2.2.43}$$

and for $\theta = \frac{5\pi}{3}$, the solution becomes

$$\begin{bmatrix} \tilde{\alpha}_\lambda(\tilde{y}) \\ \tilde{\beta}_\lambda(\tilde{y}) \end{bmatrix} = e^{i\pi n} C_1 \begin{bmatrix} \phi_{\lambda+1}(\tilde{y}) \\ \pm\phi_\lambda(\tilde{y}) \end{bmatrix}. \tag{2.2.44}$$

With these solutions, we could write the original α and β coefficients. However, we want to compare these results with numerical ones obtained through diagonalization of the tight-binding Hamiltonian. This is much easier to do if the coefficients are real, which is not the case for the α and β coefficients.

2.3 Minimal Coupling

Up until here, we worked with a tight-binding Hamiltonian where we introduced a Peierls phase, and from there worked the equations that gave us the wavefunctions. Another approach to this problem is to define the Hamiltonian in the continuum without the magnetic field, and then introduce it through the minimal coupling $\boldsymbol{p} \to \boldsymbol{p} + e\boldsymbol{A}$.

$$H_{\boldsymbol{q}} = v_F \boldsymbol{\sigma} \cdot (\boldsymbol{p} + e\boldsymbol{A}) \tag{2.3.1}$$

Writing the vector potential as $\boldsymbol{A} = B(y, 0)$, this Hamiltonian becomes

$$H_{\boldsymbol{q}} = v_F \begin{pmatrix} 0 & \hbar q_x + eyB - \hbar i q_y \\ \hbar q_x + eyB + i\hbar q_y & 0 \end{pmatrix} \tag{2.3.2}$$

Here, we chose to write the momentum in the position representation. Doing so, it becomes clear that the eigenvectors dependence on x will be just a plane wave. Thus, the eigenvectors will have the form

$$\psi_{q_x}(x,y) = e^{iq_x x}\begin{pmatrix} \phi^A(y) \\ \phi^B(y) \end{pmatrix} \tag{2.3.3}$$

Applying the Hamiltonian to this eigenvector results in

$$v_F\frac{\hbar}{l_B}\begin{pmatrix} 0 & l_B q_x + \frac{y}{l_B} - l_B\partial_y \\ l_B q_x + \frac{y}{l_B} + l_B\partial_y & 0 \end{pmatrix}\psi_{q_x}(x,y) = E\psi_{q_x}(x,y) \tag{2.3.4}$$

where we wrote the constants in terms of $l_B = \sqrt{\hbar/eB}$. Now, the procedure is essentially the same as done before: we write $\tilde{y} = l_B q_x + \frac{y}{l_B}$, identify the creation and destruction operators as functions of $\tilde{y}$ and $\partial_{\tilde{y}}$ and calculate the functions ϕ_1 and ϕ_2. Because the calculations are the same as we did in the previous section, we will skip them and write the wavefunctions

$$\psi_{q_x}(x,y) = C_\lambda e^{iq_x x}\begin{pmatrix} \phi^A_{\lambda+1}(\tilde{y}) \\ \pm\phi^B_\lambda(\tilde{y}) \end{pmatrix} \tag{2.3.5}$$

where the $\pm$ denotes that the signal of the energy of the state and C_λ is the normalization coefficient. This solution, however, is only valid on points with $q \sim 0$. The other solution, for the Hamiltonian near $\boldsymbol{K'}$ is obtained in an equivalent way:

$$\psi_{q'_x}(x,y) = C_\lambda e^{iq'_x x}\begin{pmatrix} \phi^A_\lambda(\tilde{y}) \\ \pm\phi^B_{\lambda+1}(\tilde{y}) \end{pmatrix}. \tag{2.3.6}$$

Now, we need to know if these solution correspond to the ones found in the previous section. Taking $\boldsymbol{k}$ to be the Dirac points, we obtain 4 solutions for each Dirac point. From these four solutions, one of them, centered around $n = 0$ for both Dirac points, corresponds to these ones. However, the other three solutions do not appear when we use the minimal coupling. In order to study why, we will start by going back to the tight-binding Hamiltonian.

As for the energy, the expression obtained through this method is the same as the one in eq.(2.2.40).

2.3.1 Expansion of the Peierls Phase to First Order

As the solutions we found through minimal coupling are centered on $n = 0$, we will expand the Peierls phase around it and see what results we obtain. Doing it, the tight-binding Hamiltonian becomes

$$H = H_0 - t\sum_{m,n} i\pi\frac{\phi}{\phi_0}n\left(a^\dagger(m,n)b(m,n) - a^\dagger(m,n)b(m-1,n)\right) \tag{2.3.7}$$

where H_0 is the Hamiltonian without the magnetic field. In the same way as before, we write a general eigenstate of this Hamiltonian as

$$|\psi\rangle = \sum_{m,n}\alpha(m,n)a^\dagger(m,n) + \beta(m,n)b^\dagger(m,n) \tag{2.3.8}$$

which leads to the following set of equations

$$E\alpha(m,n) = -t\left[\left(1+i\pi\frac{\phi}{\phi_0}n\right)\beta(m,n) + \left(1-i\pi\frac{\phi}{\phi_0}n\right)\beta(m-1,n) + \beta(m,n-1)\right] \tag{2.3.9}$$

$$E\beta(m,n) = -t\left[\left(1-i\pi\frac{\phi}{\phi_0}n\right)\alpha(m,n) + \left(1+i\pi\frac{\phi}{\phi_0}n\right)\alpha(m+1,n) + \alpha(m,n+1)\right] \tag{2.3.10}$$

we will make a variable change to α and β so that we may write their derivatives in momentum space as the momentum near the Dirac point

$$\alpha(m,n) = e^{i\boldsymbol{K}\cdot\boldsymbol{r}}\tilde{\alpha}(m,n) \tag{2.3.11}$$

$$\beta(m,n) = e^{i\boldsymbol{K}\cdot\boldsymbol{r}}\tilde{\beta}(m,n). \tag{2.3.12}$$

Replacing the α and β coefficients, the equations become

$$E\tilde{\alpha}(m,n) = -te^{i\boldsymbol{K}\cdot\boldsymbol{\delta}}\left[\left(1+i\pi\frac{\phi}{\phi_0}n\right)\tilde{\beta}(m,n) + \left(1-i\pi\frac{\phi}{\phi_0}n\right)e^{-i\boldsymbol{K}\cdot\boldsymbol{a}_1}\tilde{\beta}(m-1,n) + e^{-i\boldsymbol{K}\cdot\boldsymbol{a}_2}\tilde{\beta}(m,n-1)\right] \tag{2.3.13}$$

$$E\tilde{\beta}(m,n) = -te^{-i\boldsymbol{K}\cdot\boldsymbol{\delta}}\left[\left(1-i\pi\frac{\phi}{\phi_0}n\right)\tilde{\alpha}(m,n) + \left(1+i\pi\frac{\phi}{\phi_0}n\right)e^{i\boldsymbol{K}\cdot\boldsymbol{a}_1}\tilde{\alpha}(m+1,n) + e^{i\boldsymbol{K}\cdot\boldsymbol{a}_2}\tilde{\alpha}(m,n+1)\right]. \tag{2.3.14}$$

Although we cannot solve exactly this discrete model, as seen before, we can approximate the coefficients of the neighboring sites by expanding them up to first order. Expanding $\tilde{\beta}(m-1,n)$ and $\tilde{\beta}(m,n-1)$ up to first order, the right-hand side of eq.(2.3.13) becomes

$$\begin{aligned} E\tilde{\alpha}(m,n) &= -te^{i\boldsymbol{K}\cdot\boldsymbol{\delta}}\left[1+\left(1-\frac{d}{dm}\right)e^{-i\boldsymbol{K}\cdot\boldsymbol{a}_1} + \left(1-\frac{d}{dn}\right)e^{-i\boldsymbol{K}\cdot\boldsymbol{a}_2} + .\right. && (2.3.15)\\ &\quad \left. +i\pi\frac{\phi}{\phi_0}n\left(1-\left(1-\frac{d}{dm}\right)e^{-i\boldsymbol{K}\cdot\boldsymbol{a}_1}\right)\right]\tilde{\beta}(m,n). && (2.3.16)\end{aligned}$$

Let us start by considering the terms without ϕ/ϕ_0. Using the definition of the lattice vectors, we can write the derivatives in the previous equations as derivatives in order to x and y

$$\frac{d}{dm} = a\partial_x \tag{2.3.17}$$

$$\frac{d}{dn} = \frac{a}{2}\left(\partial_x - \sqrt{3}\partial_y\right). \tag{2.3.18}$$

Writing the derivatives in the momentum representation ($\partial_x = iq_x$), the terms without magnetic field are given by

$$v_F\hbar\left(q_x - iq_y\right)\tilde{\beta}(m,n) \tag{2.3.19}$$

which is the result we obtained in eq.(2.1.22), when no magnetic field is applied. This makes sense, as this term is the only one when $B = 0$. Going through the same procedure for eq.(2.3.14), we obtain a similar result

$$v_F\hbar\left(q_x + iq_y\right)\tilde{\alpha}(m,n) \tag{2.3.20}$$

which, again, agrees with the results of Section 2.1.

As for the terms multiplied by ϕ/ϕ_0, we can start by noticing that the ∂_x term is actually a second order term. This is because the $n\phi/\phi_0$ is already a first order term, so when multiplied by q_x, it

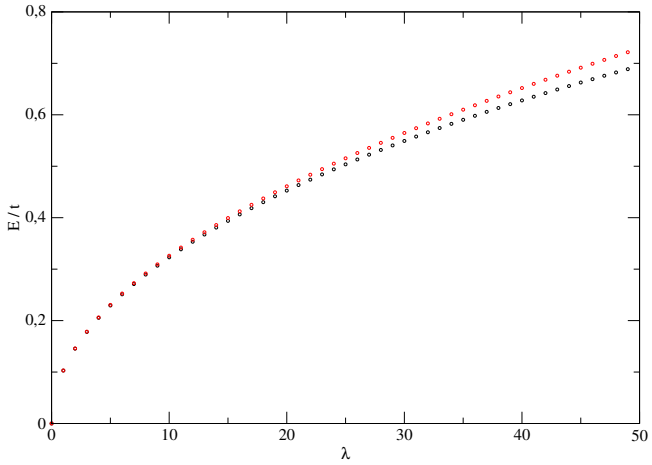

Figure 2.3: Energy levels of a periodic graphene lattice with $L = 4096$ and $\phi/\phi_0 = 1/2048$. Black dots represent the energy calculated through numerical diagonalization of the Hamiltonian in eq.(2.2.12). Red dots represent the energy calculated using eq.(2.2.40).

becomes second order. Ignoring q_x, this part of the expression becomes

$$-te^{i\boldsymbol{K}\cdot\boldsymbol{\delta}}i\pi\frac{\phi}{\phi_0}n\left(1-\left(-\frac{1}{2}+i\frac{\sqrt{3}}{2}\right)\right)\tilde{\beta}(m,n)=v_F eBy\tilde{\beta}(m,n). \tag{2.3.21}$$

Writing these results in eqs.2.3.13 and 2.3.14, we obtain

$$E\begin{pmatrix}\tilde{\alpha}(m,n)\\ \tilde{\beta}(m,n)\end{pmatrix}=\begin{pmatrix}0 & \hbar q_x+eyB-i\hbar q_y\\ \hbar q_x+eyB+i\hbar q_y & 0\end{pmatrix}\begin{pmatrix}\tilde{\alpha}(m,n)\\ \tilde{\beta}(m,n)\end{pmatrix} \tag{2.3.22}$$

which is equal to the result obtained in earlier in eq.(2.3.2). With this, it becomes clear that when we use the minimal coupling to introduce the magnetic field in graphene, what we are actually doing is expanding the Peierls phase up to first order around $n = 0$. Thus, it is only natural that the wavefunctions we find be the ones centered around $n = 0$, and that we do not find any of the other ones.

2.4 Numerical Results and Comparison

Just as in the square lattice, we will now proceed to compare the analytical expressions we obtained with the results obtained through diagonalization of the Hamiltonian in eq.(2.2.12).

2.4.1 Energy

In Fig.2.3 we plot the values of the energy obtained with eq.(2.2.40) against the ones obtained by diagonalization of the Hamiltonian. For values of the energy up to $0.3t$, the agreement between both sets is very good. From there on, the values yielded through the two methods start to diverge from one another.

We can also see how the energy varies by changing the system's parameters, as we did for the square lattice. As suggested by eq.(2.2.40), the energy spectrum does not depend on either the period of the lattice L or k_x, as can be verified by diagonalizing Ham 2.2.12 for different values of these parameters. When varying the magnetic field, we obtain the same behavior we observed in the square lattice: the spacing between energy levels increases with the magnetic field.

2.4.2 Wavefunctions

In Fig.2.4, we plot the wavefunctions for $E = 0$, $k_1 = 0$ and $\frac{\phi}{\phi_0} = \frac{2}{L}$. We see that there are four localized wavefunctions, two of which are smooth, and the other two have an oscillating phase. According to eq.(2.2.23), the smooth solutions should be centered around $n' = \frac{L}{3}, \frac{2L}{3}$ and the oscillating ones around $n' = \frac{L}{6}, \frac{5L}{6}$. Looking at the figure, we see that this is the case.

From Fig.2.4 we can also verify the relation between the $\tilde{\alpha}$ and $\tilde{\beta}$ for the smooth wavefunctions. Looking at eq.(2.2.41), we see that for the lowest energy level, $\tilde{\alpha} = 0$ and $\tilde{\beta} = \phi_0$, where this ϕ_0 refers to the harmonic oscillator wavefunction of the lowest energy and not the quantum of flux. In the graphic, we can see that $\tilde{\alpha}$ is zero around $n' = \frac{L}{3}$, and $\tilde{\beta}$ appears to have the of ϕ_0.

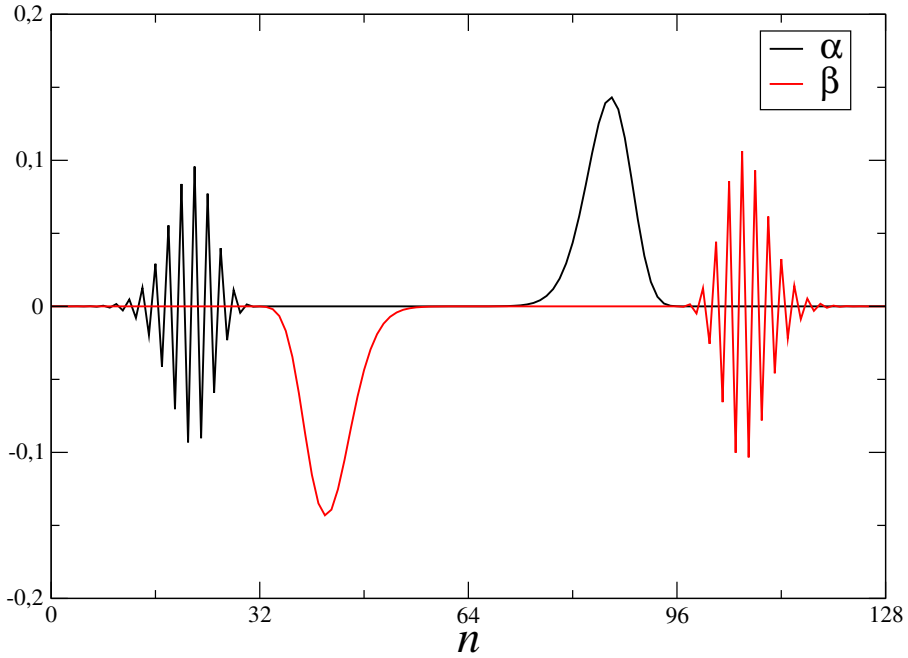

Figure 2.4: Wavefunctions for $E = 0$, $\frac{\phi}{\phi_0} = \frac{2}{L}$, $L = 128$ and $k_1 = 0$. The black and red curves represent the $\tilde{\alpha}$ and $\tilde{\beta}$ coefficients respectively.

This last point can be checked by plotting ϕ_0 against these curves, which is represented in Fig.2.5. In this figure, we plot ϕ_0 centered in $\frac{2L}{3}$ and $\frac{5L}{6}$, in addition to the module of the wavefunctions. The reason we used the module in this representation is because it is impossible to visually determine the accuracy of the fit for the fast-oscillating wavefunctions. We can see in this figure that the fit is best in the center of the curves, and that near the base, it starts to wear off. This is because, as we go away from the center, we will start entering the domain of another solution, which means that away from n', the different solutions interact, thus deforming the approximated curves whose expression we obtained.

Another aspect that we can represent is how the solutions behave for symmetric values of the energy. According to the equations we obtained for the wavefunctions, the difference between a positive and negative energy solution will be a minus sign in one of the coefficients. In Fig.2.6, we see precisely that: comparing the wavefunctions for a certain n' for both energies, one of the curves (either $\tilde{\alpha}$ or $\tilde{\beta}$) has a different sign.

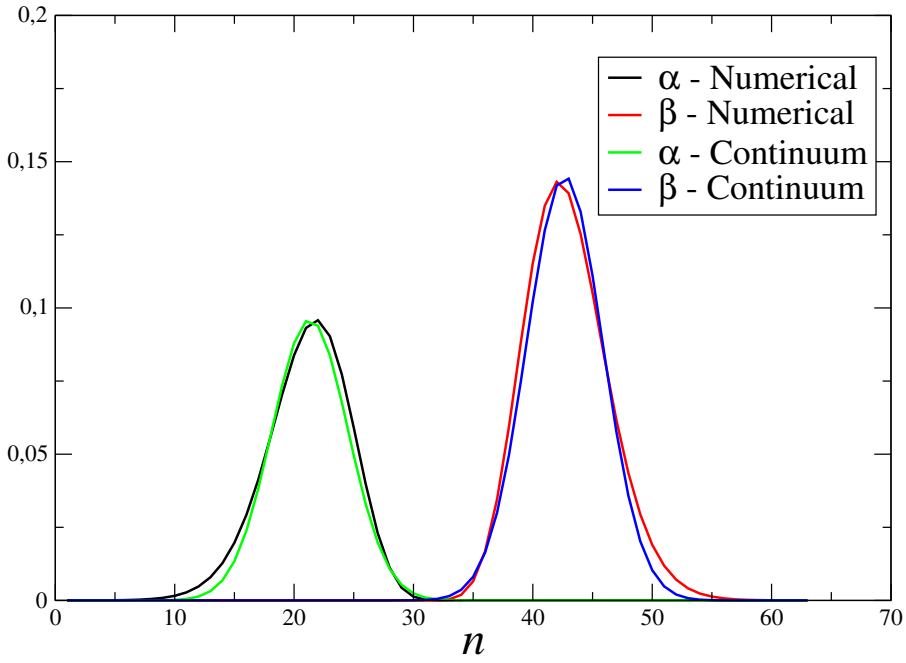

Figure 2.5: Wavefunctions for $\frac{\phi}{\phi_0} = \frac{2}{L}$, $L = 128$ and $k_1 = 0$ as function of n. Black and red curves represent the $\tilde{\alpha}$ and $\tilde{\beta}$ coefficients respectively, calculated through diagonalization of the Hamiltonian in eq.(2.2.12). The green and blue curves represent the $\tilde{\alpha}$ and $\tilde{\beta}$ coefficients calculated in the continuum approximation through eqs.(2.2.42) and (2.2.44) respectively. The wavefunctions are represented in module so it becomes easier to compare the results.

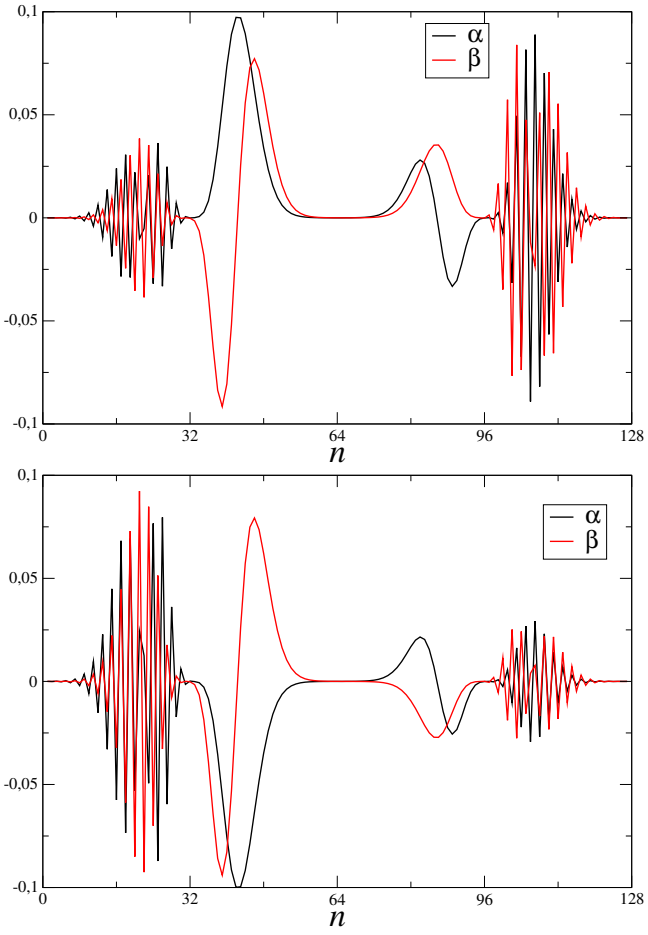

Figure 2.6: Eigenfunctions for the first non-zero energy levels. The first figure represents the wavefunctions for the positive energy and the second one for the negative energy. The other parameters remain the same ($\frac{\phi}{\phi_0} = \frac{2}{L}$, $L = 128$ and $k_1 = 0$).

Regarding the dependence on k_1, the result we obtained for graphene is the same as in the square lattice: changing k_1 will only inflict a translation upon the wavefunctions. In Fig.2.7 we represent the lowest energy wavefunctions for $k_1 = \frac{1}{3}$ which corresponds to one of the Dirac points. Using the equation for n' (eq.(2.2.23)) and using this value of k_1, we see that the values of n' will be translated by $\frac{L}{3}$. Looking at the figure, this is exactly what happens. Furthermore, as we used the k_1 of one of the Dirac points, we expect to see a smooth solution around $n' = 0$, which is also verified in Fig.2.7.

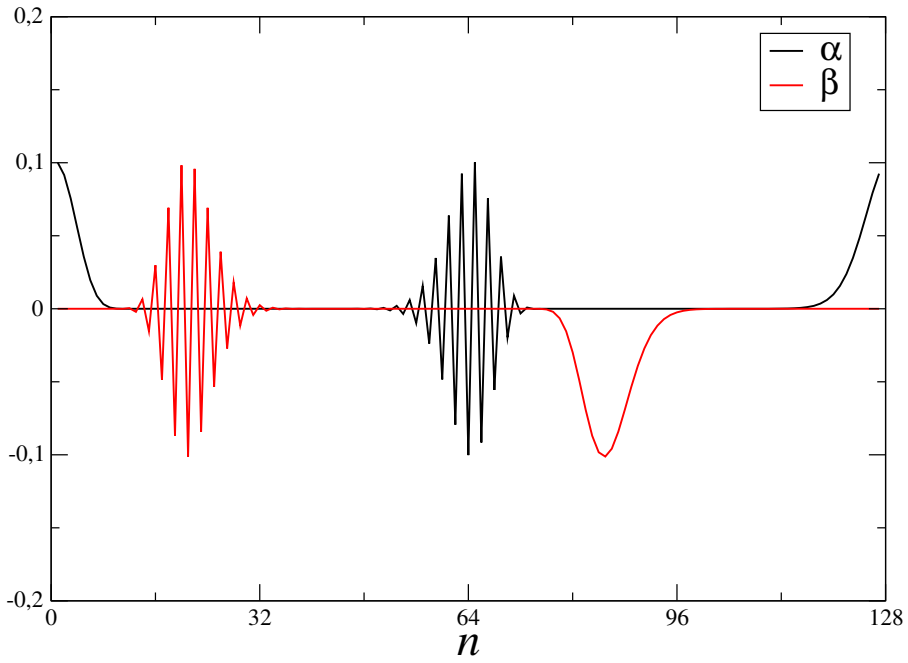

Figure 2.7: Wavefunctions for $E = 0$, $\frac{\phi}{\phi_0} = \frac{2}{L}$, $L = 128$ and $k_1 = \frac{1}{3}$

Finally, we can also vary the magnetic field and see what effects it has on the wavefunctions. In Fig.2.8 we see that the wavefunctions are the same ones we had for $\frac{\phi}{\phi_0} = \frac{2}{L}$, but duplicated. This result is the same as the one we obtained for the square lattice, where the number of points n' is directly proportional to the flux. Increasing the magnetic field also decreases the width of the wavefunctions, as was also seen for the case of the square lattice.

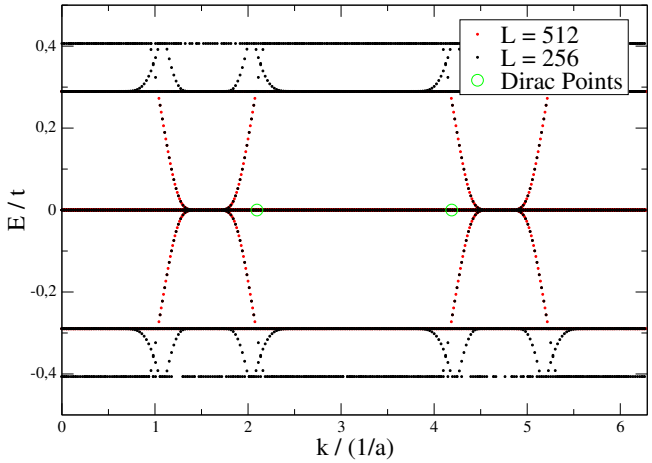

Figure 2.9: Landau Levels of graphene with open boundary conditions and $\phi/\phi_0 = 1/128$.

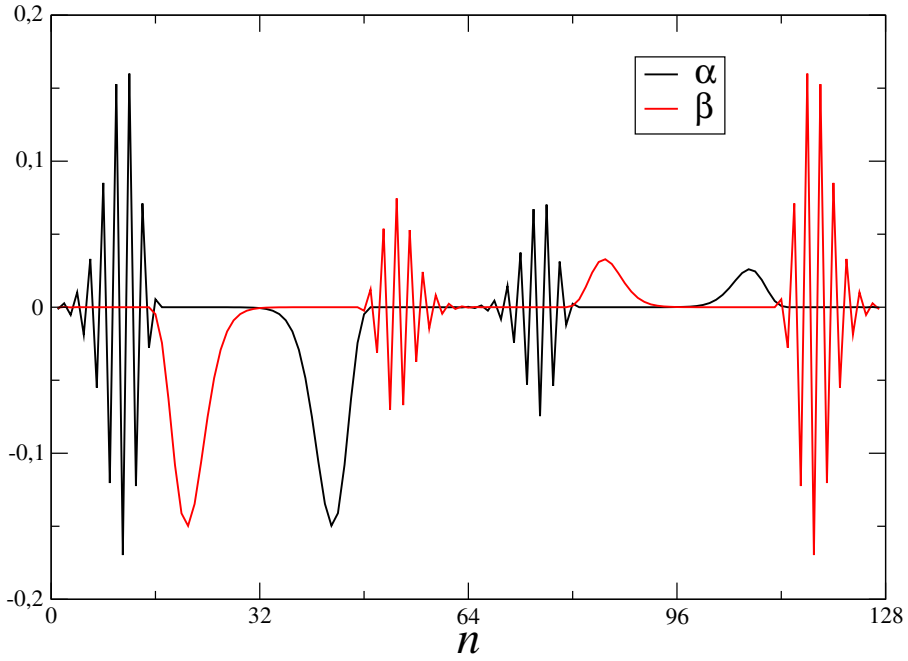

Figure 2.8: Wavefunctions for $E = 0$, $\frac{\phi}{\phi_0} = \frac{4}{L}$, $L = 128$ and $k_1 = 0$.

2.4.3 Open Boundary Conditions

We can also study the effect of open boundary conditions on graphene. We start by plotting the energy as function of k_1 in Fig.2.9. Unlike the case with periodic boundaries, here there are energy levels that depend on k_1. These levels are the ones associated with the edge states that are not present when we impose periodic boundaries on the system.

In Fig.2.10 we show the density of states for both boundaries. Just as we observed for the square lattice, as we increase the size of the graphene lattice with open boundaries, its density of states will tend to the one calculated with periodic boundary conditions. This can be seen both in the increase of the height of the peaks, and in the decrease of the amplitude of the states between peaks.

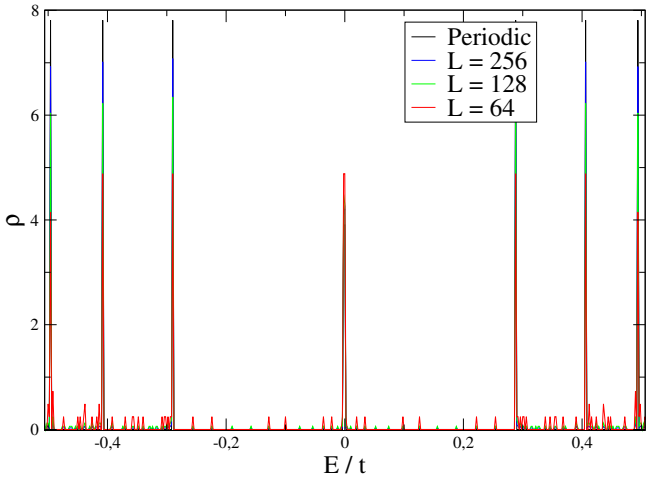

Figure 2.10: Density of states of graphene with both open and periodic boundary conditions and $\phi/\phi_0 = 1/256$

Chapter 3

General Response Theory

In this chapter, we will determine an expression for the conductivity of a crystal as a function of its Hamiltonian. In order to do so, we need to calculate the mean value of the current density $\boldsymbol{J}$, which is done using the Kubo formula. The calculations in this chapter are based on Chapters 2 and 3 of [15].

3.1 Average of an operator

The conductivity of a system can be obtained by the expression for the average of the current $\boldsymbol{J}$. With this in mind, we will arrive at an equation that yields the expected value of an operator for a system with a small time-dependent perturbation $V(t)$ to an Hamiltonian H_0 whose solutions we know. This equation is known as Kubo's formula.

The average of a fermionic operator is given by [12]

$$\langle J \rangle (t) = \sum_n f(\epsilon_n) \langle n|J|n\rangle \tag{3.1.1}$$

where the states $|n\rangle$ are the eigenstates of the Hamiltonian and $f(\epsilon_n)$ is the Fermi-Dirac distribution

$$f(\epsilon_n) = \frac{1}{1 + e^{-\beta\epsilon_n}} \tag{3.1.2}$$

Introducing the density matrix

$$\rho = \sum_n f(\epsilon_n)|n\rangle\langle n| \tag{3.1.3}$$

allows us to write eq.(3.1.1) as

$$\sum_n f(\epsilon_n) \langle n|J|n\rangle = \sum_m \langle m|J\rho|m\rangle = \mathrm{Tr}\,(\rho J)\,. \tag{3.1.4}$$

The problem with this expression is that it uses the eigenstates of the full Hamiltonian, which we do not know. In order to solve this, we want to determine the time evolution of the eigenstates of H_0.write these states as the time evolution from the eigenstates of H_0.

3.1.1 Schrödinger Picture

In quantum mechanics, the temporal evolution of a state is given by Schrödinger's equation [12]

$$i\hbar\frac{\partial}{\partial t}|\psi(t)\rangle = H|\psi(t)\rangle \tag{3.1.5}$$

We can define a time-evolution operator $\mathcal{U}(t,t_0)$ that relates a state in an instant t_0 to an instant t

$$|\psi(t)\rangle = \mathcal{U}(t,t_0)|\psi(t_0)\rangle \tag{3.1.6}$$

This operator $\mathcal{U}(t,t_0)$ can be found using Schrödinger's equation. For the case where H does not depend on time, we have

$$\mathcal{U}(t,t_0) = e^{-iH(t-t_0)/\hbar} \tag{3.1.7}$$

so, a state $|\psi(t)\rangle$ can be written as

$$|\psi(t)\rangle = e^{-iH(t-t_0)/\hbar}|\psi(t_0)\rangle \tag{3.1.8}$$

However, our Hamiltonian has a time dependence, which makes it impossible to solve its Schrödinger equation.

3.1.2 Interaction Picture

In the interaction picture, it is assumed that we can separate the Hamiltonian into two parts: a time independent Hamiltonian H_0 whose solutions we already know, and a time-dependent perturbation $V(t)$. We start by writing the definitions of the states and operators in this picture:

$$|\psi_I(t)\rangle = e^{iH_0t/\hbar}|\psi_S(t)\rangle \tag{3.1.9}$$

$$J_I(t) = e^{iH_0t/\hbar}J_S(t)e^{-iH_0t/\hbar} \tag{3.1.10}$$

where the S and I subscripts denote the Schrödinger and Interaction pictures respectively. From these expressions, we can see that the average value of an operator is left invariant.

From the Schrödinger equation, we can arrive at the equation for the time evolution of the wave-functions in the Interaction Picture:

$$\begin{aligned}
i\hbar\frac{\partial}{\partial t}|\psi_S(t)\rangle &= (H_0 + V_I(t))\,|\psi_S(t)\rangle \qquad (3.1.11)\\
i\hbar\frac{\partial}{\partial t}\left(e^{-iH_0t/\hbar}|\psi_I(t)\rangle\right) &= (H_0 + V_I(t))\left(e^{-iH_0t/\hbar}|\psi_I(t)\rangle\right)\\
H_0e^{-iH_0t/\hbar}|\psi_I(t)\rangle + i\hbar e^{-iH_0t/\hbar}\frac{\partial}{\partial t}|\psi_I(t)\rangle &= (H_0 + V_I(t))\left(e^{-iH_0t/\hbar}|\psi_I(t)\rangle\right)\\
i\hbar\frac{\partial}{\partial t}|\psi_I(t)\rangle &= V_I(t)|\psi_I(t)\rangle. \qquad (3.1.12)
\end{aligned}$$

From this equation, we can find an expression for $|\psi_I(t)\rangle$ as a function of its value at $t = t_0$ and the perturbation $V(t)$. Integrating both sides of the equation on time from t_0 to t, we obtain

$$|\psi_I(t)\rangle = |\psi_I(t_0)\rangle + \frac{1}{i\hbar}\int_{t_0}^{t} dt_1 V(t_1)|\psi_I(t_1)\rangle \tag{3.1.13}$$

We can now replace the $|\psi_I(t')\rangle$ inside the integral with the whole second member, which results in

$$|\psi_I(t)\rangle = |\psi_I\,(t_0)\rangle + \frac{1}{i\hbar}\int_{t_0}^{t} dt_1 V\,(t_1)\left(|\psi_I\,(t_0)\rangle + \frac{1}{i\hbar}\int_{t_0}^{t_1} dt_2 V\,(t_2)\,|\psi_I\,(t_2)\rangle\right). \tag{3.1.14}$$

Repeating this procedure, we obtain higher-order terms in $V(t)$, assuming this series converges

$$|\psi_I(t)\rangle = \left[1 + \frac{1}{i\hbar}\int_{t_0}^{t} dt_1 V(t_1) + \left(\frac{1}{i\hbar}\right)^2 \int_{t_0}^{t} dt_1 V(t_1) \int_{t_0}^{t_1} dt_2 V(t_2) + ...\right] |\psi_I(t_0)\rangle. \tag{3.1.15}$$

As the perturbation will be proportional to the electric field and we are interested in studying the conductivity for the lowest orders, we will truncate this sum at some order.

3.1.3 Kubo Formula

Going back to our equation for the average of an operator

$$\langle J\rangle = \mathrm{Tr}\,(\rho J) \tag{3.1.16}$$

we can write the density matrix operator in the Interaction Picture as

$$\rho_I = \sum_n f(\epsilon_n)|n_I(t)\rangle\langle n_I(t)| \tag{3.1.17}$$

$$= \sum_n f(\epsilon_n)\left(1 - \frac{1}{i\hbar}\int_{t_0}^{t} dt_1 V(t_1)\right)|n_I(t_0)\rangle\langle n_I(t_0)|\left(1 + \frac{1}{i\hbar}\int_{t_0}^{t} dt_1 V(t_1)\right) + \mathcal{O}(V^2) \tag{3.1.18}$$

where we only wrote explicitly the terms up to first order. As we will only focus on the response of first order, we will only keep these terms, ignoring all higher-order contributions. Doing so, we can write the density matrix as

$$\rho_I^{(1)} = \sum_n f(\epsilon_n)|n_I(t_0)\rangle\langle n_I(t_0)| - f(\epsilon_n)\frac{1}{i\hbar}\int_{t_0}^{t} dt_1 V(t_1)\,|n_I(t_0)\rangle\langle n_I(t_0)| \tag{3.1.19}$$

$$+ f(\epsilon_n)|n_I(t_0)\rangle\langle n_I(t_0)|\frac{1}{i\hbar}\int_{t_0}^{t} dt_1 V(t_1) \tag{3.1.20}$$

where the first term is the density matrix for H_0, which we will call ρ_0. Replacing this in the expression for the average of an operator

$$\mathrm{Tr}\,(\rho_I J_I) = \mathrm{Tr}\left[\rho_0 J_I(t) + \frac{1}{i\hbar}\int_{t_0}^{t} dt_1 \left(V(t_1)\rho_0 - \rho_0 V(t_1)\right) J_I(t)\right]. \tag{3.1.21}$$

Due to cyclic property of the trace, the second term in the above expression can be written as

$$\mathrm{Tr}\left[\left(V(t_1)\rho_0 - \rho_0 V(t_1)\right) J_I(t)\right] = \mathrm{Tr}\left[\rho_0\left[J_I(t), V(t_1)\right]\right]. \tag{3.1.22}$$

With this, we finally arrive at the Kubo Formula for first-order:

$$\langle J\rangle(t) = \langle J_I(t)\rangle_0 + \frac{1}{i\hbar}\int_{t_0}^{t} dt_1 \langle[J_I(t), V(t_1)]\rangle_0. \tag{3.1.23}$$

where the subscript zero denotes that the average is done in respect with ρ_0 instead of $\rho_I(t)$. Now, we only need an expression for the $V(t)$ and $J_I(t)$ so we can get to an expression for the conductivity.

3.2 Current Density and Conductivity

The relation between a current density $\boldsymbol{J}$ and a constant electric field $\boldsymbol{E}$ is often introduced in the form of Ohm's Law:

$$\boldsymbol{J} = \sigma \boldsymbol{E} \tag{3.2.1}$$

where the factor σ that relates them is called conductivity. The conductivity is a response function that relates an applied electric field at a certain point in time and space $(\boldsymbol{r}', t')$ to the current density at $(\boldsymbol{r}, t)$. For a constant field, this conductivity does not depend on any coordinates, but the same cannot be said for fields that are not constant. In this case, Ohm's Law takes a more general form [16]:

$$\boldsymbol{J}(\boldsymbol{r}, t) = \int d\boldsymbol{r}' dt' \sigma(\boldsymbol{r} - \boldsymbol{r}', t - t') \boldsymbol{E}(\boldsymbol{r}', t'). \tag{3.2.2}$$

From here on, we are going to focus on electrical fields that are uniform in space, so we can drop the spatial dependence. For simple systems this description is enough, but in general, the conductivity behaves as a tensor. This leads to an expression for the conductivity with higher-order terms in the electric field:

$$J_\alpha(t) = \int dt_1 \sigma_{\alpha\beta}(t - t_1) E_\beta(t_1) + \int dt_1 dt_2 \sigma_{\alpha\beta\gamma}(t - t_1, t - t_2) E_\beta(t_1) E_\gamma(t_2) + ... \tag{3.2.3}$$

This is the general form of the current density. We can see that there is not one conductivity tensor, but an infinity of them, due to the higher-order terms.

In general, it is more useful to write the conductivity as a function of frequency, rather than time. This is done by taking the Fourier transform in both members of eq.(3.2.3). Applying this to the linear term, we have

$$\int_{-\infty}^{+\infty} dt e^{i\omega t} J_\alpha^{(1)}(t) = \int_{-\infty}^{+\infty} dt e^{i\omega t} \int_{-\infty}^{+\infty} dt_1 \int_{-\infty}^{+\infty} \frac{d\omega'}{2\pi} e^{-i\omega'(t-t_1)} \sigma_{\alpha\beta}(\omega') \int_{-\infty}^{+\infty} \frac{d\omega''}{2\pi} e^{-i\omega'' t_1} E_\beta(\omega'') \tag{3.2.4}$$

As the only dependences in t and t_1 are in the exponentials, we can perform the integrations in time, yielding

$$J_\alpha^{(1)}(\omega) = \int_{-\infty}^{+\infty} \frac{d\omega'}{2\pi} 2\pi \delta(\omega - \omega') \sigma_{\alpha\beta}(\omega') \int_{-\infty}^{+\infty} \frac{d\omega''}{2\pi} 2\pi \delta(\omega' - \omega'') E_\beta(\omega'') \tag{3.2.5}$$

We can now use the second delta function to eliminate the integral in ω'', which leads to the general expression for the first order term

$$J_\alpha^{(1)}(\omega) = \int_{-\infty}^{+\infty} \frac{d\omega'}{2\pi} 2\pi \delta(\omega - \omega') \sigma_{\alpha\beta}(\omega') E_\beta(\omega'). \tag{3.2.6}$$

We could simplify this expression even further because of the delta that remains, but in order to see the similarities with higher-order terms, this expression will be kept in this form.

The calculations for higher-order terms are done in the same way as for first-order, resulting in the following expression for the n^{th} order term

$$J_{\alpha}^{(n)}(\omega) = \int \frac{d\omega_1}{2\pi} ... \frac{d\omega_n}{2\pi} 2\pi\delta\left(\omega - \omega_1 - ... - \omega_n\right) \sigma_{\alpha\alpha_1...\alpha_n}\left(\omega_1, ..., \omega_n\right) E_{\alpha_1}\left(\omega_1\right) ... E_{\alpha_n}\left(\omega_n\right) \tag{3.2.7}$$

where the coefficient $\sigma_{\alpha\alpha_1...\alpha_n}\left(\omega_1, ..., \omega_n\right)$ is the n^{th} order conductivity. These are the objects we ultimately want to calculate, although in this work we will settle for the lowest order ones.

3.3 Time-dependent Electric Field in the Tight-Binding Hamiltonian

From classical electrodynamics we know that we can write $\boldsymbol{E}$ and $\boldsymbol{B}$ in terms of a scalar and vector potential:

$$\boldsymbol{E}(\boldsymbol{r}, t) = -\nabla\phi(\boldsymbol{r}, t) - \frac{\partial \boldsymbol{A}(\boldsymbol{r}, t)}{\partial t} \tag{3.3.1}$$

$$\boldsymbol{B}(\boldsymbol{r}, t) = \nabla \times \boldsymbol{A}(\boldsymbol{r}, t). \tag{3.3.2}$$

As mentioned before, we will consider an electric field that is spatially uniform. Such a field can be obtained by a scalar potential that is linear in space

$$\boldsymbol{E} = -\nabla\phi(\boldsymbol{r}, t), \quad \boldsymbol{A}(\boldsymbol{r}, t) = \boldsymbol{0} \tag{3.3.3}$$

by a spatially uniform vector potential

$$\boldsymbol{E} = -\tfrac{\partial \boldsymbol{A}(t)}{\partial t}, \quad \phi(\boldsymbol{r}, t) = \phi(t) \ . \tag{3.3.4}$$

or by a linear combination of both. Usually, only one potential is used to describe the electric field, as it simplifies the calculations. In this work, the scalar potential description will be called length gauge, while the vector potential description will be called velocity gauge.

3.3.1 Length Gauge

A scalar potential is added to the Hamiltonian as [12]

$$H_{\boldsymbol{E}} = H_0 - e\phi(\boldsymbol{r}, t) \tag{3.3.5}$$

where e is the electron charge and $H_{\boldsymbol{E}}$ is the Hamiltonian in the length gauge. Writing ϕ in terms of the electric field, the Hamiltonian in this gauge becomes

$$H_{\boldsymbol{E}} = H_0 + e\boldsymbol{E}(t) \cdot \boldsymbol{r}. \tag{3.3.6}$$

This Hamiltonian can describe an open system imbued in an electric field, but the linear dependence on $\boldsymbol{r}$ renders it unable to describe a system with periodic boundaries. Knowing this, we will see whether we can use the Hamiltonian on the velocity gauge to study such systems.

3.3.2 Velocity Gauge

We will build the Hamiltonian in velocity gauge from the length gauge one. Starting from the fact that the velocity gauge Hamiltonian must obey the Schrödinger equation

$$i\hbar\frac{\partial|\psi_{\boldsymbol{A}}\rangle}{\partial t} = H_{\boldsymbol{A}}(t)|\psi_{\boldsymbol{A}}\rangle \tag{3.3.7}$$

we multiply both sides of the equation by a unitary operator $\mathcal{U}(t) = e^{i\alpha(\boldsymbol{r},t)}$:

$$i\hbar\mathcal{U}(\boldsymbol{r},t)\frac{\partial|\psi_{\boldsymbol{A}}\rangle}{\partial t} = \mathcal{U}(\boldsymbol{r},t)H_{\boldsymbol{A}}(t)|\psi_{\boldsymbol{A}}\rangle \tag{3.3.8}$$

$$i\hbar\frac{\partial}{\partial t}\left(\mathcal{U}(\boldsymbol{r},t)|\psi_{\boldsymbol{A}}\rangle\right) = \mathcal{U}(\boldsymbol{r},t)H_{\boldsymbol{A}}(t)\mathcal{U}^{\dagger}(\boldsymbol{r},t)\mathcal{U}(\boldsymbol{r},t)|\psi_{\boldsymbol{A}}\rangle - \hbar\frac{\partial\alpha(\boldsymbol{r},t)}{\partial t}\mathcal{U}(\boldsymbol{r},t)|\psi_{\boldsymbol{A}}\rangle. \tag{3.3.9}$$

Making the following identifications

$$H_{\boldsymbol{A}} = \mathcal{U}^{\dagger}(\boldsymbol{r},t)H_0\mathcal{U}(\boldsymbol{r},t) \tag{3.3.10}$$

$$|\psi_{\boldsymbol{A}}\rangle = \mathcal{U}^{\dagger}(\boldsymbol{r},t)|\psi_{\boldsymbol{E}}\rangle \tag{3.3.11}$$

$$\alpha(\boldsymbol{r},t) = i\frac{e}{\hbar}\boldsymbol{A}(t)\cdot\boldsymbol{r} \tag{3.3.12}$$

we see that eq.(3.3.9) becomes the Schrödinger equation for the length gauge. Thus, these identifications are the Hamiltonian and the wave functions for the velocity gauge. Translating this into the tight-binding Hamiltonian:

$$H_{\boldsymbol{A}} = e^{-i\frac{e}{\hbar}\boldsymbol{A}(t)\cdot\boldsymbol{r}}\left(-\sum_{i,j}t_{ij}|i\rangle\langle j|\right)e^{i\frac{e}{\hbar}\boldsymbol{A}(t)\cdot\boldsymbol{r}} = -\sum_{i,j}t_{ij}e^{i\frac{e}{\hbar}\boldsymbol{A}(t)\cdot(\boldsymbol{r}_j-\boldsymbol{r}_i)}|i\rangle\langle j| \tag{3.3.13}$$

where $|i\rangle$ is the occupation state in position basis. The introduction of this phase is the Peierls substitution. We now have our Hamiltonian written in the velocity gauge, which, as seen in previous chapters, can describe a system with periodic boundaries due to the periodicity of the complex exponential.

3.4 Current Density Operator

The current is obtained from the Hamiltonian from the variational principle [15]

$$J_\alpha = -\frac{1}{V}\frac{dH_{\boldsymbol{A}}(t)}{dA_\alpha} \tag{3.4.1}$$

where V is the volume of the system. In order to separate the contributions at various orders, we expand the Peierls phase, obtaining

$$H_{\boldsymbol{A}} = \sum_{i,j}t\left(\boldsymbol{r}_i,\boldsymbol{r}_j\right)e^{i\frac{e}{\hbar}\boldsymbol{A}(t)\cdot(\boldsymbol{r}_j-\boldsymbol{r}_i)}|i\rangle\langle j| \tag{3.4.2}$$

$$= \sum_{i,j}t\left(\boldsymbol{r}_i,\boldsymbol{r}_j\right)\left(1 + i\frac{e}{\hbar}\boldsymbol{A}(t)\cdot(\boldsymbol{r}_j-\boldsymbol{r}_i) + \left(i\frac{e}{\hbar}\boldsymbol{A}(t)\cdot(\boldsymbol{r}_j-\boldsymbol{r}_i)\right)^2 + ...\right)|i\rangle\langle j|$$

$$= H_0 + \sum_{i,j}t\left(\boldsymbol{r}_i,\boldsymbol{r}_j\right)\left(i\frac{e}{\hbar}\boldsymbol{A}(t)\cdot(\boldsymbol{r}_j-\boldsymbol{r}_i) + \left(i\frac{e}{\hbar}\boldsymbol{A}(t)\cdot(\boldsymbol{r}_j-\boldsymbol{r}_i)\right)^2 + ...\right)|i\rangle\langle j| \tag{3.4.3}$$

where in the last step we separated the non-perturbed Hamiltonian H_0 from the perturbation $V(t)$. As H_0 does not depend on $\boldsymbol{A}(t)$, the current is just

$$J^{\alpha} = -\frac{1}{V}\frac{\delta V(t)}{\delta A^{\alpha}}. \tag{3.4.4}$$

which, applied to eq.(3.4.3), yields

$$J^{\alpha}(t) = -\frac{1}{V}\sum_{i,j}\left(ev_{ij}^{\alpha} + e^2 v_{ij}^{\alpha\beta}A^{\beta}(t) + ...\right)|i\rangle\langle j| \tag{3.4.5}$$

where the n^{th} order coefficient v_{ij} is written as

$$v_{ij}^{\alpha\alpha_1...\alpha_n} = \left(\frac{i}{\hbar}\right)^{n+1} t\left(\boldsymbol{r}_i, \boldsymbol{r}_j\right)\left(r_j^{\alpha} - r_i^{\alpha}\right)\left(r_j^{\alpha_1} - r_i^{\alpha_1}\right)...\left(r_j^{\alpha_n} - r_i^{\alpha_n}\right). \tag{3.4.6}$$

These coefficients can be written in as commutators of H_0 and the position operator. In order to do so, let us start by writing the hopping integral as

$$t\left(\boldsymbol{r}_i, \boldsymbol{r}_j\right) = \langle i|H_0|j\rangle. \tag{3.4.7}$$

Note that we can also write a position vector as the action of the position operator on a state

$$\boldsymbol{r}_i|i\rangle = \hat{\boldsymbol{r}}|i\rangle. \tag{3.4.8}$$

With this, we can take the coefficient of the first-order term in eq.(3.4.5) and write it as

$$v_{ij}^{\alpha} = \frac{i}{\hbar}\langle i|H_0|j\rangle\left(r_j^{\alpha} - r_i^{\alpha}\right) = \frac{i}{\hbar}\langle i|H_0 r^{\alpha}|j\rangle - \langle i|r^{\alpha}H_0|j\rangle \tag{3.4.9}$$

$$= \frac{i}{\hbar}\langle i|\left[H_0, r^{\alpha}\right]|j\rangle = \frac{i}{\hbar}\left[H_0, r^{\alpha}\right]_{i,j} \tag{3.4.10}$$

where we use v_{ij}^{α}. Going to second order, we have

$$\left(i\frac{e}{\hbar}\right)^2 t\left(\boldsymbol{r}_i, \boldsymbol{r}_j\right)\left(r_j^{\alpha} - r_i^{\alpha}\right)\left(r_j^{\beta} - r_i^{\beta}\right) = \left(i\frac{e}{\hbar}\right)^2\langle i|\left[H_0, r^{\alpha}\right]|j\rangle\left(r_j^{\beta} - r_i^{\beta}\right) \tag{3.4.11}$$

$$= \left(i\frac{e}{\hbar}\right)^2\langle i|\left[\left[H_0, r^{\alpha}\right], r^{\beta}\right]|j\rangle$$

$$= \left(i\frac{e}{\hbar}\right)^2\left[\left[H_0, r^{\alpha}\right], r^{\beta}\right]_{i,j}. \tag{3.4.12}$$

With these two results, we can write the n^{th} order coefficient as

$$v_{ij}^{\alpha\alpha_1...\alpha_n} = \left(\frac{i}{\hbar}\right)^{n+1}\left[\left[\left[\left[H_0, r^{\alpha}\right], r^{\alpha_1}\right], ..., r^{\alpha_n}\right]\right]_{ij}. \tag{3.4.13}$$

Using the expression for $J^{\alpha}(t)$, we can write it in the Interaction picture as

$$J_I^{\alpha}(t) = e^{\frac{itH_0}{\hbar}}J^{\alpha}(t)e^{-\frac{itH_0}{\hbar}}. \tag{3.4.14}$$

Writing the current in a many-particle basis, this expression becomes

$$J_I^{\alpha}(t) = -\frac{1}{V}\sum_{i,j}\left(ev_{ij}^{\alpha} + e^2 v_{ij}^{\alpha\beta}A^{\beta}(t) + ...\right)c_i^{\dagger}(t)c_j(t) \tag{3.4.15}$$

where $c_i^\dagger(t)$ and $c_j(t)$ are the creation and annihilation operators in the interaction picture.

Finally, we can replace this expression in Kubo formula and arrive at an expression for the average of the current:

$$\langle J^\alpha \rangle (t) = -\frac{1}{V}\sum_{i,j} \left\langle c_i^\dagger(t) c_j(t) \right\rangle_0 \left(e v_{ij}^\alpha + e^2 v_{ij}^{\alpha\beta} A^\beta(t) \right) \tag{3.4.16}$$

$$- \frac{ie^2}{V\hbar}\sum_{i,j,k,l} v_{ij}^\alpha v_{kl}^\beta \int_{t_0}^t dt_1 \left\langle \left[c_i^\dagger(t) c_j(t), c_k^\dagger(t_1) c_l(t_1) \right] \right\rangle_0 A^\beta(t_1). \tag{3.4.17}$$

This expression for the average of $\boldsymbol{J}$ depends only on the commutators of H_0 with the position operator and the average of the creation and annihilation operators in the interaction picture.

There is, however, one problem with this expression: the creation and annihilation operators are expressed in position basis when we only know how to calculate their averages in the eigenbasis. To solve this, we will rewrite transform the sums over position states into sums in eigenstates. Looking at the first term, we can write it as

$$-\frac{e}{V}\sum_{i,j} \left\langle c_i^\dagger(t) c_j(t) \right\rangle_0 v_{ij}^\alpha = -\frac{e}{V} \left\langle \sum_{i,j} G_{ji}(t) v_{ij}^\alpha \right\rangle_0 \tag{3.4.18}$$

where we defined the operator $G_{ji}(t)$ as $c_i^\dagger(t) c_j(t)$. This sum can be written as the trace of the operators

$$\sum_{ij} G_{ji}(t) v_{ij}^\alpha = \mathrm{Tr}\left[G(t) v^\alpha \right] \tag{3.4.19}$$

which means that they can be written in any basis. In particular, we will write them in the eigenbasis:

$$\sum_{i,j} G_{ji}(t) v_{ij}^\alpha = \sum_{m,n} G_{nm}(t) v_{mn}^\alpha \tag{3.4.20}$$

where the labels m and n denote states in the eigenbasis. The same procedure can be made for all the other operators in eq.(3.4.17). Using the results that are obtained in Appendix A for the averages of creation and annihilation operators

$$\langle c_m^\dagger(t_1) c_n(t_2) \rangle_0 = \delta_{mn} f(\epsilon_m) e^{\frac{i}{\hbar}\epsilon_m (t_1 - t_2)} \tag{3.4.21}$$

$$\left\langle \left[c_m^\dagger(t) c_n(t), c_p^\dagger(t_1) c_q(t_1) \right] \right\rangle_0 = \delta_{np}\delta_{mq} (f(\epsilon_m) - f(\epsilon_n)) e^{\frac{i}{\hbar}(\epsilon_m - \epsilon_n)(t - t_1)} \tag{3.4.22}$$

the expression for the average of the current becomes

$$\langle J^\alpha \rangle (t) = -\frac{1}{V}\sum_m f(\epsilon_m) \left(e v_{mm}^\alpha + e^2 v_{mm}^{\alpha\beta} A^\beta(t) \right)$$

$$- \frac{ie^2}{V\hbar}\sum_{m,n} v_{mn}^\alpha v_{nm}^\beta (f(\epsilon_m) - f(\epsilon_n)) \int_{t_0}^t dt_1 e^{\frac{i}{\hbar}(\epsilon_m - \epsilon_n)(t - t_1)} A^\beta(t_1). \tag{3.4.23}$$

3.5 First-order Conductivity

With an expression for the average of the current, we can now proceed to calculate the conductivity. For the zero-order term of eq.(3.4.23)

$$\left\langle J_\alpha^{(0)} \right\rangle (t) = -\frac{e}{V}\sum_m f(\epsilon_m) v_{mm}^\alpha \tag{3.5.1}$$

we can expand v_{mm}^α, obtaining

$$v_{mm}^\alpha = \frac{i}{\hbar}\left[H_0, r^\alpha\right]_{m,m} = \frac{i}{\hbar}\langle m|H_0 r^\alpha - r^\alpha H_0|m\rangle = \frac{i}{\hbar}\epsilon_m(\langle m|r^\alpha|m\rangle - \langle m|r^\alpha|m\rangle) = 0 \tag{3.5.2}$$

This manipulation is only valid for a system with open boundaries. For periodic boundaries, we identify the operator $\boldsymbol{r}$ with the covariant derivative [17]. Due to time inversion symmetry, v_{ii}^α also becomes zero. This result makes sense, as the zero-order term represents the average of the current when no electric field is applied, which should be zero.

For the first-order conductivity, we start by writing the average of the current in the space of frequencies, as mentioned in Section 3.2. Applying $\int dt e^{i\omega t}$ to both terms of eq.(3.4.23), we obtain

$$J_\alpha^{(1)}(\omega) = \int_{-\infty}^{+\infty} dt e^{i\omega t}\left[\frac{e^2}{V}\sum_m f(\epsilon_m) v_{mm}^{\alpha\beta} A^\beta(t)\right. . \tag{3.5.3}$$

$$\left. + \frac{ie^2}{V\hbar}\sum_{m\neq n} v_{mn}^\alpha v_{nm}^\beta (f(\epsilon_m) - f(\epsilon_n)) \int_{t_0}^t dt_1 e^{\frac{i}{\hbar}(\epsilon_m - \epsilon_n)(t-t_1)} A^\beta(t_1)\right] \tag{3.5.4}$$

In the second sum, we wrote that the sum is for $m \neq n$. This is because, as $v_{mm}^\alpha = 0$, in the case of $m = n$, the result would be zero. The first term can be written as

$$\begin{aligned}\frac{e^2}{V}\sum_m f(\epsilon_m) v_{mm}^{\alpha\beta}\int_{-\infty}^{+\infty} dt e^{i\omega t} A^\beta(t) &= \frac{e^2}{V}\sum_m f(\epsilon_m) v_{mm}^{\alpha\beta} A^\beta(\omega) \\ &= \frac{e^2}{V}\sum_m f(\epsilon_m) v_{mm}^{\alpha\beta}\int_{-\infty}^{+\infty}\frac{d\omega'}{2\pi} 2\pi\delta(\omega-\omega') A^\beta(\omega')\end{aligned} \tag{3.5.5}$$

where in the last step we wrote the expression in the same form as in eq.(3.2.6). As for the second term, the calculations become more complicated. Looking only at the terms that depend on t or t_1, we can write it as

$$\int_{-\infty}^{+\infty} dt \int_{t_0}^t dt_1 e^{i\omega t} e^{\frac{i}{\hbar}\omega_{mn}(t-t_1)} A^\beta(t_1) \tag{3.5.6}$$

where we wrote $(\epsilon_i - \epsilon_j)/\hbar$ as ω_{mn}. Expanding $A^\beta(t_1)$ in a Fourier series, this expression becomes

$$\int_{-\infty}^{+\infty}\frac{d\omega'}{2\pi}\int_{-\infty}^{+\infty} dt \int_{t_0}^t dt_1 e^{i(\omega+\omega_{mn})t} e^{-i(\omega'+\omega_{mn})t_1} A^\beta(\omega'). \tag{3.5.7}$$

The major difficulty in this expression comes from the limits of the integral in t_1. In Appendix B, we use the integral representation of the Heaviside function to solve these integrals, which yield

$$\int_{-\infty}^{+\infty} dt \int_{-\infty}^t dt_1 e^{i(\omega+\omega_{mn})t} e^{-i(\omega'+\omega_{mn})t_1} = \frac{2\pi i\delta(\omega-\omega')}{\omega+\omega_{mn}+i0^+} \tag{3.5.8}$$

we can write the first-order term of the average of the current as

$$J_\alpha^{(1)}(\omega) = \int_{-\infty}^{+\infty} \frac{d\omega'}{2\pi} 2\pi\delta(\omega-\omega') \left[\frac{e^2}{V} \sum_m f(\epsilon_m) v_{mm}^{\alpha\beta} - \frac{e^2}{V\hbar} \sum_{m\neq n} v_{mn}^{\alpha} v_{nm}^{\beta} \frac{(f(\epsilon_m) - f(\epsilon_n))}{\omega + \omega_{mn} + i0^+} \right] A^\beta(\omega'). \quad (3.5.9)$$

In order to obtain the conductivity, we only need to replace $A^\beta(\omega')$ by the corresponding electric field. Eq.(3.3.4) gives a relation between $\boldsymbol{A}(t)$ and $\boldsymbol{E}(t)$ which we can use to determine their relation in the frequency space. Taking the Fourier transform of both terms of eq.(3.3.4), we get

$$\boldsymbol{E}(\omega) = i\omega \boldsymbol{A}(\omega). \quad (3.5.10)$$

Using this result in eq.(3.5.9), we obtain

$$J_\alpha^{(1)}(\omega) = \int_{-\infty}^{+\infty} \frac{d\omega'}{2\pi} 2\pi\delta(\omega-\omega') \left[-\frac{ie^2}{V\omega'} \sum_m f(\epsilon_m) v_{mm}^{\alpha\beta} + \frac{ie^2}{V\hbar\omega'} \sum_{m\neq n} v_{mn}^{\alpha} v_{nm}^{\beta} \frac{(f(\epsilon_m) - f(\epsilon_n))}{\omega' + \omega_{mn} + i0^+} \right] E^\beta(\omega') \quad (3.5.11)$$

From this expression, we can write the conductivity as

$$\sigma^{\alpha\beta}(\omega') = \frac{ie^2}{V\omega'} \left[-\sum_m f(\epsilon_m) v_{mm}^{\alpha\beta} + \frac{1}{\hbar} \sum_{m\neq n} v_{mn}^{\alpha} v_{nm}^{\beta} \frac{(f(\epsilon_m) - f(\epsilon_n))}{\omega' + \omega_{mn} + i0^+} \right]. \quad (3.5.12)$$

As we have not made any assumptions about H_0, this expression is valid for any crystal.

Chapter 4

Transport in Graphene

Having obtained the wavefunctions of graphene under a constant magnetic field in Chapter 2, and a general expression for the first-order conductivity in Chapter 3, we will now calculate graphene's linear conductivity. After reaching an expression for it, we will compare it with numerical results obtained using the KITE software, which uses the Kernel Polynomial Method (KPM) to efficiently calculate transport coefficients. As such, a brief introduction to KPM and an example for the calculation of the density of states will be presented.

4.1 Conductivity in the Length Gauge

The expression we obtained for the conductivity is written in the velocity gauge. However, when using an approximated Hamiltonian H_0, the length gauge yields better results. As such, we will write the conductivity in the length gauge. As mentioned before, this is only valid for systems with open boundary conditions, where the $\boldsymbol{r}$ operator is well-defined. Expanding $v^{\alpha\beta}_{mm}$ in the expression for the conductivity (eq.(3.5.12))

$$-\frac{ie^2}{V\omega}\sum_m f(\epsilon_i)v^{\alpha\beta}_{mm} = -\frac{ie^2}{V\omega}\sum_m f(\epsilon_m)\frac{i}{\hbar}\left[v^\alpha, r^\beta\right]_{mm} = \frac{e^2}{V\omega\hbar}\sum_{m\neq n} v^\alpha_{mn}r^\beta_{nm}\left(f(\epsilon_m)-f(\epsilon_n)\right). \tag{4.1.1}$$

and $v^\alpha_{mn}v^\beta_{nm}$ as

$$\begin{aligned}\frac{ie^2}{V\hbar\omega}\sum_{m\neq n} v^\alpha_{mn}v^\beta_{nm}\frac{(f(\epsilon_m)-f(\epsilon_n))}{\omega+\omega_{mn}+i0^+} &= \frac{ie^2}{V\hbar\omega}\sum_{m\neq n} v^\alpha_{mn}\frac{i}{\hbar}\left(\epsilon_m-\epsilon_n\right)r^\beta_{nm}\frac{(f(\epsilon_m)-f(\epsilon_n))}{\omega+\omega_{mn}+i0^+}\\ &= \frac{e^2}{V\hbar\omega}\sum_{m\neq n} v^\alpha_{mn}\left(\omega_{mn}+\omega'+i0^+-\omega'-i0^+\right)r^\beta_{nm}\frac{(f(\epsilon_m)-f(\epsilon_n))}{\omega+\omega_{mn}+i0^+}\\ &= \frac{e^2}{V\hbar\omega}\sum_{m\neq n} v^\alpha_{mn}r^\beta_{nm}(f(\epsilon_m)-f(\epsilon_n)) - \frac{e^2}{\hbar}\sum_{m,n} v^\alpha_{mn}r^\beta_{nm}\frac{(f(\epsilon_m)-f(\epsilon_n))}{\omega+\omega_{mn}+i0^+}.\end{aligned}$$

The first term of this expression cancels with the one obtained in eq.(4.1.1), leaving only

$$\sigma^{\alpha\beta}(\omega) = -\frac{e^2}{V\hbar}\sum_{m\neq n} v^\alpha_{mn}r^\beta_{nm}\frac{(f(\epsilon_m)-f(\epsilon_n))}{\omega+\omega_{mn}+i0^+}. \tag{4.1.2}$$

This is the conductivity in the length gauge for a system with open boundary conditions.

4.2 Equivalence Between Gauges for Periodic Boundaries

For periodic boundaries, we cannot handle the position operator as we do for open boundaries; instead, we define it as

$$r^{\alpha}_{mn} = i(\delta_{mn}\frac{\partial}{\partial k^{\alpha}} - i\boldsymbol{\xi}^{\alpha}_{mn}) \tag{4.2.1}$$

where ξ^{α}_{mn} is the Berry connection, defined as

$$\xi^{\alpha}_{mn} = i\langle m|\frac{\partial}{\partial k^{\alpha}}|n\rangle. \tag{4.2.2}$$

Using this definition of $\boldsymbol{r}$, we can write the $r^{\beta}_{nm}(f(\epsilon_m) - f(\epsilon_n))$ term in eq.(4.1.2) as

$$r^{\beta}_{nm}(f(\epsilon_m) - f(\epsilon_n)) = \left[r^{\beta}, \rho_0\right]_{nm} = i\left[\delta_{mn}\frac{\partial}{\partial k^{\beta}}f(\epsilon_n) - i\xi^{\beta}_{knm}(f(\epsilon_m) - f(\epsilon_n))\right] \tag{4.2.3}$$

The commutation relations we used in this calculation are written in eq.(34) of reference [17]. Furthermore, using eq.(28) of the same reference, we can write v^{α}_{mn} as

$$v^{\alpha}_{mn} = -\frac{i}{\hbar}\left[r^{\alpha}, H_0\right]_{mn} = \frac{1}{\hbar}\left[\delta_{mn}\frac{\partial\epsilon_m}{\partial k_{\alpha}} - i\xi^{\alpha}_{kmn}(\epsilon_n - \epsilon_m)\right]. \tag{4.2.4}$$

Joining these two expression in eq.(4.1.2), the equation we obtain for the first-order conductivity is

$$\sigma^{\alpha\beta}(\omega) = -\frac{ie^2}{V\hbar^2}\left[\sum_m \frac{1}{\omega}\frac{\partial\epsilon_m}{\partial k_{\alpha}}\frac{\partial\epsilon_n}{\partial k_{\beta}}\frac{\partial f(\epsilon_n)}{\partial\epsilon_n} - \sum_{m,n}\xi^{\alpha}_{mn}(\epsilon_n - \epsilon_m)\frac{\xi^{\beta}_{nm}(f(\epsilon_m) - f(\epsilon_n))}{\omega + \omega_{mn} + i0^+}\right]. \tag{4.2.5}$$

The first term in this expression is called the intra band term, and the second one the inter band term. This expression is the same as eq.(89) of [17], where the first-order response of a crystal in length gauge for periodic boundary conditions is studied. This means that eq.(4.1.2) can also be applied to systems with periodic boundary conditions.

4.3 Graphene's Conductivity

With this expression, we only need to calculate v^{α}_{mn} and r^{α}_{mn}. In order to determine these quantities we will use the Dirac Hamiltonian of eq.(2.3.1) as H_0, in similarity to what is done in [2]. Doing so, we obtain for v^{α}_{mn}

$$v^{\alpha}_{mn} = \frac{i}{\hbar}v_F\left[\boldsymbol{\sigma}\cdot(\boldsymbol{p} + e\boldsymbol{A}(\boldsymbol{r})), r^{\alpha}\right]_{mn} \tag{4.3.1}$$

where $\boldsymbol{\sigma} = \sigma^x\hat{e}_x + \sigma^y\hat{e}_y$ and σ^x and σ^y are the Pauli matrices, such that

$$\sigma^x\hat{e}_x + \sigma^y\hat{e}_y = \begin{pmatrix} 0 & \hat{e}_x - i\hat{e}_y \\ \hat{e}_x + i\hat{e}_y & 0 \end{pmatrix}. \tag{4.3.2}$$

As $\boldsymbol{A}(\boldsymbol{r})$ is a function of $\boldsymbol{r}$, their commutator is zero. This leaves only the term in $\boldsymbol{p}$, whose commutator with $\boldsymbol{r}$ is

$$\left[p^{\alpha}, r^{\beta}\right] = -i\hbar\delta_{\alpha\beta}.$$

Using this in the expression for v^{α}_{mn}, it becomes

$$v^{\alpha}_{mn} = \frac{i}{\hbar}v_F\left[\boldsymbol{\sigma}\cdot\boldsymbol{p}, r^{\alpha}\right]_{mn} = v_F\sigma^{\alpha}_{mn}. \tag{4.3.3}$$

As for the value of r^{α}_{mn}, we start by expanding v^{α}_{mn}

$$v^{\alpha}_{mn} = \frac{i}{\hbar}\left[H_0, r^{\alpha}\right]_{mn} = \frac{i}{\hbar}\left(\epsilon_m - \epsilon_n\right) r^{\alpha}_{mn}. \tag{4.3.4}$$

Equaling this to the result we obtained in eq.(4.3.3), we get

$$r^{\alpha}_{mn} = \frac{-iv_F}{\omega_{mn}}\sigma^{\alpha}_{mn}.$$

Replacing these results in eq.(4.1.2), we get an expression for the conductivity

$$\sigma^{\alpha\beta}(\omega) = -\frac{ie^2}{V\hbar}\sum_{m\neq n}\frac{v_F^2}{\omega_{mn}}\sigma^{\alpha}_{mn}\sigma^{\beta}_{nm}\frac{(f(\epsilon_m) - f(\epsilon_n))}{\omega + \omega_{mn} + i0^+}$$

where the σ^{α}_{mn} and σ^{β}_{nm} are not to be confused with the conductivity.

4.3.1 Calculation of $\sigma^{xx}(\omega)$

All that is left is to calculate are the σ^{α}_{mn} objects. A state with energy ϵ_m is written as

$$\psi_{m,k_x,n'}(x,y) = e^{-ik_x x}\begin{pmatrix}\alpha_m(k_x, y, n')\\ \beta_m(k_x, y, n')\end{pmatrix}$$

as determined in Chapter 2. Thus, we can write $\boldsymbol{\sigma}_{mn}$ as

$$\boldsymbol{\sigma}_{mn} = N\sum_{k_x,k_x'}\int_{-\infty}^{+\infty} dxdy\psi^{\dagger}_{m,k_x,n'}(x,y)\boldsymbol{\sigma}\psi_{n,k_x',n'}(x,y)$$

where N is the number of states with energy ϵ_m. Notice that the n' for both ψ is the same. As the wavefunctions are centered around n', if its value were to be different for both ψ, there would be no region where both wavefunctions were non-zero. As such n' has to take the same value for the integral to be non-zero. Furthermore, the expression we will obtain for σ^{α}_{mn} will be the same for any n', i.e., for any of the solutions found in Chapter 2. Being so, we will only present the calculations for one of the solutions obtained.

Writing $\psi_{m,k_x,n'}(x,y)$ as

$$\psi_{m,k_x,n'}(x,y) = C_m e^{-ik_x x}\begin{pmatrix}sgn(m)\phi_{|m|-1}(\tilde{y})\\ \phi_{|m|}(\tilde{y})\end{pmatrix} \tag{4.3.5}$$

$\boldsymbol{\sigma}_{mn}$ becomes

$$NC_mC_n\int_{-\infty}^{+\infty} dxdye^{-ix(k_x-k_x')}\begin{pmatrix}\frac{m}{|m|} & \phi_{|m|-1}(\tilde{y}'), & \phi_{|m|}(\tilde{y}')\end{pmatrix}\begin{pmatrix}0 & \hat{e}_x + i\hat{e}_y\\ \hat{e}_x - i\hat{e}_y & 0\end{pmatrix}\begin{pmatrix}\frac{n}{|n|}\phi_{|n|-1}(\tilde{y})\\ \phi_{|n|}(\tilde{y})\end{pmatrix}.$$

Notice that the arguments $\tilde{y}$ are different for both wavefunctions, as they depend on k_x. Starting by solving the integral in x, we get

$$\int_{-\infty}^{+\infty} dxe^{-ix(k_x-k_x')} = L\delta(k_x - k_x')$$

leaving us with

$$LNC_mC_n\delta(k_x-k'_x)\left[sgn(m)(\hat{e}_x+i\hat{e}_y)\int_{-\infty}^{+\infty}dy\phi_{|m|-1}(\tilde{y})\phi_{|n|}(\tilde{y})\right.$$
$$\left.+sgn(n)\,(\hat{e}_x-i\hat{e}_y)\int_{-\infty}^{\infty}dy\phi_{|m|}(\tilde{y})\phi_{|n|-1}(\tilde{y})\right].$$

The remaining integral can be solved using the orthogonality relations of the ϕ_m functions

$$\int_{-\infty}^{+\infty}dy\phi_m(\tilde{y})\phi_n(\tilde{y})=\delta_{mn}$$

which lead to

$$\boldsymbol{\sigma}_{mn}=LNC_mC_n\left[sgn(m)(\hat{e}_x+i\hat{e}_y)\delta_{|m|-1,|n|}+sgn(n)\,(\hat{e}_x-i\hat{e}_y)\,\delta_{|m|,|n|-1}\right]. \tag{4.3.6}$$

As for the number of solutions N, we have already seen that they increase linearly with L. Knowing that for $\frac{\phi}{\phi_0}=\frac{2}{L}$ we have four solutions, we can write the total number of solutions N as

$$N=2\frac{\phi}{\phi_0}L.$$

Using these results to calculate $\sigma^{xx}(\omega)$, we obtain

$$\sigma^{xx}(\omega)=-2\frac{\phi}{\phi_0}L^2\frac{ie^2}{V\hbar}\sum_{m\neq n}\frac{(C_mC_n)^2\,v_F^2}{\omega_{mn}}\frac{(f(\epsilon_m)-f(\epsilon_n))}{\omega+\omega_{mn}+i0^+}$$
$$\cdot\left(sgn(m)\delta_{|m|-1,|n|}+sgn(n)\delta_{|m|,|n|-1}\right)\left(sgn(n)\delta_{|n|-1,|m|}+sgn(m)\delta_{|n|,|m|-1}\right) \tag{4.3.7}$$

Simplifying the terms with the deltas and writing the volume of the system as $L^2\frac{\sqrt{3}}{2}a^2$, we obtain

$$\sigma^{xx}(\omega)=-\frac{2}{\pi l_B^2}\frac{ie^2}{\hbar}\sum_{m\neq n}\frac{(C_mC_n)^2\,v_F^2}{\omega_{mn}}\frac{(f(\epsilon_m)-f(\epsilon_n))}{\omega+\omega_{mn}+i0^+}\left(\delta_{|m|-1,|n|}+\delta_{|m|,|n|-1}\right). \tag{4.3.8}$$

For $\sigma^{xy}(\omega)$ the result is very similar:

$$\sigma^{xy}(\omega)=\frac{2}{\pi l_B^2}\frac{e^2}{\hbar}\sum_{m\neq n}\frac{(C_mC_n)^2\,v_F^2}{\omega_{mn}}\frac{(f(\epsilon_m)-f(\epsilon_n))}{\omega+\omega_{mn}+i0^+}\left(\delta_{|m|-1,|n|}-\delta_{|m|,|n|-1}\right). \tag{4.3.9}$$

These expressions coincide with the ones that have already been derived in literature, such as in [18].

These are the expressions we will use in the comparisons with numerical results.

4.4 Kernel Polynomial Method - KPM

The Kernel Polynomial Method (KPM) is a numerical method that allows to efficiently calculate quantities that are written as a trace of operators. This is done by expanding all functions of operators in Chebyshev polynomials, whose recursion relations make it much faster to calculate said quantities. The introduction made here is based on [15].

4.4.1 Chebyshev Polynomials

The Chebyshev polynomial of n^{th} order is defined as

$$T_n(x) = \cos(n \arccos(x))$$

First of all, this means both the argument is defined in the interval $]-1, 1[$. This is important, because usually the arguments of the functions we want to use are not in this range, so a scaling will be needed in order to apply this method. Second, the Chebyshev polynomials obey the following recursion relation

$$T_{n+1}(x) = 2xT_n(x) - T_{n-1}$$

which can be easily proved from its definition, replacing x by $\cos(\theta)$:

$$\begin{aligned} T_{n+1}(\cos(\theta)) &= \cos((n+1)\theta) = \cos(n\theta)\cos(\theta) - \sin(n\theta)\sin(\theta) \\ &= 2\cos(\theta)\cos(n\theta) - \cos(\theta)\cos(n\theta) - \sin(\theta)\sin(n\theta) \\ &= 2\cos(\theta)T_n(\cos(\theta)) - [\cos(-\theta)\cos(n\theta) - \sin(-\theta)\sin(n\theta)] \\ &= 2\cos(\theta)T_n(\cos(\theta)) - T_{n-1}(\cos(\theta)) \end{aligned}$$

Taking the first two polynomials form their definition,

$$\begin{aligned} T_0(x) &= 1 \\ T_1(x) &= x \end{aligned}$$

we can now obtain any polynomial from just these two.

These polynomials also satisfy an orthogonality relation:

$$\int_{-1}^{1} \frac{dx}{\pi\sqrt{1-x^2}} T_m(x)T_n(x) = \frac{1+\delta_{n0}}{2}\delta_{mn}$$

4.4.2 Expansion of a function in a series of Chebyshev Polynomials

Any function $f :]-1, 1[\to \mathbb{R}$ can be expressed in a series of Chebyshev polynomials:

$$f(x) = \sum_{n=0}^{\infty} a_n T_n(x)$$

The coefficients a_n can be determined using the orthogonality relation:

$$\int_{-1}^{1} \frac{dx}{\pi\sqrt{1-x^2}} T_n(x)f(x) = a_n \frac{1+\delta_{n0}}{2} \Rightarrow a_n = \frac{2}{1+\delta_{n0}} \int_{-1}^{1} \frac{dx}{\pi\sqrt{1-x^2}} T_n(x)f(x)$$

As an example, let us apply this to a function that appears in the expression for the density of states: the Dirac Delta.

$$\delta(x-\epsilon) = \sum_{n=0}^{\infty} a_n(\epsilon)T_n(x)$$

The coefficients $a_n(\epsilon)$ are given by:

$$a_n(\epsilon) = \frac{2}{1+\delta_{n0}} \int_{-1}^{1} \frac{dx}{\pi\sqrt{1-x^2}} T_n(x)\delta(x-\epsilon) = \frac{2}{1+\delta_{n0}} \frac{T_n(\epsilon)}{\pi\sqrt{1-\epsilon^2}}$$

We can thus write the Dirac-delta as:

$$\delta(x-\epsilon) = \frac{1}{\pi\sqrt{1-\epsilon^2}} \left[1 + 2\sum_{n=1}^{\infty} T_n(\epsilon)T_n(x)\right]$$

Another important point that we have to take care of is that the functions that can be expanded in Chebyshev polynomials have to have their arguments in the interval $]-1,1[$. As the functions we are expanding depend on the Hamiltonian, we need to define the action of a function of the Hamiltonian. For a eigenket of the Hamiltonian $|n\rangle$ with eigenvalue ϵ_n, we can write:

$$f(H)|n\rangle = f(\epsilon_n)|n\rangle$$

This means that for rescaling the Hamiltonian, what we have to take into account are its eigenvalues. Thus, the new Hamiltonian and energy become

$$\tilde{H} = (H-b)/\lambda$$
$$\tilde{E} = (E-b)\lambda$$

with $b = (E_{max} + E_{min})/2$ and $\lambda = (E_{max} - E_{min})/(2+\epsilon)$. The ϵ is an arbitrarily small value, and is in the definition of λ to ensure that the arguments do not fall in the boundaries of the interval $]-1,1[$. Let us now apply this to the density of states:

$$\rho(\epsilon) = \frac{1}{V}\sum_n \delta(\epsilon-\epsilon_n) = \frac{1}{V}\mathrm{Tr}\left[\delta(\epsilon-H)\right] = \frac{1}{V}\mathrm{Tr}[\delta(\lambda(\tilde{\epsilon}-\tilde{H}))] == \frac{1}{\lambda V}\sum_n a_n(\tilde{\epsilon})\mathrm{Tr}[T_n(\tilde{H})]$$

with the $a_n(\epsilon)$ coefficients determined earlier. As we can see, this expression is formally the same as the original one, the only difference being the additional λ factor in the denominator.

For other functions, such as the conductivity, other quantities that depend on the energy, such as the frequency, chemical potential and temperature, also have to be rescaled; however, the resulting expression will always be formally identical to the original one.

4.4.3 Evaluation of Traces

Although for the density of states, we only need to calculate the trace of the Chebyshev polynomials, in the general case, we have to calculate the trace of the product of operators and Chebyshev polynomials, such as:

$$\mathrm{Tr}\left[v^{\alpha} i g^{R}\left(\frac{\epsilon}{\hbar}+\omega\right) v^{\beta}\delta(\epsilon-H)\right] \tag{4.4.1}$$

where g^R is the retarded Green function. Although this may look time-consuming at first, using the Chebyshev polynomials' recursion relation, it becomes a very fast process. Let us start by analyzing the simple case with just one operator and a Chebyshev polynomial. Taking $|\phi\rangle$ and $|\psi\rangle$ to be arbitrary states, we can write the general element we have to calculate as:

$$\mu_n^{\psi\phi} = \langle\psi\,|AT_n(H)|\,\phi\rangle = \langle\psi_A|\phi_n\rangle$$

Here, $|\phi_n\rangle = 2H|\phi_{n-1}\rangle - |\phi_{n-2}\rangle$, so we can recursively calculate the next μ_n just by knowing the previous ones. This saves a lot of time, because if we did not have these recurrence relation, for every μ_n we would have to calculate explicitly the corresponding polynomial, which would take a lot more time.

When there is more than one Chebyshev polynomial, such as in eq.(4.4.1), the procedure we apply is the following: we define our object,

$$\mu_{nm}^{\psi\phi} = \langle\psi\,|AT_n(H)BT_m(H)|\,\phi\rangle$$

and now we fix a value of m, for which μ_{nm} becomes $\langle\psi\,|AT_n(H)|\,\phi_m^B\rangle$. Now this is just like the previous case, where we can recursively obtain all $T_n(H)|\phi_m^B\rangle$. After obtaining these values for all n and fixed m, we increase m, obtaining $|\phi_{m+1}\rangle$ by recursion and repeat the same procedure again for all n, and so on for all values of m. For objects which have more than two Chebyshev polynomials, the procedure is analogous.

Finally, we just need to calculate the trace. In order to do that, let us start by considering a random vector defined as

$$|r\rangle = \sum_{i=0}^{D-1} \xi_{ir}|\phi_i\rangle$$

where $\{|\phi_i\rangle\}$ is a basis of the system, D is the number of states of the system and ξ_{ri} is a complex random variable with the following properties:

$$\begin{aligned}\langle\xi_{ri}\rangle &= 0\\ \langle\xi_{r'i}\xi_{rj}\rangle &= 0\\ \langle\xi^*_{r'i}\xi_{rj}\rangle &= \delta_{r'r}\delta_{ij}.\end{aligned}$$

We can write the object $\langle r\,|A|\,r\rangle$ as

$$\langle r\,|A|\,r\rangle = \sum_{ij}\xi^*_{ri}\xi_{rj}A_{ij}$$

and calculating its average, using the properties we imposed to ξ_{ri}, we get

$$\langle\langle r\,|A|\,r\rangle\rangle = \sum_{ij}\langle\xi^*_{r'i}\xi_{rj}\rangle\,A_{ij} = \sum_i A_{ii} = \mathrm{Tr}\,[A]\,.$$

This means that with a random distribution with the properties mentioned above, we can calculate the trace of operators from random vectors. There is, however, a question that arises from this method: how good of an approximation is this method? As this result is only valid on average, there is bound to be some error from the actual quantity, so we need to quantify that. We can do that by defining the average over R realizations:

$$\Theta = \frac{1}{R}\sum_{r=0}^{D-1}\langle r\,|A|\,r\rangle$$

The variation around the average is given by $(\delta\Theta)^2 = \left\langle \Theta^2 \right\rangle - \left\langle \Theta \right\rangle^2$, whose expression is:

$$(\delta\Theta)^2 = \frac{1}{R}\left[\mathrm{Tr}\left(A^2\right) + \left(\left\langle |\xi_{ri}|^4 \right\rangle - 2\right)\sum_{i=0}^{D-1} A_{ii}^2\right]$$

The first thing that stands out is that the variation depends on the random distribution chosen, which means that we want to chose one that minimizes the variation. The minimum value for the $\left\langle |\xi_{ri}|^4 \right\rangle$ is 1, and can be demonstrated as follows. Let $x = |\xi_{ri}|$. Now, taking the variance of x^2, we get:

$$\left\langle \left(x^2 - \left\langle x^2 \right\rangle\right)^2 \right\rangle = \left\langle x^4 - 2x^2\left\langle x^2 \right\rangle + \left\langle x^2 \right\rangle^2 \right\rangle = \left\langle x^4 \right\rangle - \left\langle x^2 \right\rangle^2$$

As we already know that $\left\langle x^2 \right\rangle$ is 1 from the established properties of the distribution, added to the fact that the variance is cannot be negative, we have that $\left\langle x^4 \right\rangle \geq 1$. This leads to the smallest variance possible being:

$$(\delta\Theta)^2_{min} = \frac{1}{R}\left[\mathrm{Tr}\left[A^2\right] - \sum_{i=0}^{D-1} A_{ii}\right]$$

which would be exactly zero in the basis in which A is diagonal. However, it is due to the difficulty of finding such a basis that we are taking this procedure.

4.4.4 Kernels

When approximating a function with a finite number of Chebyshev polynomials, as it will happen when running numerical simulations, there will be some oscillations near points where the function is not continuous. A way to improve the approximation [15] is by introducing a new coefficient w_n (weight function) in every term of the expansion such that the oscillations are reduced. A constraint for this w_n is that as $N \to \infty$:

$$f_{KPM}(x) = \frac{1}{\pi}\frac{1}{\sqrt{1-x^2}}\sum_{n=0}^{N} w_n a_n T_n(x) \to f(x)$$

so that in this limit we get our initial function. With this weight function defined, we can introduce the Kernel function:

$$K_N(x,y) = \sum_{n=0}^{N-1}\frac{2}{1+\delta_{n0}} w_n T_n(x)\frac{T_n(y)}{\pi\sqrt{1-y^2}}$$

The kernel gives us a mapping between the function that we are trying to approximate and approximated function:

$$f_{KPM}(x) = \int_{-1}^{1} K_N(x,y) f(y) dy$$

From the various kernels that can be used, the most common ones are listed below:

4.4.4.1 Dirichlet Kernel

The Dirichlet kernel is obtained with $w_n^D = 1$ and is equivalent to the truncation of the series without a weight function. This kernel remains a good approximation as long as the function $f(x)$ does not

contain any discontinuities.

4.4.4.2 Fejér Kernel

The Fejér kernel can be obtained from the Dirichlet kernel in the following way:

$$K_N^F(x,y) = \frac{1}{N}\sum_{n=0}^{N} K_n^D(x,y)$$

which results in the coefficients

$$w_n^F = 1 - \frac{n}{N}$$

This kernel has the advantage of lowering the weight of higher-order coefficients of the Chebyshev expansion, which are the ones responsible for oscillations near discontinuities. With these features, this kernel is more appropriated for functions with discontinuities than the Dirichlet kernel.

4.4.4.3 Jackson Kernel

The Jackson kernel is a kernel that tries to minimize the spreading of sharp features of the function; as such, we will use it to approximate Dirac deltas. Its weight function is given by:

$$w_n^J = \frac{(N-n+1)\cos\left(\frac{\pi n}{N+1}\right) + \sin\left(\frac{\pi n}{N+1}\right)\cot\left(\frac{\pi}{N+1}\right)}{N+1}$$

To see how this kernel behaves when approximating a Dirac delta, we are going to calculate the approximated function's average and variance.

$$\langle x\rangle = \int_{-1}^{1} x\delta_{KPM}(x)dx$$

We can write x as $T_1(x)$ and $\delta_{KPM}(x)$ using the previously obtained expression, but this time with the added weight. This results in:

$$\langle x\rangle = \int_{-1}^{1}\sum_{n=0}^{N-1}\frac{1}{\pi\sqrt{1-x^2}}\frac{2w_n}{1+\delta_{n0}}T_n(x)T_n(\epsilon)T_1(x)dx$$

As we are making $\epsilon = 0$, we will have to work with the Chebyshev polynomials in zero, which are simply 0 for odd n, and $(-1)^{n/2}$ for even n.

$$\langle x\rangle = \sum_{n=0}^{N-1}\frac{2w_n}{1+\delta_{n0}}T_n(0)\int_{-1}^{1}\frac{T_n(x)T_1(x)dx}{\pi\sqrt{1-x^2}} == \sum_{n=0}^{N-1} w_n T_n(0)\delta_{n,1} = w_1T_1(0) = 0$$

which is the expected result for the Dirac delta. Moving on to the variance, we need only calculate $\langle x^2\rangle$, as the average was already seen to be zero. Writing x^2 as $T_2(x) + T_0(x)$, we have

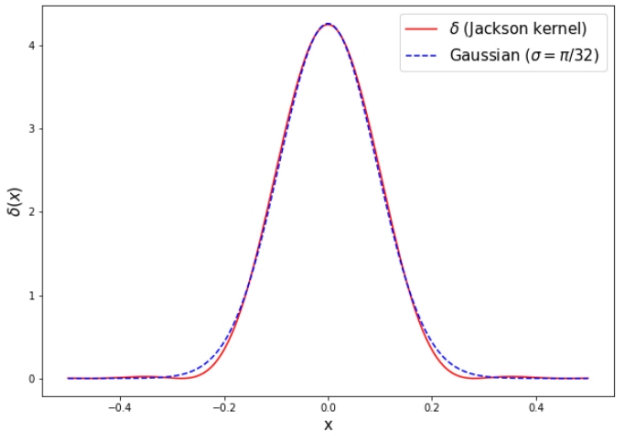

Figure 4.1: Comparison of a Gaussian with $\sigma = \pi/32$ with $\delta_{KPM}(x)$ calculated with 32 polynomials [15]

$$\begin{aligned}\langle x^2 \rangle &= \int_{-1}^{1} \sum_{n=0}^{N-1} \frac{1}{\pi\sqrt{1-x^2}} \frac{2w_n}{1+\delta_{n0}} T_n(x) T_n(0) \left[\frac{T_2(x)+T_0(x)}{2}\right] dx \\ &= \frac{1}{2} \sum_{n=0}^{N-1} w_n \left(\delta_{n,0} - \delta_{n,2}\right) = \frac{1}{2}\left(w_0 - w_2\right)\end{aligned}$$

Substituting the w coefficients in the equation and working the expression, we get to the result:

$$\langle x^2 \rangle = \frac{N \sin^2\left(\frac{\pi}{N+1}\right)}{N+1}$$

We can now take the limit for large N, from which we obtain an expression for the standard deviation:

$$\sigma \approx \left|\sin\left(\frac{\pi}{N}\right)\right| \approx \frac{\pi}{N}$$

In order to evaluate this result, we can compare it with a Gaussian with σ equal to the result obtained. The results are in represented in Fig.4.1.

Although near the peak, the two curves coincide almost completely, near the base, a difference emerges. We can analyze this difference by calculating higher-order moments for this distribution. Calculating $\langle x^4 \rangle$, we get the following expression:

$$\langle x^4 \rangle \approx 1 - 2\left(\frac{\pi}{N}\right)^2$$

which differs from the one for a Gaussian distribution:

$$\langle x^4 \rangle = 3\sigma^4 \approx 3\left(\frac{\pi}{N}\right)^2 \to 0$$

These results mean that, although this kernel gives us a good approximation of the Dirac delta for a small value of N, the same does not apply for distributions of the form $x^n\delta(x)$, where oscillations will start to appear.

4.4.4.4 Lorentz Kernel

Although the Jackson kernel is the best choice for functions with sharp features, it is not for Green functions, whose imaginary part approaches a Lorentzian rather than a Gaussian, as is the case for the Dirac delta. The weight function for the Lorentz kernel is:

$$w_n^L = \frac{\sinh\left[\lambda\left(1 - n/N\right)\right]}{\sinh(\lambda)}$$

Here, λ is a free parameter that represents a compromise between good resolution and damping of the oscillations.

4.4.5 Example - Density of States

We will now apply this method to the calculation of the density of states on graphene with periodic boundary conditions. As seen before, the density of states is given by:

$$\rho(\tilde{\epsilon}) = \frac{1}{\lambda V}\sum_n a_n(\tilde{\epsilon})\mathrm{Tr}[T_n(\tilde{H})]$$

First, we need to define the action of the Hamiltonian on the basis states. The basis we are going to use is $\{|a,m,n\rangle, |b,m,n\rangle\}$, where $|a,m,n\rangle$ denotes an electron on an atom A at position (m,n) in lattice coordinates. The same goes for $|b,m,n\rangle$, but this represents a B atom. Remembering the Hamiltonian for graphene in a magnetic field (eq.(2.2.12)):

$$H = -t\sum_{m,n} e^{i\frac{\pi\phi}{\phi_0}n}a^\dagger(m,n)b(m,n) + e^{-i\frac{\pi\phi}{\phi_0}n}a^\dagger(m,n)b(m-1,n) + a^\dagger(m,n)b(m,n-1) + h.c$$

we can apply it to the basis vectors, obtaining:

$$\begin{aligned} H|a,m,n\rangle &= e^{-i\frac{\pi\phi}{\phi_0}n}|b,m,n\rangle + e^{i\frac{\pi\phi}{\phi_0}n}|b,m-1,n\rangle + |b,m,n-1\rangle \\ H|b,m,n\rangle &= e^{i\frac{\pi\phi}{\phi_0}n}|a,m,n\rangle + e^{-i\frac{\pi\phi}{\phi_0}n}|a,m+1,n\rangle + |a,m,n+1\rangle. \end{aligned}$$

With this information, we can now create a program that calculates the density of states using KPM. The random distribution used to generate random vectors will be

$$\xi_j = \exp(2\pi i x_j)$$

where x_j is a random number between 0 and 1 with uniform distribution. Its properties can easily be checked:

$$\begin{aligned} \langle\xi_j\rangle &= \int_0^1 dx_j e^{2\pi i x_j} = 0 \\ \langle\xi_i^*\xi_j\rangle &= \langle\xi_i^*\rangle\langle\xi_j\rangle(-\delta_{ij}+1) + \delta_{ij}\langle\xi_i^*\xi_i\rangle = \delta_{ij}\int_0^1 dx_i e^{2\pi i(x_i-x_i)} = \delta_{ij} \\ \langle\xi_i\xi_j\rangle &= \langle\xi_i\rangle\langle\xi_j\rangle(-\delta_{ij}+1) + \delta_{ij}\langle\xi_i\xi_i\rangle = \delta_{ij}\int_0^1 dx_i e^{4\pi i x_i} = 0 \end{aligned}$$

With this random distribution, we made a program in python that calculates the density of states

of graphene with periodic boundary conditions. In addition to the density of states calculated with KPM, we also calculated the eigenvalues of the Hamiltonian and plotted them in the same graphic, in order to check if they coincide with the peaks of the Landau levels. The results are in Fig.4.2

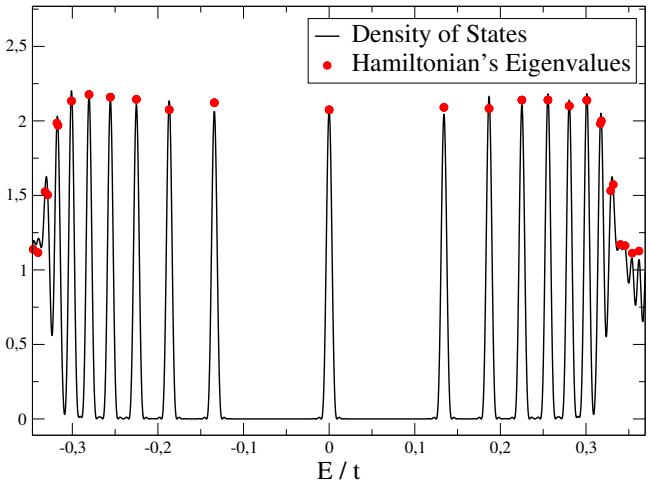

Figure 4.2: Density of states of a graphene lattice 128×128 with periodic boundary conditions calculated using KPM using 1024 Chebyshev polynomials, $\phi/\phi_0 = 2/L$ and Jackson Kernel (black line) and eigenvalues of the Hamiltonian (red dots) for low energies.

As it can be seen, the peaks of the Landau levels all coincide with the obtained eigenvalues, which demonstrates the accuracy of the KPM.

We can also vary the number of polynomials and see how it affects the resolution of the peaks. The results are on Fig.4.3. In here, we can clearly see that as the number of Chebyshev polynomials increase, the Landau levels become more defined. For 1024 polynomials, the density of states is almost entirely comprised of Landau levels, which means that for this case, this number of polynomials is good enough to have an accurate description of the density of states of graphene.

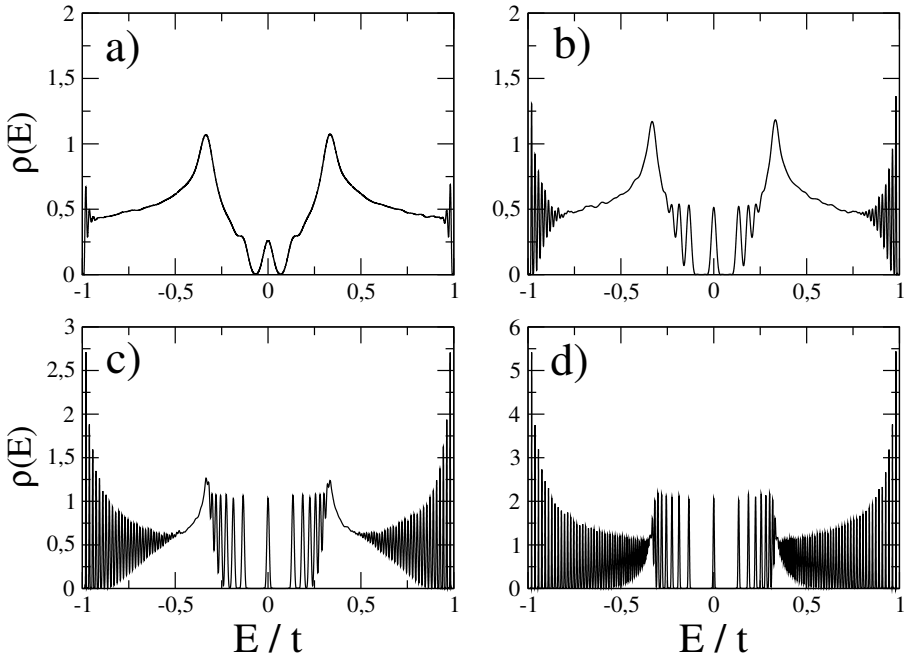

Figure 4.3: Density of states as calculated with the same parameters as in Fig.4.2, but with different number of Chebyshev polynomials: a)128; b)256; c)512 and d)1024

4.5 KITE Results

In this section, we will compare results obtained with KITE with the expressions obtained earlier. The expressions we will use are those of eqs.(4.3.8) and (4.3.9)

$$\sigma^{xx}(\omega) = -\frac{2}{\pi l_B^2}\frac{ie^2}{\hbar}\sum_{m\neq n}\frac{(C_m C_n)^2 v_F^2}{\omega_{mn}}\frac{(f(\epsilon_m)-f(\epsilon_n))}{\omega+\omega_{mn}+i\gamma}\left(\delta_{|m|-1,|n|}+\delta_{|m|,|n|-1}\right) \tag{4.5.1}$$

$$\sigma^{xy}(\omega) = \frac{2}{\pi l_B^2}\frac{e^2}{\hbar}\sum_{m\neq n}\frac{(C_m C_n)^2 v_F^2}{\omega_{mn}}\frac{(f(\epsilon_m)-f(\epsilon_n))}{\omega+\omega_{mn}+i\gamma}\left(\delta_{|m|-1,|n|}-\delta_{|m|,|n|-1}\right). \tag{4.5.2}$$

where γ is a phenomenological parameter that describes the inelastic scattering of phonons. It is also necessary to the assure that the conductivity converges when $\omega = \omega_{mn}$.

We start by plotting the results obtained by KITE against eq.(4.3.8) in Fig.4.4 a). The distinctive feature of this conductivity is that there are peaks that correspond to the energy differences between Landau levels (ω_{mn}). We can also see how for lower frequencies, both the analytical and numerical results strongly agree; however, for higher frequencies, larger differences between the curves start to arise, especially in the case of the imaginary part. This behavior happens because we have to truncate the sum in eq.(4.3.8) at some energy level, and also because the wavefunctions we used are approximations for low energies.

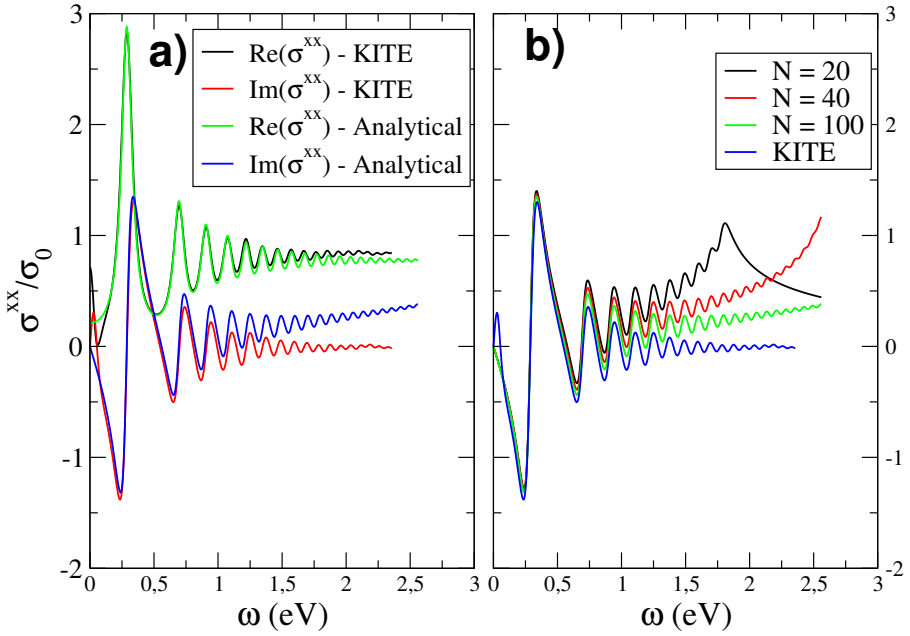

Figure 4.4: a) Plot of σ^{xx} for $\epsilon_F = 0.1$ eV , $\frac{\phi}{\phi_0} = \frac{1}{1024}$ and $\gamma = 0.05$ eV. The analytical curves are obtained from eq.(4.3.8) and the sums are made for the lowest 100 energy levels. b) Representation of the imaginary part of $\sigma^{xx}(\omega)$ for different numbers N of states used in the calculation through eq.(4.3.8) and comparison with the KITE result. The other parameters are the same as in a).

The effect of the truncation of the sum can also be studied. In Fig.4.4 b) we plot the imaginary part of $\sigma^{xx}(\omega)$ for three values of N, where N is the number of terms we consider in the sum over m and n in eq.(4.3.8). In this figure, we can see that, although the agreement between all the curves is very good for the first peak, for higher energies, we get improved results for higher values of N. This means that for a high enough N, we can get a very good agreement even for high energies between the analytical and numerical curves.

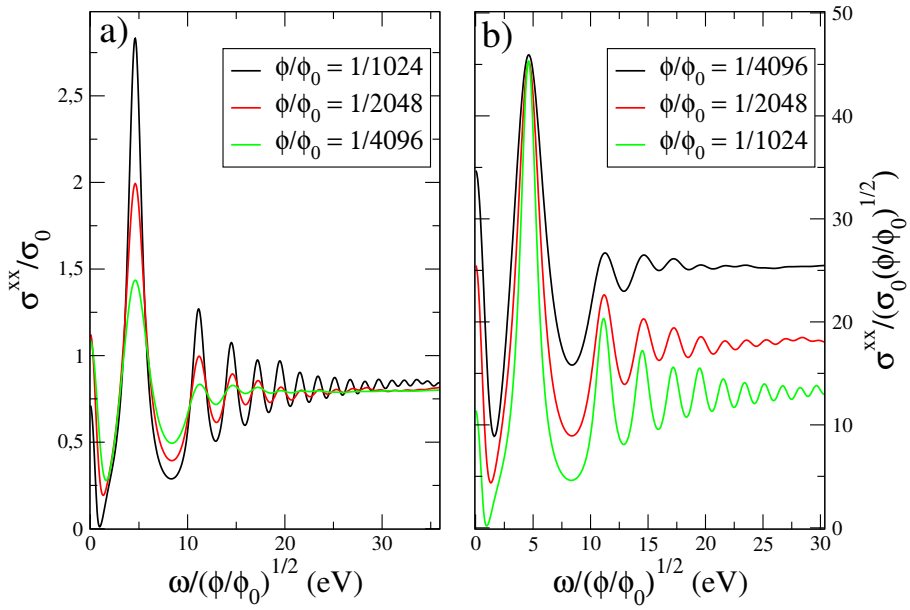

Figure 4.5: Real part of σ^{xx} as function of $\omega\sqrt{\frac{\phi_0}{\phi}}$ for $\epsilon_F = 0.1$ eV and $\gamma = 0.05$ eV calculated using KITE; b) σ^{xx} calculated with the same parameters as that of a), but the conductivity has been divided by $\sqrt{\frac{\phi}{\phi_0}}$..

We now shift our focus to the effect the variation of the magnetic field has on the conductivity. In Fig.4.5 a) we plotted σ^{xx} as function of $\omega\sqrt{\frac{\phi_0}{\phi}}$. The reason we scaled ω by such a factor is that, as said before, the position of the peaks correspond to the differences in energy between the Landau levels. As we saw before, these energies depend on $\sqrt{B}$, which means that by representing σ^{xx} as we do, the position of the peaks should be the same independently of the value of the magnetic field. This is exactly what we observe in Fig.4.5 a), where the peaks are all in the same position.

Another aspect of this graphic, is that the amplitude of the peaks increases with the magnetic field. Looking at eq.(4.3.8), we see that the dependence in B are in l_B and ω_{mn}. In the peaks, the term with the largest contribution to the amplitude is the one in which $\omega \approx \omega_{mn}$, making it so that the factors that contribute to the dependence on B are

$$\frac{1}{l_B^2\omega_{mn}} \propto \sqrt{B}.$$

The larger the peak, the more irrelevant the contributions from other terms are, meaning that this tendency should be better observed the largest peaks. In contrast, for higher frequencies, as the peaks will be shorter, the weight of the term where $\omega \approx \omega_{mn}$ will be smaller; in turn, the $\frac{1}{\omega+\omega_{mn}+i\gamma}$ factor will have an increased weight, which will make it so the conductivity does not depend on B.

This dependence on the square root of the magnetic field is not obvious in Fig.4.5 a), so we rescale these conductivities in Fig.4.5 b). We can see that for the first peak, the three curves have very close values. As the energy increases, the curves grow apart, until they take different constant values. Looking back at Fig.4.5 a), we see that these constant values are the same for all curves, which means that for high energies, the conductivity does not depend on the magnetic field.

Another interesting aspect of the conductivity is its dependence on the Fermi energy. In Fig.4.6 we represent $\sigma^{xx}(\omega)$ for $\epsilon_F = 0.5$ eV. Unlike the previous cases, with this Fermi energy, the peaks of the conductivity are much less pronounced. Additionally, we can see that for $\omega \sim 1$eV, there is a sudden increase for all the curves. This behavior is also present in graphene without magnetic field, where

there is a step at $\omega = 2\epsilon_F$ [19]. As the Fermi energy in this case is 0.5 eV, we can see that the position of the step in the case when there is no magnetic field is in the area where the sudden rise of the σ^{xx} happens with magnetic field.

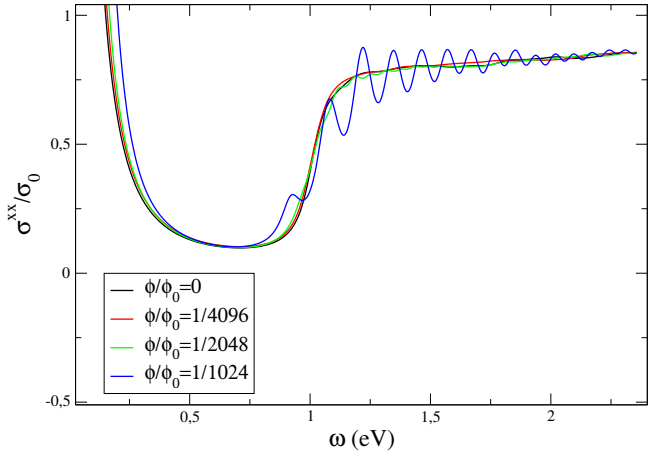

Figure 4.6: Plot of the linear conductivity σ^{xx} by KITE with parameters $\epsilon_F = 0.5$ eV and $\gamma = 0.05$ eV.

Finally, we compute $\sigma^{xy}(\omega)$, which is plotted in Fig.4.7. In this case, the agreement between the analytical and numerical results is even better than for σ^{xx}, as the curves almost coincide. We can also see that there are no peaks in the plot of $\sigma^{xy}(\omega)$, which is due to the minus sign in one of the deltas.

/home/joao/xy_B_2048_ef_0.1_scat_0.05.agr

Figure 4.7: Representation of $\sigma^{xy}(\omega)$ for $\epsilon_F = 0.1$ eV, $\frac{\phi}{\phi_0} = \frac{1}{2048}$, $\gamma = 0.05$ eV, calculated with KITE and through eq.(4.3.9).

In all the comparisons between numerical and analytical results, we see that there is a discrepancy at $\omega = 0$. This is due to the broadning of the peaks, which is a consequence of the fact that γ is non-zero. The Landau levels, which should be highly localized around the Landau energies, acquire a finite width, which introduce states that are not physical. Furthermore, numerically, for low frequencies, the conductivity is calculated through the sum of two divergent terms. If there is not enough resolution, they cancel exactly.

Chapter 5

Conclusions

In Chapter 1, we found a good approximation for the wavefunctions and energy of a square lattice with periodic boundary conditions by working the equations obtained by the Peierls substitution on the tight-binding Hamiltonian. The solutions obtained are valid for low energies and have the form of the wavefunctions of the quantum harmonic oscillator. Furthermore, we also saw that for systems with size $L \sim 10^3$ with open boundaries is described with good accuracy by a periodic boundaries description. In the last section of this chapter, we determined an expression for the vector potential that respects periodic boundary conditions for any crystal.

In Chapter 2, we used two different gauges to implement the Peierls phase in graphene's tight-binding Hamiltonian, which yield different constraints to the flux after applying periodic boundary conditions. Working the resulting equations, we arrived at two types of solutions for the wavefunctions: smooth ones, and ones with an oscillating phase. Just as in the square lattice, the approximated solutions for low energy in graphene with a magnetic field are the wavefunctions of the quantum harmonic oscillator. However, unlike the square lattice, the Landau levels go with $\sqrt{\lambda}$ and not with λ. Additionally, we also deduced the energy and wavefunctions of graphene through minimal coupling in the Dirac Hamiltonian, which we interpreted to be equivalent to an approximation of first-order of the Peierls phase. Comparing the analytical results with numerical ones, we saw that our approximated solution for low energies were in good agreement with the ones obtained from the diagonalization of the Hamiltonian. Once more, we checked that systems with open boundaries are well described by periodic boundary conditions for $L \sim 10^3$.

In Chapter 3, we presented a deduction of Kubo formula, which enables us to calculate the average of an operator up until any order. After writing the first-order Kubo formula, we worked an expression for the current density operator, thus obtaining an expression for its average.

In Chapter 4, we wrote the expression for the first-order conductivity in the length gauge, both for systems with periodic or boundary conditions. Replacing H_0 with the Dirac Hamiltonian, we obtained the first-order conductivities $\sigma^{xx}(\omega)$ and $\sigma^{xy}(\omega)$. Using the KITE software, we were able to compare the obtained expressions with numerical results. These expressions proved to describe the conductivity accurately for low frequencies; as for high frequencies, the truncation of the sums in the analytical expressions constitutes a barrier to better results. Another important point is that we could identify the dependence of the conductivity in B in the graphics we obtained.

Summing up, we were able to obtain a good approximation for wavefunctions of graphene under a magnetic field, and used them to calculate its linear conductivity accurately.

Chapter 6

Appendices

6.1 Appendix A - Averages of Creation and Annihilation Operators

Calculation of $\left\langle c_i^\dagger(t) c_j(t) \right\rangle_0$

From eq.(3.1.10), we can write the time evolution equation for an operator in the interaction picture as

$$\frac{d}{dt} J_I = \frac{i}{\hbar} \left[H_0, J_I \right].$$

Applying this equation for a creation operator, we get

$$\frac{d}{dt}\left(c_i^\dagger(t)\right) = \frac{i}{\hbar}\left[H_0, c_i^\dagger(t)\right] == e^{\frac{itH_0}{\hbar}} \frac{i}{\hbar}\left[H_0, c_i^\dagger\right] e^{-\frac{itH_0}{\hbar}} \tag{6.1.1}$$

where $c_i^\dagger(t)$ is the creation operator in the Interaction picture and $c_i^\dagger$ is the one in the Schrödinger picture. The commutator $\left[H_0, c_i^\dagger\right]$ yields

$$\left[H_0, c_i^\dagger\right] = \epsilon_i c_i^\dagger.$$

Putting this result in eq.(6.1.1), we obtain

$$\frac{d}{dt}\left(c_i^\dagger(t)\right) = \frac{i}{\hbar}\epsilon_i c_i^\dagger(t)$$

whose solution is

$$c_i^\dagger(t) = c_i^\dagger e^{\frac{i}{\hbar}\epsilon_i (t - t_0)}$$

where t_0 is the instant the perturbation is turned on. As for the annihilation operator, the solution is just the hermitian conjugate

$$c_i(t) = c_i e^{-\frac{i}{\hbar}\epsilon_i (t - t_0)}.$$

With this, we can write $\langle c_i^\dagger(t_1) c_j(t_2) \rangle_0$ as

$$\langle c_i^\dagger(t_1) c_j(t_2) \rangle_0 = \langle c_i^\dagger c_j \rangle_0 e^{\frac{i}{\hbar}\epsilon_i (t_1 - t_0)} e^{-\frac{i}{\hbar}\epsilon_j (t_2 - t_0)}.$$

Having dealt with the time dependence, we need to calculate the average of the operators in the Schrödinger picture. We can start by writing it as

$$\langle c_i^\dagger c_j \rangle_0 = \mathrm{Tr}\left[\rho_0 c_i^\dagger c_j\right]$$

Using Wick theorem for finite temperature, this average yields

$$\langle c_i^\dagger c_j \rangle_0 = \delta_{ij} f(\epsilon_i)$$

where $f(\epsilon_i)$ is the Fermi-Dirac distribution.

Finally, putting this expression in the average of the operators in the interaction picture, we obtain

$$\langle c_i^\dagger(t_1) c_j(t_2) \rangle_0 = \delta_{ij} f(\epsilon_i) e^{\frac{i}{\hbar}\epsilon_i(t_1-t_2)}.$$

Calculation of $\left\langle \left[c_i^\dagger c_j, c_k^\dagger c_l \right] \right\rangle_0$

In order to calculate this average, we start by expanding the commutator:

$$\begin{aligned}
\left[c_i^\dagger c_j, c_k^\dagger c_l \right] &= c_i^\dagger c_j c_k^\dagger c_l - c_k^\dagger c_l c_i^\dagger c_j \\
&= c_i^\dagger c_j c_k^\dagger c_l + c_k^\dagger c_i^\dagger c_l c_j - c_k^\dagger \left\{ c_l c_i^\dagger \right\} c_j \\
&= c_i^\dagger c_j c_k^\dagger c_l + c_i^\dagger c_k^\dagger c_j c_l - \delta_{il} c_k^\dagger c_j \\
&= c_i^\dagger \left\{ c_k^\dagger c_j \right\} c_l - \delta_{il} c_k^\dagger c_j \\
&= \delta_{kj} c_i^\dagger c_l - \delta_{il} c_k^\dagger c_j
\end{aligned}$$

Putting this result back into the average, what we get is

$$\left\langle \left[c_i^\dagger c_j, c_k^\dagger c_l \right] \right\rangle_0 = \left\langle \delta_{kj} c_i^\dagger c_l - \delta_{il} c_k^\dagger c_j \right\rangle_0 == \delta_{kj} \left\langle c_i^\dagger c_l \right\rangle_0 - \delta_{il} \left\langle c_k^\dagger c_j \right\rangle_0$$

Using the result from the previous section, we obtain the following result

$$\left\langle \left[c_i^\dagger c_j, c_k^\dagger c_l \right] \right\rangle_0 = \delta_{kj}\delta_{il} \left(f(\epsilon_i) - f(\epsilon_j) \right)$$

Calculation of $\left\langle \left[c_i^\dagger c_j, \left[c_k^\dagger c_l, c_m^\dagger c_n \right] \right] \right\rangle_0$

Similarly to the previous case, we want to expand this commutator in terms of the previous order term. Expanding $\left\langle \left[c_i^\dagger c_j, \left[c_k^\dagger c_l, c_m^\dagger c_n \right] \right] \right\rangle_0$ we obtain

$$\left[c_i^\dagger c_j, \left[c_k^\dagger c_l, c_m^\dagger c_n \right] \right] = \left[c_i^\dagger c_j, c_k^\dagger c_l c_m^\dagger c_n \right] - \left[c_i^\dagger c_j, c_m^\dagger c_n c_k^\dagger c_l \right] \tag{6.1.2}$$

From this expression, we can rearrange the order of the operators $c_k^\dagger c_l c_m^\dagger c_n$ in the first commutator so as to match that of the second one, and cancel it, thus leaving only the commutators that were needed.

$$\begin{aligned}
c_k^\dagger c_l c_m^\dagger c_n &= c_k^\dagger c_n \left\{ c_m^\dagger, c_l \right\} - c_k^\dagger c_m^\dagger c_l c_n \\
&= c_k^\dagger c_n \left\{ c_m^\dagger, c_l \right\} - c_m^\dagger c_k^\dagger c_n c_l \\
&= c_k^\dagger c_n \left\{ c_m^\dagger, c_l \right\} - c_m^\dagger c_l \left\{ c_k^\dagger, c_n \right\} + c_k^\dagger c_l c_m^\dagger c_n
\end{aligned}$$

Replacing this into the first term in eq.(6.1.2),

$$\left[c_i^\dagger c_j, c_k^\dagger c_l c_m^\dagger c_n \right] = \left\{ c_m^\dagger, c_l \right\} \left[c_i^\dagger c_j, c_k^\dagger c_n \right] - \left\{ c_k^\dagger, c_n \right\} \left[c_i^\dagger c_j, c_m^\dagger c_l \right] + \left[c_i^\dagger c_j, c_k^\dagger c_l c_m^\dagger c_n \right]$$

We can now see that the last term in this expression cancels the last one on eq.(6.1.2), which leads to:

$$\left\langle \left[c_i^\dagger c_j, \left[c_k^\dagger c_l, c_m^\dagger c_n\right]\right]\right\rangle_0 = \left\{c_m^\dagger, c_l\right\}\left\langle \left[c_i^\dagger c_j, c_k^\dagger c_n\right]\right\rangle_0 - \left\{c_k^\dagger, c_n\right\}\left\langle \left[c_i^\dagger c_j, c_m^\dagger c_l\right]\right\rangle_0$$

As we already have the result of the averages that are left, we can replace it, obtaining

$$\left\langle \left[c_i^\dagger c_j, \left[c_k^\dagger c_l, c_m^\dagger c_n\right]\right]\right\rangle_0 = \delta_{ml}\delta_{kj}\delta_{in}\left[f(\epsilon_i) - f(\epsilon_j)\right] - \delta_{kn}\delta_{mj}\delta_{il}\left[f(\epsilon_i) - f(\epsilon_j)\right]$$

6.2 Appendix B - Integrals of complex exponentials

In Chapter 4, we need to calculate the result of

$$\int_{-\infty}^{+\infty} dt \int_{-\infty}^{t} dt' e^{i(\omega+\omega_{pq})t} e^{-i(\omega'+\omega_{pq})t'}$$

When both integrals in time go from $-\infty$ to $+\infty$, this integral becomes easy to calculate; however, in this case, one of the upper limits of the integral is not $+\infty$ but t. This can be solved by inserting an Heaviside function

$$\Theta(t) = \int_{-\infty}^{+\infty} \frac{d\omega}{2\pi i} \frac{e^{i\omega t}}{\omega - i\epsilon}$$

such that for $t_1 > t$ it becomes zero. This makes us able to prolong the second integral until $+\infty$, yielding

$$\begin{aligned}
\int_{-\infty}^{+\infty} dt \int_{-\infty}^{t} dt' e^{i(\omega+\omega_{pq})t} e^{-i(\omega'+\omega_{pq})t'} &= \int_{-\infty}^{+\infty} dt \int_{-\infty}^{+\infty} dt' \int_{-\infty}^{+\infty} \frac{d\omega''}{2\pi i} \frac{e^{i\omega''(t-t')}}{\omega'' - i\epsilon} e^{i(\omega+\omega_{pq})t} e^{-i(\omega'+\omega_{pq})t'} \\
&= \int_{-\infty}^{+\infty} dt \int_{-\infty}^{+\infty} dt' \int_{-\infty}^{+\infty} \frac{d\omega''}{2\pi i} \frac{1}{\omega'' - i\epsilon} e^{i(\omega+\omega_{pq}+\omega'')t} e^{-i(\omega'+\omega_{pq}+\omega'')t'} \\
&= \int_{-\infty}^{+\infty} \frac{d\omega''}{2\pi i} \frac{2\pi\delta(\omega+\omega_{pq}+\omega'')}{\omega'' - i\epsilon} 2\pi\delta(\omega'+\omega_{pq}+\omega'') \\
&= i\frac{\delta(\omega-\omega')}{\omega'+\omega_{pq}+i\epsilon} 2\pi\delta(\omega'+\omega_{pq}+\omega'')
\end{aligned}$$

In order to calculate the second-order conductivity, we need to calculate the next order integral

$$\int_{-\infty}^{+\infty} dt \int_{-\infty}^{t} dt_1 \int_{-\infty}^{t_1} dt_2 e^{i(\omega+\omega_{pi})t} e^{-i(\omega_1+\omega_{pm})t_1} e^{-i(\omega_2+\omega_{mi})t_2}$$

which is done in exactly the same fashion as the previous one. In this one, we need to introduce two Heaviside functions, which results in

$$\begin{aligned}
&\int_{-\infty}^{+\infty} dt \int_{-\infty}^{t} dt_1 \int_{-\infty}^{t_1} dt_2 \int \frac{d\omega'}{2\pi i} \int \frac{d\omega''}{2\pi i} \frac{e^{i(\omega+\omega_{pi}+\omega')t}}{\omega'-i\epsilon} \frac{e^{-i(\omega_1+\omega_{pm}+\omega'-\omega'')t_1}}{\omega''-i\epsilon} e^{-i(\omega_2+\omega_{mi}+\omega'')t_2} \\
&= \int \frac{d\omega'}{2\pi i} \int \frac{d\omega''}{2\pi i} \frac{2\pi\delta(\omega+\omega_{pi}+\omega')}{\omega'-i\epsilon} \frac{2\pi\delta(\omega_1+\omega_{pm}+\omega'-\omega'')}{\omega''-i\epsilon} 2\pi\delta(\omega_2+\omega_{mi}+\omega'') \\
&= 2\pi \int d\omega' \frac{\delta(\omega+\omega_{pi}+\omega')}{\omega'-i\epsilon} \frac{\delta(\omega_1+\omega_2+\omega_{mi}+\omega_{pm}+\omega')}{\omega_2+\omega_{mi}+i\epsilon} \\
&= -2\pi \frac{\delta(\omega-\omega_1-\omega_2)}{\omega_1+\omega_2+\omega_{pi}+i\epsilon} \frac{1}{\omega_2+\omega_{mi}+i\epsilon}
\end{aligned}$$

where in the third to fourth step we used that $\omega_{mi} + \omega_{pm} = \omega_{pi}$. For the second term we need to calculate, it is exactly the same procedure, where only the indices of the energy differences in the exponential change. Substituting them, we get that the second integral is given as

$$-2\pi \frac{\delta(\omega - \omega_1 - \omega_2)}{\omega_1 + \omega_2 + \omega_{pm} + i\epsilon} \frac{1}{\omega_2 + \omega_{pi} + i\epsilon}$$

6.3 Appendix C - Calculation of $\nabla \times \boldsymbol{A}$

The magnetic field $\boldsymbol{B}$ can be written as the curl of $\boldsymbol{A}$

$$\boldsymbol{B} = (\partial_x A_y - \partial_y A_x)\, \hat{e}_z.$$

Although we normally write $\boldsymbol{A}$ in its components along the reciprocal lattice vectors, we can convert it into cartesian coordinates. Writing the reciprocal lattice vectors along in its components along the coordinate axes

$$\boldsymbol{b}_1 = b_{1x}\hat{e}_x + b_{1y}\hat{e}_y$$

$$\boldsymbol{b}_2 = b_{2x}\hat{e}_x + b_{2y}\hat{e}_y$$

the vector potential becomes

$$\boldsymbol{A}(\boldsymbol{r}) = A_1(\boldsymbol{r})\boldsymbol{b}_1 + A_2(\boldsymbol{r})\boldsymbol{b}_2 = (A_1(\boldsymbol{r})b_{1x} + A_2(\boldsymbol{r})b_{2x})\hat{e}_x + (A_1(\boldsymbol{r})b_{1y} + A_2(\boldsymbol{r})b_{2y})\hat{e}_y$$

Replacing this result in the equation for the magnetic field, we obtain

$$\boldsymbol{B} = (\partial_x(A_1(\boldsymbol{r})b_{1y} + A_2(\boldsymbol{r})b_{2y}) - \partial_y(A_1(\boldsymbol{r})b_{1x} + A_2(\boldsymbol{r})b_{2x}))\, \hat{e}_z.$$

We now have to ascertain the dependence on x and y inside A_1 and A_2. Writing the position vector as $\boldsymbol{r} = m_1\boldsymbol{a}_1 + m_2\boldsymbol{a}_2$, where m_1 and m_2 can take any real value, we can write the components of $\boldsymbol{A}$ as

$$A_1(\boldsymbol{r}) = \sum_j A_{1j}\boldsymbol{r}\cdot\boldsymbol{b}_j = 2\pi\sum_j A_{1j}m_j$$
$$A_2(\boldsymbol{r}) = \sum_j A_{2j}\boldsymbol{r}\cdot\boldsymbol{b}_j = 2\pi\sum_j A_{2j}m_j$$

However, what we need to calculate are the derivatives in order to x and y, so we need to write x_1 and x_2 as their function. Rewriting $\boldsymbol{r}$, we have

$$\boldsymbol{r} = (m_1 a_{1x} + m_2 a_{2x})\hat{e}_x + (m_1 a_{1y} + m_2 a_{2y})\hat{e}_y$$

From here, we can we can write equations for m_1 and m_2 as function of x and y:

$$m_1 = \left(\frac{a_{2y}x - a_{2x}y}{V}\right)$$
$$m_2 = -\left(\frac{a_{1y}x - a_{1x}y}{V}\right)$$

where $V = a_{11}a_{22} - a_{12}a_{21}$ is the area of a unit cell. Replacing in the expression for A_1 and A_2, we have

$$A_1(\boldsymbol{r}) = \frac{2\pi}{V}\left(A_{11}\left(a_{2y}x - a_{2x}y\right) - A_{12}\left(a_{1y}x - a_{1x}y\right)\right)$$
$$A_2(\boldsymbol{r}) = \frac{2\pi}{V}\left(A_{21}\left(a_{2y}x - a_{2x}y\right) - A_{22}\left(a_{1y}x - a_{1x}y\right)\right)$$

We can now put these expressions in the equation for the magnetic field

$$\boldsymbol{B} = \frac{2\pi}{V}\left(\left(A_{11}a_{2y} - A_{12}a_{1y}\right)b_{1y} + \left(A_{21}a_{2y} - A_{22}a_{1y}\right)b_{2y} + \left(A_{11}a_{2x} - A_{12}a_{1x}\right)b_{1x} + \left(A_{21}a_{2x} - A_{22}a_{1x}\right)b_{2x}\right)\hat{e}_z$$

$$\boldsymbol{B} = \frac{(2\pi)^2}{V}\left(A_{21} - A_{12}\right)\hat{e}_z$$

Writing $\boldsymbol{B} = B\hat{e}_z$, this expression becomes

$$B = \frac{(2\pi)^2}{V}\left(A_{21} - A_{12}\right) \tag{6.3.1}$$

Bibliography

[1] K. S. Novoselov, A. K. Geim, S. V. Morozov, D. Jiang, Y. Zhang, S. V. Dubonos, I. V. Grigorieva, and A. A. Firsov, Electric field effect in atomically thin carbon films, Science. 306, 666, (2004)

[2] X. Yao and A. Belyanin, Nonlinear optics of graphene in a strong magnetic field, J. Phys. Condens. Matter 25 , 054203 (2013)

[3] X. Yao and A. Belyanin, Giant optical nonlinearity of graphene in a strong magnetic field, Physical Review Letters, 2012

[4] Cheng, J. L. Vermeulen, N. Sipe, J. E.; Third order optical nonlinearity of graphene; New Journal of Physics; 2014

[5] M Tahir and K Sabeeh; Gap opening in the zeroth Landau level in gapped graphene: pseudo-Zeeman splitting in an angular magnetic field; Journal of Physics: Condensed Matter; 2012

[6] Cheng, J. L. Guo, C., Nonlinear magneto-optic effects in doped graphene and in gapped graphene: A perturbative treatment, Physical Review B, 2018

[7] Bludov, Yu V.; Vasilevskiy, M. I.; Peres, N. M.R.; Magnetic field assisted transmission of THz waves through a graphene layer combined with a periodically perforated metallic film, Physical Review B, 2018

[8] Crassee, Iris Levallois, Julien Walter, Andrew L. Ostler, Markus Bostwick, Aaron Rotenberg, Eli Seyller, Thomas van der Marel, Dirk Kuzmenko, Alexey B.; Giant Faraday rotation in single- and multilayer graphene; Nature Physics; 2010

[9] König-Otto, Jacob C.; Wang, Yongrui; Belyanin, Alexey; Berger, Claire De; Heer, Walter A.; Orlita, Milan; Pashkin, Alexej; Schneider, Harald; Helm, Manfred; Winnerl, Stephan; Four-Wave Mixing in Landau-Quantized Graphene, Nano Letters, 2017

[10] Yumoto, Go; Matsunaga, Ryusuke; Hibino, Hiroki; Shimano, Ryo; Ultrafast Terahertz Nonlinear Optics of Landau Level Transitions in a Monolayer Graphene, Physical Review Letters, 2018

[11] Moradi, Afshin; Energy density and energy flow of surface waves in a strongly magnetized graphene; Journal of Applied Physics; 2018

[12] Claude Cohen-Tannoudji, Bernard Diu, Frank Laloe; Quantum Mechanics

[13] Neil W. Ashcroft, N. David Mermin; Solid State Physics

[14] Castro, Eduardo & Peres, Nuno & Santos, João & Guinea, Francisco & Castro Neto, Antonio. (2007). An introduction to the physics of graphene layers. 111-143. 10.1142/9789812772206_0004.

[15] Simão Meneses João (2017), Non-Linear Optical Response with the Kernel Polynomial Method (Master's Thesis)

[16] Gonçalves, Paulo André & Peres, Nuno. (2016). An Introduction to Graphene Plasmonics. 10.1142/9948.

[17] Gauge covariances and nonlinear optical responses, G. B. Ventura, D. J. Passos, J. M. B. Lopes dos Santos, J. M. Viana Parente Lopes, N. M .R. Peres

[18] A. Ferreira, J. Viana-Gomes, Yu. V. Bludov, Vitor M. Pereira, N. M. R. Peres, A. H. Castro Neto; Faraday effect in graphene enclosed in an optical cavity and the equation of motion method for the study of magneto-optical transport in solids; Phys. Rev. B 84, 235410

[19] Peres, Nuno. (2010). The transport properties of graphene: an introduction. Rev. Mod. Phys. 82, 2673. Reviews of Modern Physics. 82. 10.1103/RevModPhys.82.2673.